Reconstructing the Geodetic Mass Balance of Thompson Glacier, Axel Heiberg Island, Canada

GEO 511 Master's Thesis

Author
Andreas Gantner
13-732-243

Supervised by
Prof. Dr. Michael Zemp
Dr. Laura Thomson (l.thomson@queensu.ca)

Faculty representative
Prof. Dr. Andreas Vieli

29.04.2020
Department of Geography, University of Zurich

GEO 511 Master's Thesis

Reconstructing the Geodetic Mass Balance of Thompson Glacier, Axel Heiberg Island, Canada

Author

Andreas Gantner
andreas.gantner@uzh.ch
13-732-234

Supervisors

Dr. Michael Zemp
michael.zemp@geo.uzh.ch

Dr. Laura Thomson
l.thomson@queensu.ca

Faculty Member

Prof. Dr. Andreas Vieli
andreas.vieli@geo.uzh.ch

30th of April 2020
Department of Geography, University of Zurich

Summary

This thesis aims to reconstruct the geodetic mass balance of Thompson Glacier, a large outlet glacier on Axel Heiberg Island in the Canadian Arctic. The area lies within a region which experiences some of the greatest rates of climate warming. Recent estimates show that the disappearing ice masses in northern Canada are one of the largest contributors to global sea-level rise besides Greenland and Antarctica. Yet, data in the area is very limited, with only few long-term series of glaciological measurements and geodetic mass balance values of only a dozen glaciers existing. Adding to the geodetic sample size greatly improves the understanding of climatic changes in a region where data availability is still scarce. Thus, this thesis additionally entails mass balance estimates for smaller glaciers surrounding Thompson Glacier, presenting results for a total of 8 different glaciers.

The basic framework of this thesis are two historical maps which resulted from field expeditions in 1960. The Thompson Glacier Region Map shows the area in a scale of 1:50'000. It was produced with glaciological studies in mind, thus offering incredible detail on the glacier's structures in the past. In addition, the Expedition Area Map in 1:100'000 extends the perimeter to the larger context of the study area. Using both maps, a digital elevation model of the historical glacier state is derived. Changes in glacier volume and mass balance are then assessed by creating a difference image of the historical data and the contemporary digital elevation models TanDEM-X and ArcticDEM. The most important constraint is that the accumulation area of Thompson Glacier is only charted on the less detailed map. The comparison of the historical maps to its contemporary counterpart demonstrates that the Expedition Area Map suffers from largely unrealistic elevation data. Assuming that such strong negative changes are unlikely the entire accumulation area is interpreted as a data void. This issue is then tackled using two different void filling approaches.

The first method assigns a zero-change rate to the entire accumulation area. The resulting difference image serves as an indicator of the impact generated by inaccurate historical data. To increase detail within the filled void, the second method introduces as much of the knowledge of local elevation changes as possible. Relying on the assumption that elevation change is dependent on elevation itself, so called elevation bins are used to reconstruct the accumulation area based on mean elevation changes in the respective altitudes. Regardless of the observed difference image, the resulting geodetic mass balances for Thompson Glacier turn out negative.

As each step in deriving the geodetic mass balances entails a variety of uncertainties, a statistical approach to assess error propagation is implemented. In doing so, it is possible to estimate the uncertainties within all derived values for glacier wide elevation change, mass balance and mass change. This helps to quantify the obtained results, illustrating that the modified historical elevation model is able to reconstruct a plausible scenario for Thompson Glacier. Based on this, the glacier experienced a slight negative mass balance rate over the last five decades. However, due to its large size, the corresponding loss in ice mass reveals the large impact of a changing climate. As polar glaciers are important contributors to global sea level rise, future research improving the data sample in the High Arctic is vital.

Acknowledgements

Table of Contents

Lis of Abbreviations

ACN   Arctic Canada North

AG   Astro Glacier

AHI   Axel Heiberg Island

BG   Bellevue Glacier

CAA   Canadian Arctic Archipelago

CG   Crook Glacier

dDEM   difference Digital Elevation Model;
             The difference image resulting from the subtraction of one DEM from another.

DEM   Digital Elevation Model

EXA   Expedition Area

FG   Finger Glacier

GLIMS   Global Land Ice Measurements from Space

HIF   Hidden Ice Field

IDW   Inverse Distance Weighting

MIC   Mueller Ice Cap

NAD27   North American Datum 1927

PG   Parallel Glacier

PH   Phantom Glacier

PoR   Period of record

RGI   Randolph Glacier Inventory

TG   Thompson Glacier

TGR   Thompson Glacier Region

TR   Transit Glacier

WGMS   World Glacier Monitoring Service

List of Figures

List of Tables

1. Introduction

1.1 Motivation

Retreating ice masses have become an icon of climate change (Zemp *et al.*, 2019). Melting glaciers and ice caps are contributing significantly to a rising sea level with no halt in sight (Gardner *et al.*, 2011). The impacts of a changing climate are nowhere as visible as in the Arctic, where surface air temperatures have been increasing twice as fast as the global average (Meredith *et al.*, 2019). As new extremes occur year after year, the importance of understanding the ongoing changes rises.

This thesis sets its focus on the Canadian Arctic Archipelago (CAA). The islands located off to the north-western coasts of Greenland contain around 14% of the global land-ice volume and are located in latitudes that are currently experiencing some of the greatest rates of climate warming (Sharp *et al.*, 2011). Yet, only few studies on the region's contribution to sea-level change exist (Thomson and Copland, 2017). In recent years, the Canadian Arctic lost over 60 gigatons of ice per year, rendering it one of the largest contributors to global sea-level rise besides the ice masses of Greenland and Antarctica (Gardner *et al.*, 2011). Therefore, assessing the changes of its glaciers provides valuable details to a region, where data availability is still relatively scarce (Zemp *et al.*, 2019).

At the heart of the thesis is a closer examination of Thompson Glacier, the second largest outlet glacier of the Müller Ice Cap on Axel Heiberg Island in the Canadian Arctic (Müller, 1962). In 1960, field expeditions resulted in detailed maps of the glacier, presenting a comprehensive overview of the historical extent of the outlet glacier. The maps entail various smaller glaciers, differing in size, slope and aspect, which are included into this thesis in addition to Thompson Glacier. This provides a better observational coverage of the region and allows a more extensive interpretation of the impacts of climate change.

Thanks to the field maps, the region is suitable for a geodetic mass balance reconstruction which compares the historical maps with contemporary digital elevation models (DEM). Such an analysis can serve as an important indicator for climatic changes and helps to assess a glacier's contribution to sea level rise (Zemp *et al.*, 2013). While there have been similar studies in the area (e.g. Thomson et al., 2017), this thesis additionally tackles the issue of inaccurate historical data. The map covering the accumulation area of the glacier is based on indefinite information. Thus, a solid approach to define the missing elevation data is necessary. Based on the assumption that there is a relationship between elevation change and elevation (McNabb *et al.*, 2019), the historical state of the accumulation area is reconstructed.

There is a need to better understand the changes of polar glaciers and their contribution to global sea level rise (Meredith *et al.*, 2019). This thesis provides valuable insights into the evolution of ice masses within the Canadian Arctic. Additionally, it tests the reliability of historical maps applied in glaciological studies and shows an approach to assess glaciated areas where the historical data is incomplete or vague.

1.2 Approach, Research Questions and Structure

This thesis aims to add to the understanding of changes in the Canadian Arctic by contributing to the geodetic mass balance samples in a region, where the observational coverage so far has been slim (Zemp *et al.*, 2019). The main goal is to reconstruct the geodetic mass balance of Thompson Glacier for the period of 1959 to 2014. This is based on the geodetic method which determines glacier volume change through repeated mapping and differencing of glacier surface elevations (Zemp *et al.*, 2013). In this case, the basic framework consists of a comparison of elevation data taken from historical maps to contemporary satellite DEMs. As there are large data voids present in the available historical data, this thesis furthermore entails different approaches to reconstruct data voids, as well as an assessment of uncertainties within the used data. In addition to Thompson Glacier, several smaller glaciers in the vicinity will be included in the analysis.

To achieve these goals, the following research questions will be discussed:

a.) *How did Thompson Glacier's ice mass change during the period of 1959 to 2014?*

b.) *How reliable is the use of historical maps in deriving geodetic mass balances for glaciers?*

c.) *How do different approaches to reconstruct large data voids impact the obtained results?*

d.) *How relevant is the assessment of error propagation regarding the quantification of obtained results?*

The thesis is divided into the following parts: Chapter 2 presents an overview on the study area and the field expeditions which the historical maps are based on. Chapter 3 delineates the broader scientific context. Chapter 4 introduces the data used throughout the thesis. Chapter 5 explains all implemented methods use to derive the geodetic mass balance from the historical maps, as well as the approaches to tackling the data void in the accumulation area and the accompanying uncertainties. The obtained results are presented in chapter 6 and discussed in Chapter 7. Chapter 8 concludes the thesis by revisiting the research questions and presenting a brief outlook for future research on the topic.

2. Study Area

The study area is situated on Axel Heiberg Island (AHI), the second most northern of the islands in the Canadian Arctic Archipelago (Figure 1). The island has been featured in many studies over the past half century. It presents an interesting area for glaciological research (e.g. Müller, 1962; Kälin, 1971; Thomson et al., 2017), as a wide range of glacier types is present. An older inventory compiled by Ommaney (1969) lists the following: 55% of the island's ice coverage are attributed to outlet glaciers, 26% are valley-, mountain and other glaciers with independent accumulation areas, while ice caps and ice fields account for 16% and 3%, respectively.
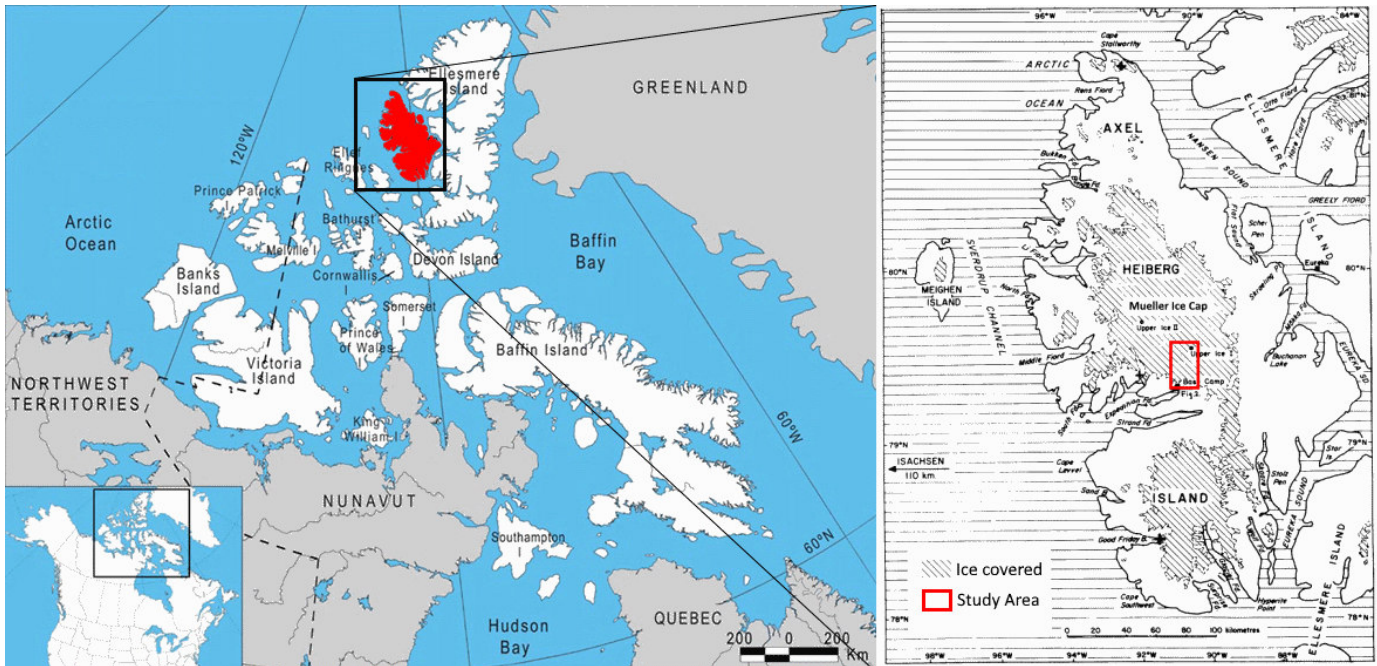
Figure 1: Geographical location of Axel Heiberg marked in red on the left map. Study area on AHI outlined in red on the right map. Left map adapted from the original by the Canadian Museum of Nature (nature.ca), Right map adapted from the original by Müller (1962: 132).

More precisely, this thesis is set in the Expedition Fiord in the center of AHI's western coast. Like the island, the fiord is shaped by many different types of glaciers; its most dominant being Thompson Glacier, a large outlet glacier from Müller Ice Cap. The area has appeared in various scientific studies since the first expeditions in 1959. These were led by Fritz Müller, the head of the forerunner of the World Glacier Monitoring Service (WGMS) with the objective of carrying out detailed mass balance investigations on multiple glaciers (Müller, 1962). Ever since, the focus of glaciological work has been set on White Glacier. Its surface mass balance values have been recorded annually, with only a single short interruption in the late 1970s. Thanks to this long running series, White Glacier serves as an important reference glacier for climatic changes in the region (WGMS, 2019).

2.1 Thompson Glacier

Thompson Glacier is the second largest outlet glacier of Müller Ice Cap (MIC). Its main tongue flows in a southward direction extending 40 km from its ice divide at an elevation of 1400 m a.s.l. to its snout at 100 m a.s.l. The glacier flows along a rather flat slope with a surface gradient averaging around 4%, its width varying between 3 and 5 km (Müller, 1962). The main tongue of the glacier flows down from MIC, but two of its larger tributaries have different accumulation conditions: Crook Glacier (CG) is a glacier confined by steep cliffs of the peaks to the west of Thompson Glacier. To the east, Wreck Glacier (WR) flows from an ice-covered ridge to the east down to where it merges with the tongue of Thompson Glacier.
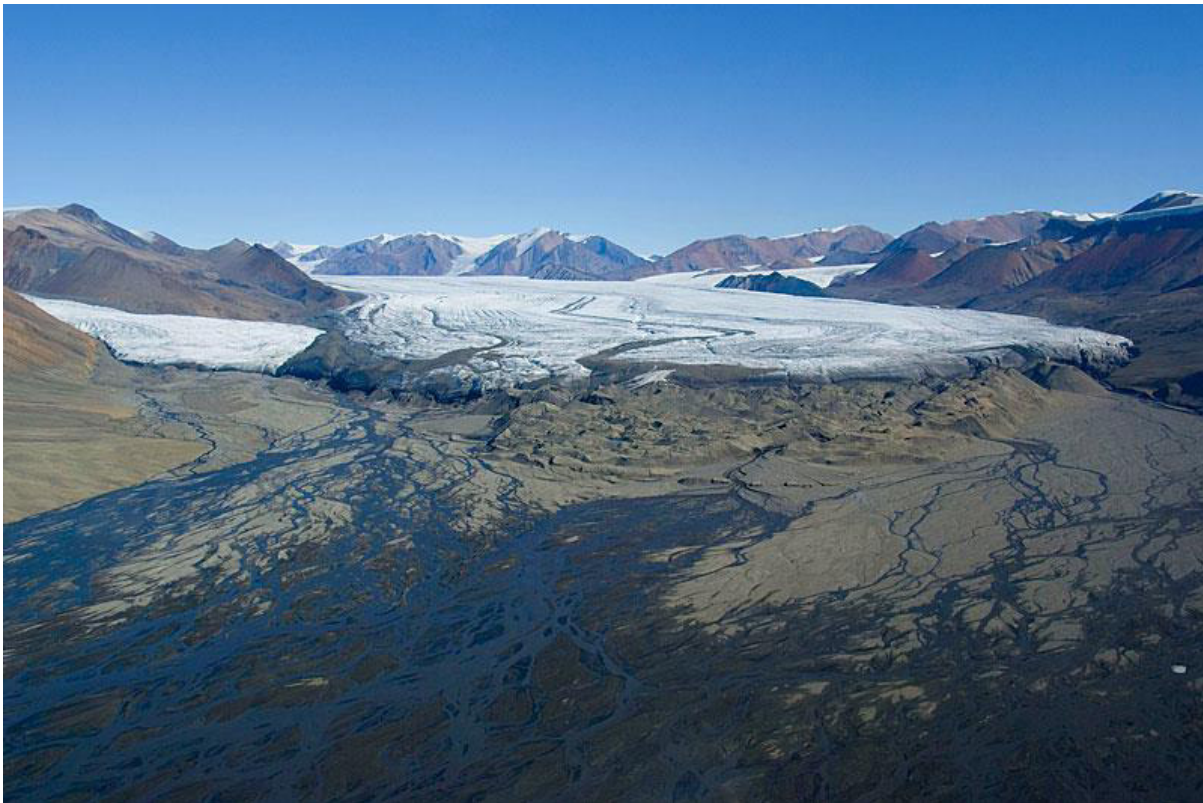
Figure 2: Aerial view of the snout of Thompson Glacier. Well visible is the distinctive push moraine in front of the glacier and the sinuous medial moraines on the glacier's tongue. Left of the snout lies the tongue of White Glacier. In the upper right, the confluence of Wreck Glacier and Thompson Glacier can be seen. Photo from Glaciers Online (Alean, 2008).

The first observations on the glacier included measurements of summer ablation and ice thickness. They were conducted during the field expeditions in the early 1960s (Müller, 1962). On Thompson Glacier, the focus of scientific work centred on its push moraine, a special feature resulting from the advance of the glacier into frozen gravel deposits (Figure 2). The behaviour of the moraine is described in detail by Kälin (1971) and Moisan and Pollard (1995), yet both concentrate on the processes within the push structure rather than on the behaviour of the glacier.

Recent length changes of Thompson Glacier are compiled in Cogley et al. (2011). The glacier had been advancing since the time of the earliest photographs in 1948 up until around 2008, when measurements of its terminus showed that it has begun a slow retreat (Figure 3a). Over that period, the glacier gained about 950 m in length. Observations between 1960 and 1977 reveal that the glacier was advancing 18 m per year on average (Figure 3b), which is especially interesting as the neighbouring White Glacier shows a persistent retreat in the same timeframe.
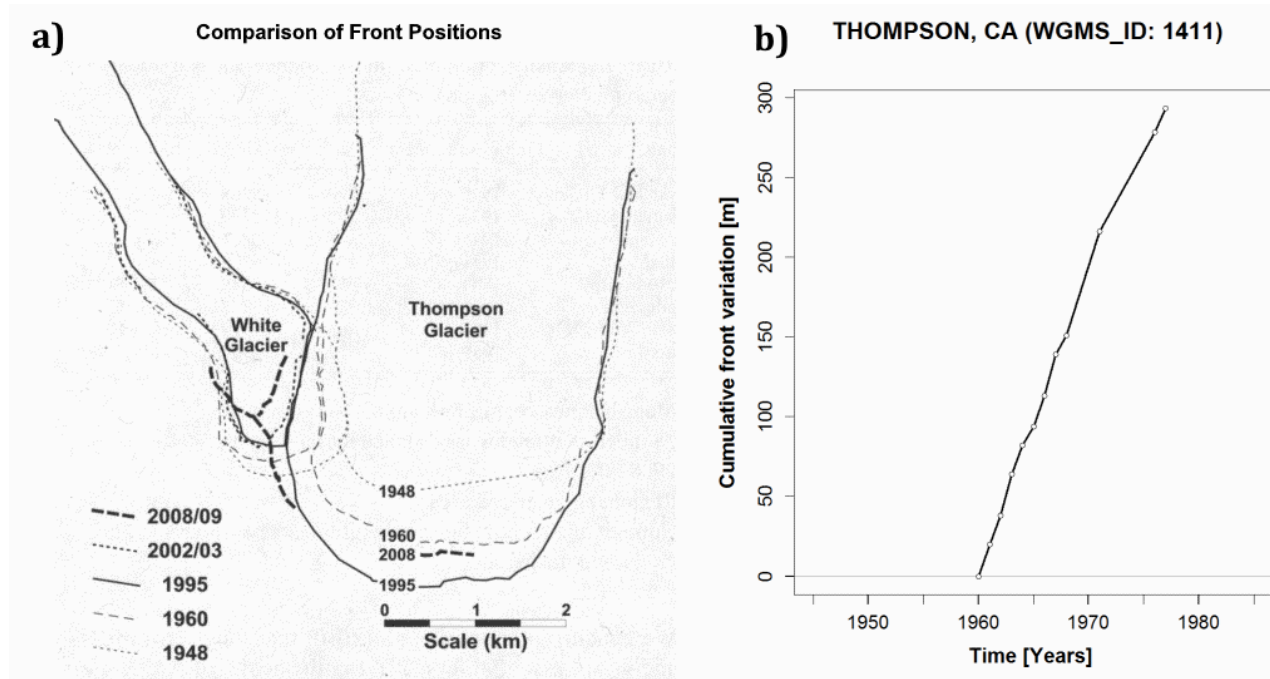
Figure 3: a) Comparison of glacier front positions of White Glacier and Thompson Glacier showing the retreat of Thompson Glacier from 1995 to 2008 (adapted from Cogley et al. (2011:373). b) Cumulative front variation from 11 observations between 1960 and 1977 showing an advance of 18 m per year during that period (WGMS FoG database, 2018).

There are different interpretations for this contrasting behaviour: Cogley and Adams (2000) refer to the large size of Thompson Glacier which would explain a longer response time. In this case, the continuous advance is the response to the cooling during the early 19th century, while the smaller White Glacier is already reacting to more recent warming. Alternatively, the sinuous medial moraines of Thompson Glacier suggest a slow surge behaviour (Copland, Sharp and Dowdeswell, 2003). This implies a cyclical, non-steady flow with an active phase during which the ice flow velocity increases, causing the glacier to advance. However, there are no in-situ measurements which confirm such a behaviour (Cogley, Adams and Ecclestone, 2011).
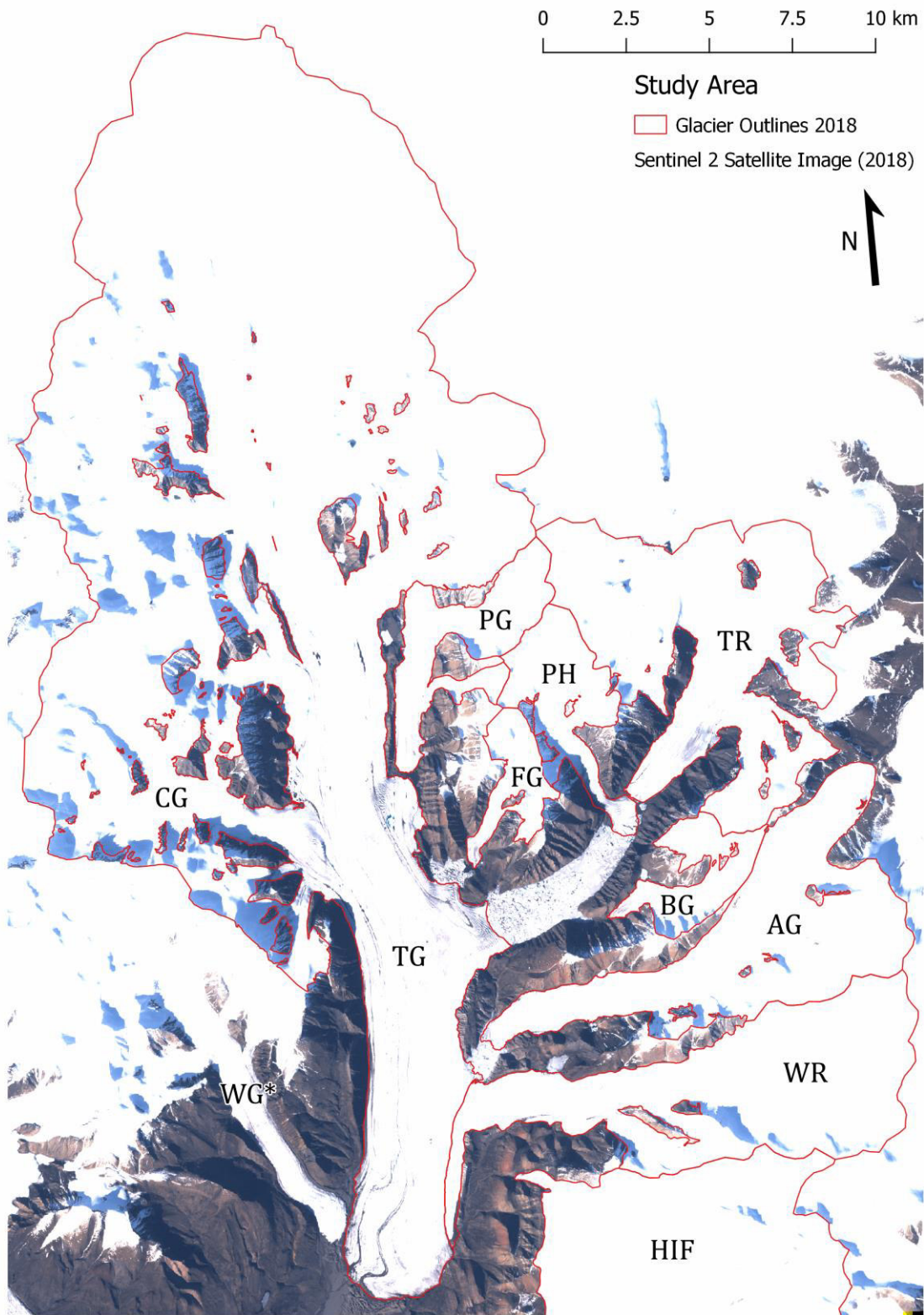
Figure 4: Study Area on Axel Heiberg Island with superimposed glacier outlines from 2018. TG = Thompson Glacier. The abbreviations of surrounding glaciers are explained in Table 1, page 7. WG*) White Glacier, to the southeast of Thompson Glacier is used for reference data. Sentinel 2 image based on Copernicus data (2018).

2.2 Surrounding Glaciers

The historical map of the Thompson Glacier Region features a number of smaller glaciers, which can be included into the assessment of geodetic mass balances within this study. This offers a more comprehensive understanding of changes in the area as the neighbouring glaciers have other characteristics and differ in size, slope and aspect. Therefore, reactions to climatic changes are not only assessable for the larger Thompson Glacier, but on a smaller scale, including the facets of the local topography. The observed surrounding glaciers are all situated to the east of Thompson Glacier. Neighbouring glaciers to the west are direct tributaries and thus included in the assessment of Thompson Glacier. The glaciers observed in this study are compiled in Table 1 below.

Table 1: Overview on the glaciers surrounding Thompson Glacier that are included in this thesis. Areas from glacier outlines are derived from the Sentinel 2 image of August 2018 and optimized by drainage divides as explained in Chapter 5.4.

Abbr.	Name	Area in 2018 [km²]
AG	Astro Glacier	38.35
BG	Bellevue Glacier	7.74
CG	Crook Glacier[1]	-
FG	Finger Glacier	5.69
HIF	Hidden Ice Field	72.88
PG	Parallel Glacier	12.14
PH	Phantom Glacier	12.06
TR	Transit Glacier	49.81
WR	Wreck Glacier[1]	-
TG	Thompson Glacier	372.11

The neighbours of Thompson Glacier in clockwise orientation are: Parallel Glacier, which originates from the more mountainous southern part of MIC. It is separated from Thompson Glacier only by a thin ridge. Finger Glacier and Phantom Glacier are two steep mountain glaciers located to both sides of Phantom Peak. Both terminate in glacial lakes dammed by Thompson Glacier, namely Five Finger Lake in the case of Finger Glacier and the prominent Phantom Lake for the latter. The large Phantom Lake is also the terminus for the larger Transit Glacier, which flows down from an outlier of MIC and incorporates its own tributary glaciers from the mountains to its side. Next, Bellevue Glacier is a small valley glacier situated between a mountain ridge of the same name and the cliffs to the side of Phantom Lake. Astro Glacier is a moderately sized valley glacier which terminates and calves into Astro Lake, which is dammed by the confluence of Thompson Glacier and its tributary Wreck Glacier. Lastly, the Hidden Ice Field is located to the south of Wreck Glacier covering the plateau around Snow Dome, one of the higher peaks in the area.

---

[1] Crook Glacier and Wreck Glacier are direct tributaries to Thompson Glacier and will therefore be directly included into the analysis of Thompson Glacier without presenting individual values. Nonetheless, trends in elevation change on the two tributaries will be described.

Figure 5: a) Parallel Glacier, separated from Thompson Glacier by the aptly named Separation Ridge.
b) Thompson Glacier calving into the western end of Phantom Lake, the smaller Finger Glacier is visible in the upper right
corner of the image.
c) The termini of Phantom Glacier (left) and Transit Glacier (right). The front part of Phantom Glacier is floating on
Phantom Lake.
d) View along Phantom Lake with Transit Glacier's tongue in the background. Bellevue Glacier is portrayed to the right.
e) Astro Glacier calving into Astro Lake. The colour difference along the lake's shore indicates the lowering of the lake's
surface over time.
f) View of Hidden Ice Field with its highest point, Snow Dome, to the upper left.

All photos are aerial images taken in July 2008, except for a) which dates back to 1977.
All photos from Glaciers Online (Alean, 2008).

3. Scientific Context

3.1 Worldwide Glacier Monitoring

For more than sixty years, glacier-wide mass balance measurements have been used to assess glacier contribution to regional runoff and sea level rise. Monitoring the changes in the mass of glaciers provides valuable information on climatic changes and how water resources transform (Zemp *et al.*, 2013). Presently, the dataset of the World Glacier Monitoring Service (WGMS) includes glaciological samples of 450 glaciers, and 19'130 glaciers are studied with geodetic samples. This corresponds to 1% of all glaciers for glaciological studies, and 9% of the total concerning the geodetic sample size, respectively. There are however large differences in the observational coverage. In some regions the geodetic sample covers 79% of the glaciated area while others have less than 1% of their area monitored (Zemp *et al.*, 2019).

These regional differences are rendered visible by comparing the geodetic sample coverage of the first-order regions from the Randolph Glacier Inventory (RGI), see Figure 6. In Alaska, 47% of a total of 84'725 km² of glaciated area have been observed. Yet equally glacierized regions, such as the Greenland Periphery (12% of 89'717 km²) or Arctic Canada North (9% of 105'111 km²) have strikingly lower coverage rates (Zemp *et al.*, 2019).
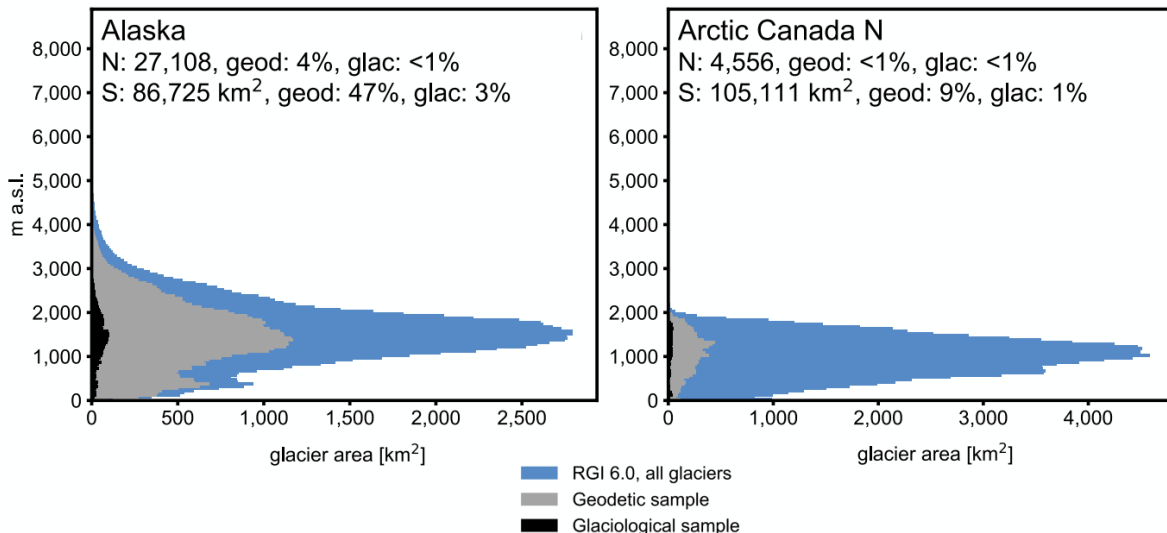
Figure 6: Regional glacier hypsometry with colour-coded observational coverage, figure by Zemp et al. (2019: 390). N: Total number of glaciers in the region. S: Total area of glaciers in the region. Percentages of geodetic and glaciological samples are presented for each N and S.

This is especially important because record mass losses are found in these areas. Sample coverage is already incomplete in Alaska, where the most extreme rates (-73 Gt yr^{-1}) can be found. But the equally large losses in the Canadian Arctic (-60 Gt yr^{-1}) and the Greenland periphery (-51 Gt yr^{-1}) are severely lacking observation (Zemp *et al.*, 2019). The absence of data in areas where mass losses are greatest shows the need to assess the changes of individual polar glaciers (Meredith *et al.*, 2019).

3.2 Ice-loss in the Canadian Arctic Archipelago

Long-term records of individual glaciers' surface mass budget exist in the CAA. The WGMS lists four reference glaciers in the region, which are glaciers with ongoing glaciological mass-balance measurements of at least thirty years (WGMS, 2019). These include two smaller ice caps (Melville and Meighen), the outlet basin of the larger Devon Ice Cap and the mountain glacier White Glacier on AHI. Additionally, there are other, less complete mass balance records available in the area. These include, for example, measurements on Baby Glacier, a small remnant glacier west of Thompson Glacier, which began in the same year as White Glacier but were interrupted in the 1980s.

In more detail, the trends of the better observed glaciers on AHI read as follows: The mass balance record of White Glacier shows a clear negative trend since the initial measurements. The geodetic mass balance over the last 54 years amounts to –9.61±0.87 m w.e., accompanied by a persistent retreat of the glacier (Thomson *et al.*, 2017). Due to its smaller size, Baby Glacier has a much shorter response time to climatic changes resulting in much more variable annual mass balances. Yet, observed over a longer time period, the small glacier also exhibits a clear negative trend (Cogley, Adams and Ecclestone, 2011).

Contrary to the mass balance trend in the entire CAA, the island wide coverage of glaciated area on AHI remained relatively stable between 1958 and 2000, with a loss of ice-covered surfaces of less than 1%. However, the details compiled in the paper by Thomson et al. (2011) show that there are opposing trends present on the island. Outlet glaciers from the island's larger ice caps exhibit minor retreats, while independent ice masses, such as valley glaciers, mountain glaciers and smaller ice caps (< 25 km^2), show significant retreat, indicating more stable accumulation conditions on the island's larger ice caps. Most of the observed glaciers behave according to the High Arctic climate regime, with a relatively low mass turnover where little accumulation and little ablation balance each other. In general, these glaciers are less sensitive to changes in precipitation and temperature than glaciers in more maritime climate regimes, where rates for both accumulation and ablation are higher (Zemp *et al.*, 2015).

However, the available glacier sample is too small to extrapolate the findings the entire region without introducing large uncertainties. Thus, existing estimates for the change in ice mass for the whole area are often based on larger scale approaches, such as airborne laser altimetry. Gardner et al. (2011) showed that, regardless of the approach, losses in ice mass have sharply increased over a relatively short time: Starting at an estimated average loss of -23 Gt per year between 1995 and 2005, it increased to an average of -31±8 Gt per year between 2004 and 2006 and even further to an average of -92±12 Gt per year between 2007 and 2009. Cumulated over the last decades, the northern part of CAA alone exhibits a change in ice mass of -1069 Gt from 1961 to 2016, equalling a global sea level rise of roughly 3 mm (Zemp et al. 2019).

4. Data

4.1 Historical Maps

4.1.1 Thompson Glacier Region (TGR)

The Thompson Glacier Region map in the scale of 1:50'000 covers the tongue of Thompson Glacier in high detail. It entails an area of roughly 1000 km², spanning from the Expedition Fiord in the southwestern corner to Hidden Ice Field in the southeast, to Eureka Pass in the northeast and the accumulation area of Crusoe Glacier in the northwest. The map is based on aerial images from 1959 and field observations made during summer 1960 (Haumann and Honegger, 1962). Regarding this thesis, note that the map does not entail the glacier's accumulation area on Müller Ice Cap.
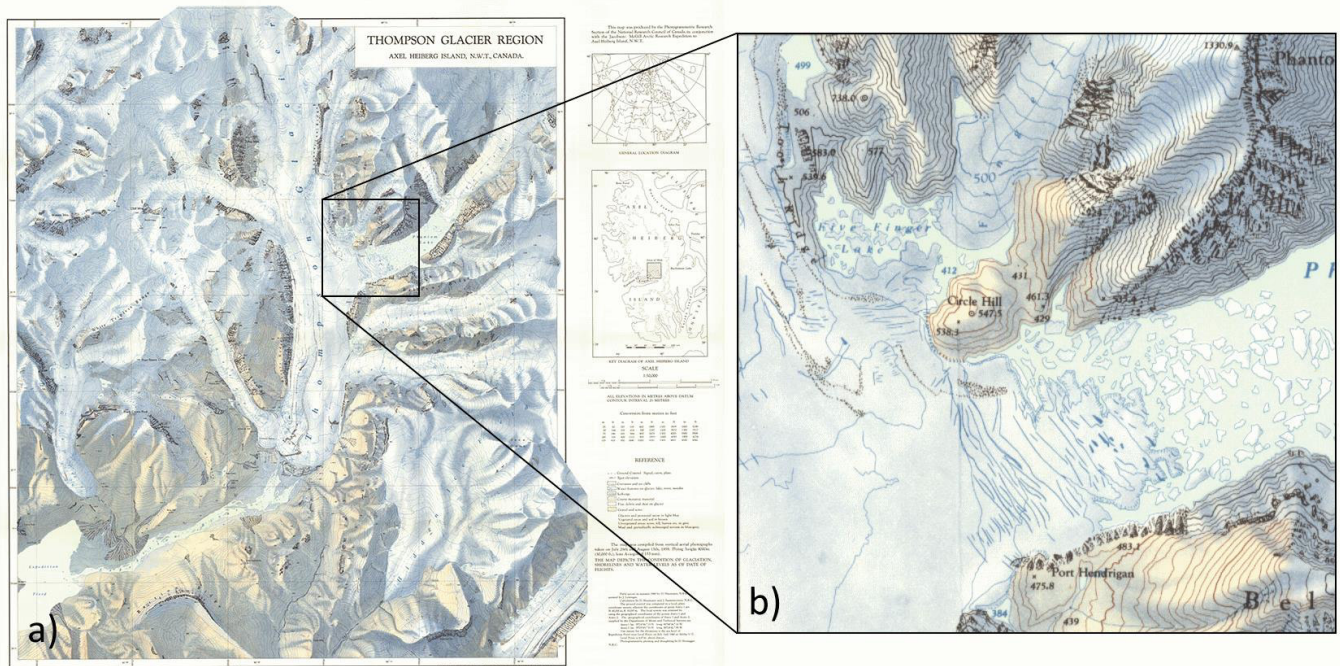
Figure 7: a) Thompson Glacier Region Map (TGR) in 1:50'000 (National Research Council, 1962). It is mapped from aerial photogrammetry in 1959 and ground surveys in 1960. b) Detailing on the map showing crevasses and ice cliffs on the glacier, icebergs on glacial lakes and steep cliffs in the ice-free terrain next to the glacier.

The TGR map is orientated along its own local planar coordinate system. It is defined by a baseline which is constructed using the coordinates of two survey points: Astro. However, the exact method of how the local planar coordinate system was constructed is missing. It is assumed that a transverse Mercator projection on a Clarke 1866 ellipsoid was used (Cogley and Jung-Rothenhäusler, 2002). The vertical datum of the map is defined by a sea level measurement at the shore of Expedition Fiord in the lower left corner of the map. This so-called Level Point was used as the first reference benchmark for elevation measurements.

4. Data

A peculiarity of the TGR map is that it was produced with glaciological research in mind (Blachut and Müller, 1966). Thus, the map is extremely detailed on glaciated terrain, depicting features such as crevasses, supraglacial streams, faults, cracks, ice cliffs and many more (Figure 7b). The map is available in two versions: one with relief shading and one without. This thesis relies on the unshaded variant, as contour lines are better visible and the cleaning of unwanted map features is easier.

The contour lines on the map are drawn in an equidistance of 25 m with colour-coding according to the underlying terrain:

- Blue: Glaciated areas and perennial snow cover
- Brown: Vegetated areas and soil
- Grey: Unvegetated areas, barren terrain
- Blue-Grey: Mud and periodically submerged terrain

4.1.3 Expedition Area (EXA)

The Expedition Area map in the scale of 1:100'000 covers an area of approximately 2500 km² of western Axel Heiberg Island. It is again centered on Thompson Glacier but expands further north to the Müller Ice Cap (Figure 8a). While not being as detailed as the TGR map, it provides a useful overview on the larger context of the area featuring a number of on-glacier survey points (e.g. Upper Ice Station I and II) and prominent mountain peaks (Figure 8b). An inset in the upper right corner of the map shows the area around White Crown Mountain, the highest peak on Axel Heiberg Island (Müller and Harrison, 1965).
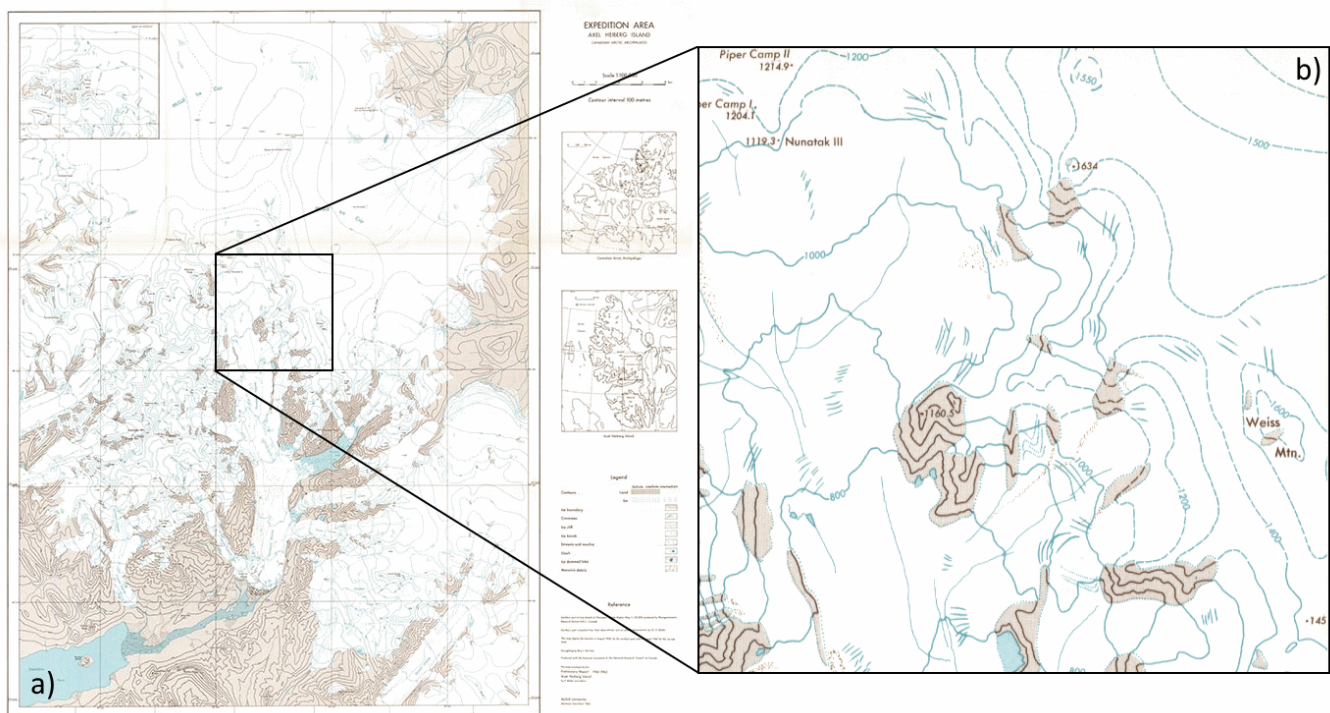
Figure 8: a) Expedition Area Map (EXA) in 1:100'000 by Müller & Harrison (1965) compiled from field observations and aerial images from 1960 as well as the Thompson Glacier Region Map in overlapping areas.
b) Detailing on the map includes nunataks in brown, survey locations with elevation data and glacial lakes. Note the difference in contour lines between definite lines (left part of the image) and indefinite dashed lines (right part of the image).

The map features contour lines with an equidistance of 100 m, classified into definite and indefinite accuracy. The latter predominate on Müller Ice Cap which results in an uncertainty regarding the accumulation area of Thompson Glacier. While the southern portion of the map is based largely on the TGR map, the Northern part of is mostly compiled from aerial images, with only few ground-survey points. This limits the accuracy of the map, especially since elevation information for Müller Ice Cap is derived from relatively few flight lines (Figure 9). The report on the aerial survey further mentions poor illumination due to the low angle of the sun, which needs to be considered regarding the quality of the EXA map (Haumann, 1963).
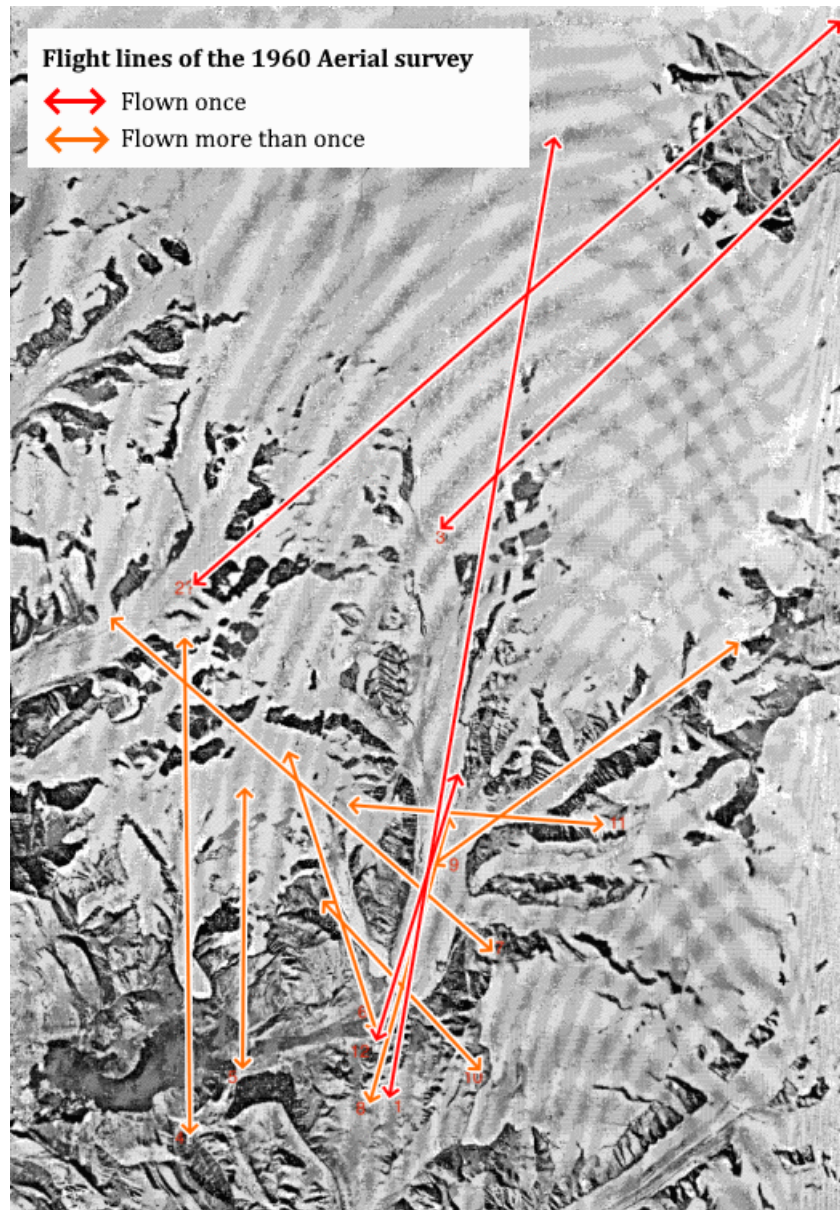
Figure 9: Flight lines from the 1960 aerial photography flight program. The higher density of flight lines in the lower half covers the extent of the TGR map. Note the lower coverage of flight lines over Müller Ice Cap in the upper half of the image. Original image from Haumann (1963: 87).

4.2 Digital Elevation Models

4.2.1 TanDEM-X

The TanDEM-X digital elevation model is one of two high resolution datasets available in the study area. It is a RADAR image which is composed of elevation data from a timeframe ranging from December 2010 to February 2014 (2012±2). The DEM has a spatial resolution of 0.4 to 1.2 arcsec, which translates to a cell size of 5.9 to 17.7 m. It covers the accumulation area and the tongue of Thompson Glacier, as well as the smaller glaciers in the eastern part of the study area. As a RADAR product, the TanDEM-X image is unaffected by atmospheric conditions, thus presenting an elevation dataset without any data voids.
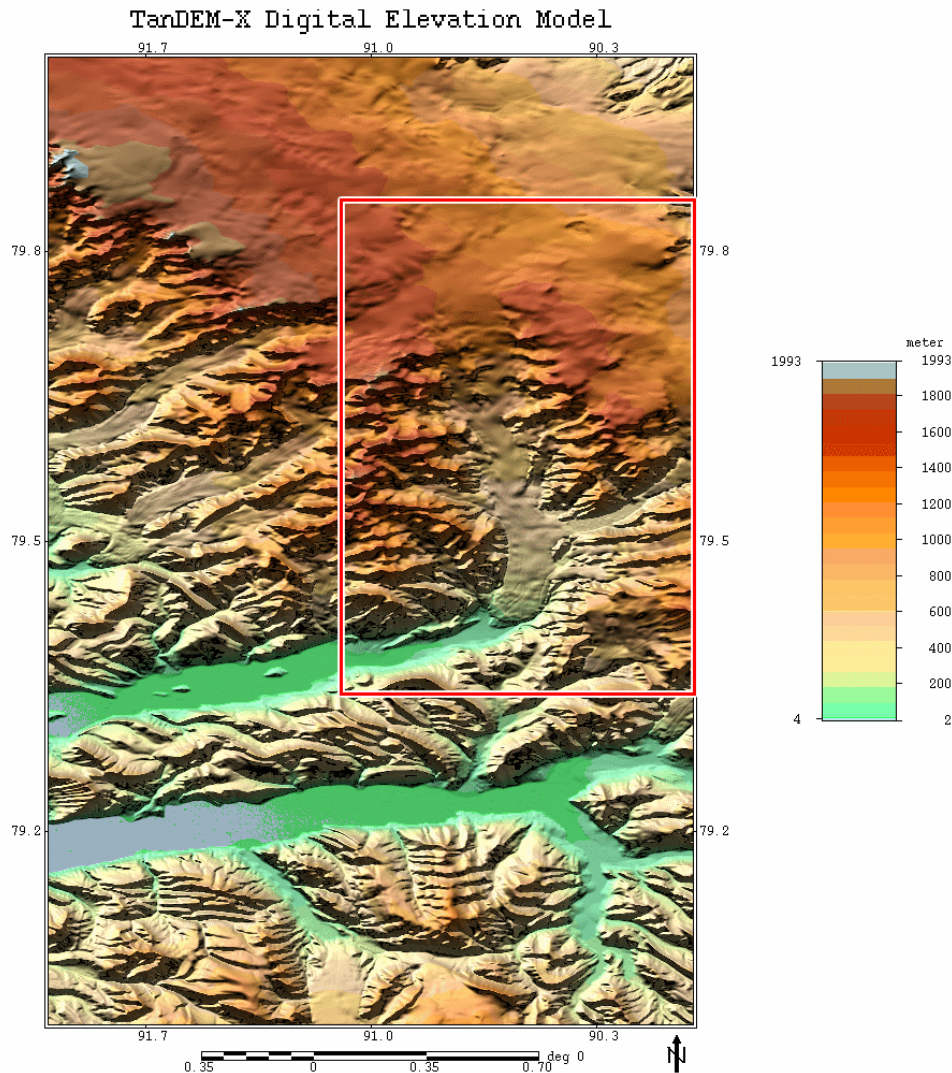
Figure 10: Expedition Fiord Area as visible on the TanDEM-X Digital Elevation Model, study area highlighted in red. Note that the accumulation areas of the eastern glaciers are cut off. TanDEM-X image by DLR, 2017.

The elevation data over the entirety of the study area has almost no detected height error, with the exception of steeper cliffs, where a height error of up to 5 m is given in the metadata. The product is cleaned from RADAR shadows and layover effects, rendering each data pixel valid (DLR, 2017).

The only important constraint is that the accumulation areas of the glaciers to the east, including the tributary Wreck Glacier, are situated outside of the perimeter of the dataset. Thus, the TanDEM-X cannot be used to derive glacier-wide values for the entirety of Thompson Glacier. However, it is a useful resource to compare the results derived from ArcticDEM data.

4.2.2 ArcticDEM

In addition, the ArcticDEM mosaic with a 2 m resolution is used throughout this thesis. This DEM is based on optical photogrammetry and is composed of aerial images that were taken over a timespan from 2012 to 2017 (2014±2.5). Unlike TanDEM-X, the ArcticDEM dataset is constrained by atmospheric conditions which can cause data voids and elevation errors in the elevation model. The advantage of this DEM is that it covers the entire study area.
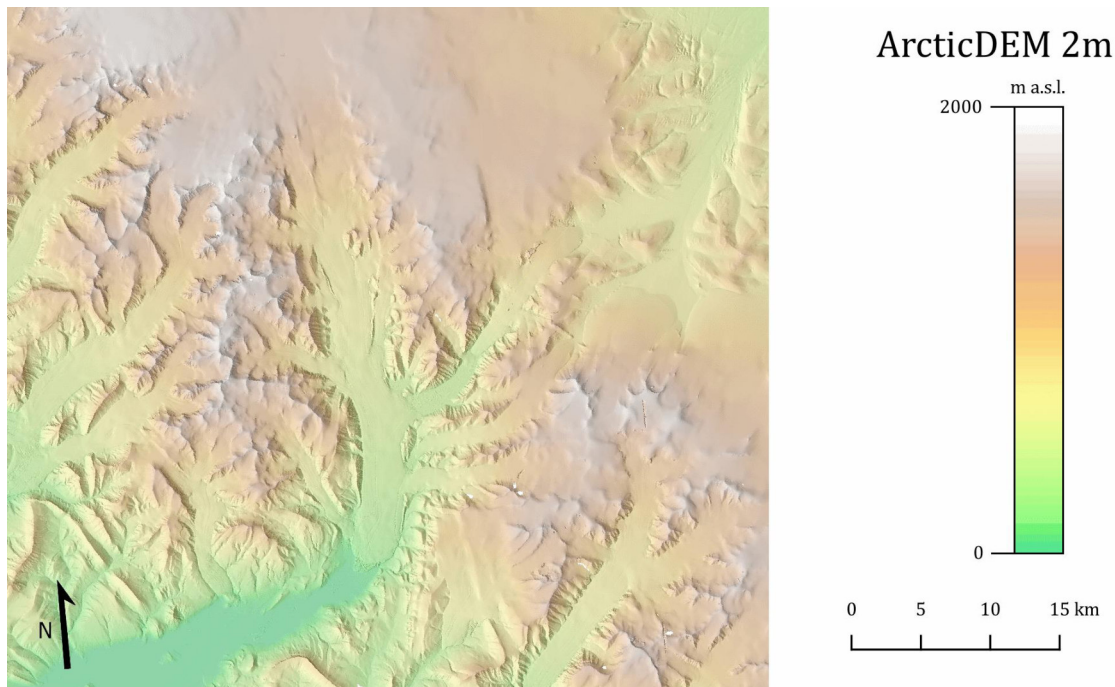
Figure 11: Hillshade of the ArcticDEM Digital Elevation Model in 2m resolution, centred on Thompson Glacier. Image rendered in QGIS, data from ArcticDEM, 2018.

The elevation data within the study area is relatively consistent with few data voids or artefacts. Data voids with no elevation information are in general small in size (Figure 12a). Since glacier-wide values are to be calculated, the impact of such data voids can be neglected. Data artefacts with wrong elevation information are also rare. Larger examples can be found in the accumulation area of Transit Glacier or on Strand Glacier (Figure 12b). Same as the data voids, these artefacts are not excluded within the calculations, as their impact is assumed to be small.
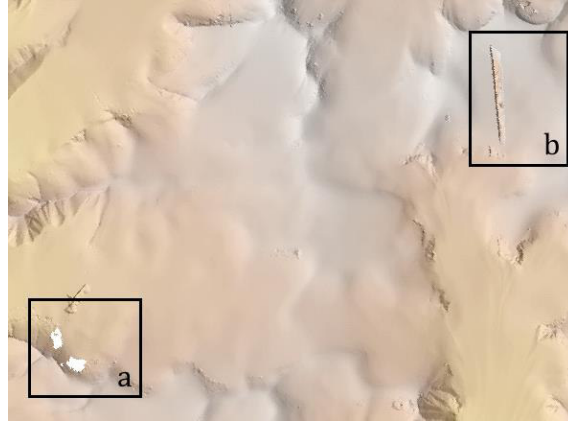
Figure 12: Faults in the ArcticDEM dataset: a) Data void with lack of elevation information. b) Data artefact with wrong elevation information. As both are small in size, they are not omitted from glacier-wide calculations. Image rendered in QGIS, data from ArcitcDEM, 2018.

4.3 Glacier Outlines

The glacier outlines from the historical maps are digitized manually. Glacier outlines on the TGR map are traceable with relatively high detail thanks to the colour coding of the contour lines (see Chapter 4.1.1). The EXA map was used to add nunataks situated outside the perimeter of the TGR map. For contemporary glacier outlines the use of the GLIMS dataset was first considered as an option, as they are readily available and applicable in glaciological studies (Paul *et al.*, 2015). However, all GLIMS outlines in the study area date from 1999, thus being significantly older than the DEMs used in this thesis. Additionally, the glacier drainage divides are indefinite and offer only a rough division of the glacier's in the region (Figure 13). Therefore, a new polygon dataset was created using a Sentinel 2 Image as the basis for glacier outlines. The process of deriving the new outlines is presented in Chapter 5.3.

Figure 13: Comparison of GLIMS and newly derived glacier outlines. Note the more detailed drained divide outlines in blue compared to the indefinite division in the GLIMS dataset in orange.

5. Methods

5.1 Workflow
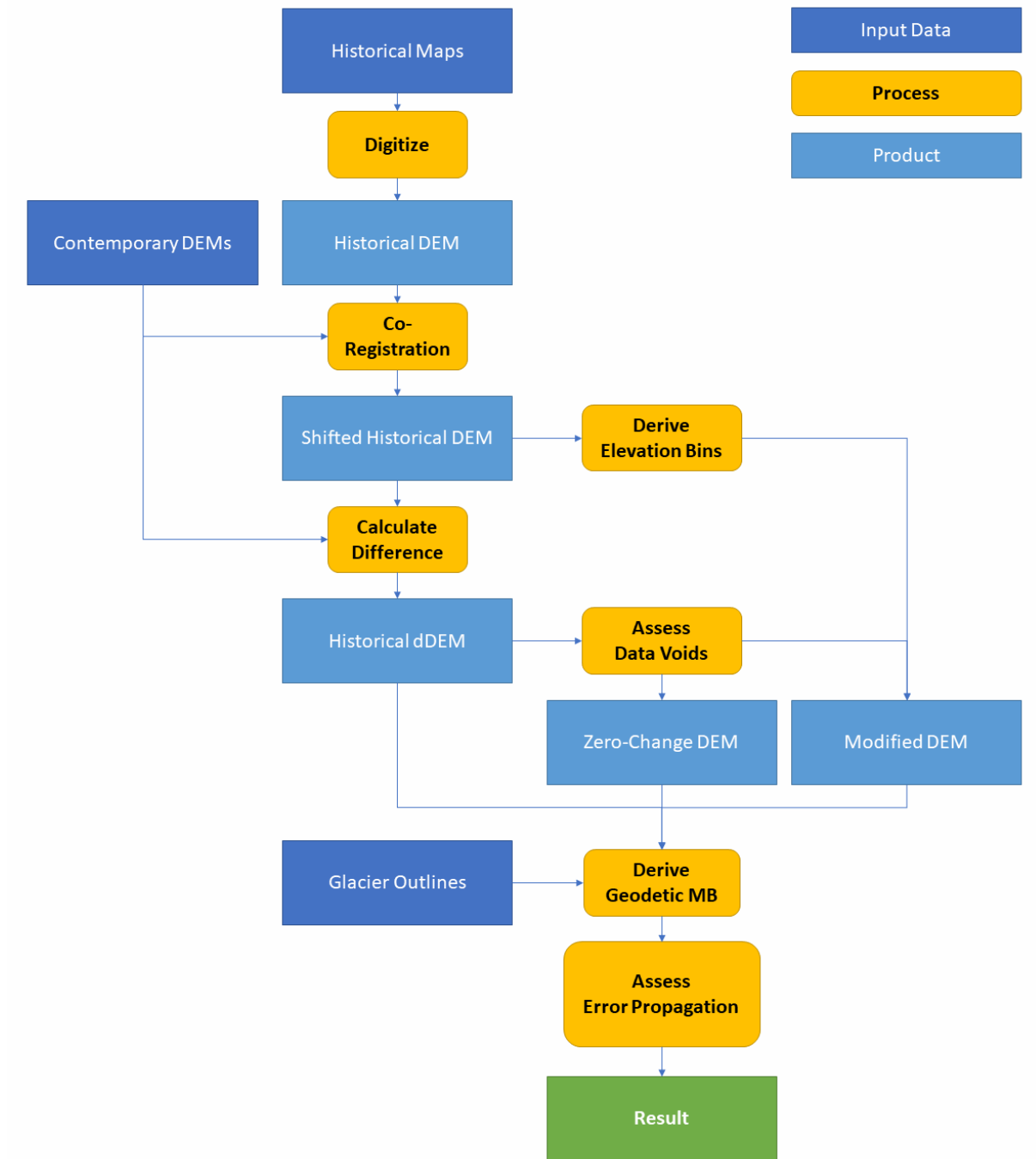
Figure 14: Simplified overview of the workflow from the historical maps to the mass balance results presented in this thesis. Each process is explained in detail in the following subchapters.

5.2 Digitizing the Historical Maps

5.2.1 Preparing the maps

The process of deriving a digital elevation model from the historical maps is based on the map versions without relief shading, as their contour line information is better visible. Nonetheless, certain measures to clean up the map for better readability are necessary (Figure 15). These include the removal of the following features: Surface water streams, as they are in the same colour as elevation information in glaciated areas and are therefore hard to tell apart. Crevasses which intersect contour lines, medial moraines, ice cliffs or outcrops within glaciated areas. And lastly, cartographic details and labels which conceal elevation information. Furthermore, the contrast of the map is enhanced, so that line features stand out more. The removal and adjustment of features is achieved through manual editing of the map using the image editing software Paint.net.
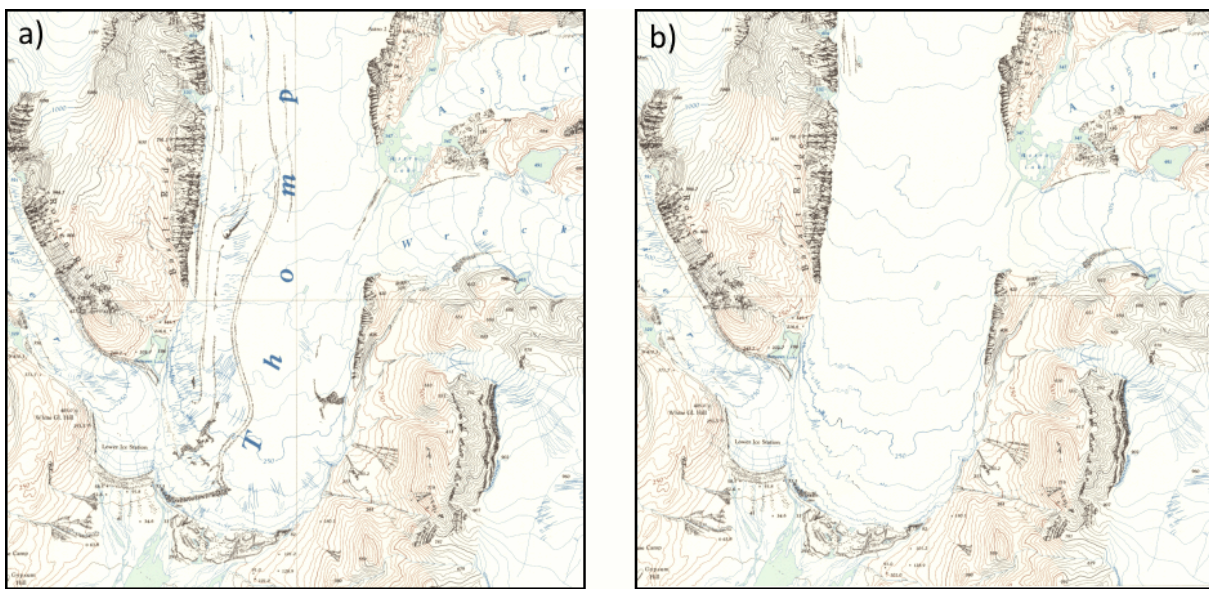
Figure 15: a) TGR Map before the clean-up. b) Map after cleaning unwanted features. On glacier surfaces only contour lines are kept, all other features are removed.

5.2.2 Georeferencing the maps

The first step in the process of deriving a digital elevation model from historical maps is to define the correct georeference. In this case, said process relies mostly on the survey points Astro 1 and Astro 2. These were used to orient the local coordinate system applied in the maps. In the Cogley and Jung-Rohtenhäusler study (2002), they assume that maps are based on the Clarke 1866 ellipsoid, which is part of the North American Datum 1927 (NAD27). The metadata on the historical maps includes the geographical coordinates in longitude and latitude of both survey points. Thus, it is possible to georeference the maps by using the Astro points as pass points for the process. The conversion of the maps into NAD27 is implemented using the georeference tool in QGIS. In this case, the use of only two pass points is sufficiently accurate, as the derived DEM needs to be fitted to the satellite DEMs in the co-registration process.

5.2.3 Vectorising Contour Lines

The vectorising of contour lines is implemented semi-automatically through ArcScan, a toolset within ArcMap 10.6. This process relies on a binary image, so the map image is classified into either colour or transparent pixels. This is achieved by selecting only one colour band of the map image which renders a greyscale image with values ranging from 0 to 255. Using only one band, the unique value of each pixel can be computed. These can then be classified into values representing contour line information and unrequired values which will be set transparent. The better the map is prepared regarding the contrast between contour lines and background, the easier is the classification. Ideally, the map background only consists of the highest value (255), while all other values can be grouped as contour line information. The tool then follows the centre line of the contour pixels to derive a vector line from the input image.

The process is highly dependent on the readability of the contour lines on the historical maps. Where contour line information is thorough, the elevation data from the maps is accurately represented. This applies to the majority of the Thompson Glacier's main tongue and flat ice-free terrain. In steeper terrain, the ArcScan Toolset tends to create coalescing contour lines (Figure 16), as the original contour lines are too close to each other. This issue can be resolved by manually correcting the contour data (Figure 17). Here, contour lines that cover glaciated terrain were addressed primarily. On ice-free terrain, the manual correction was only applied to areas which were used in the stable terrain mask.
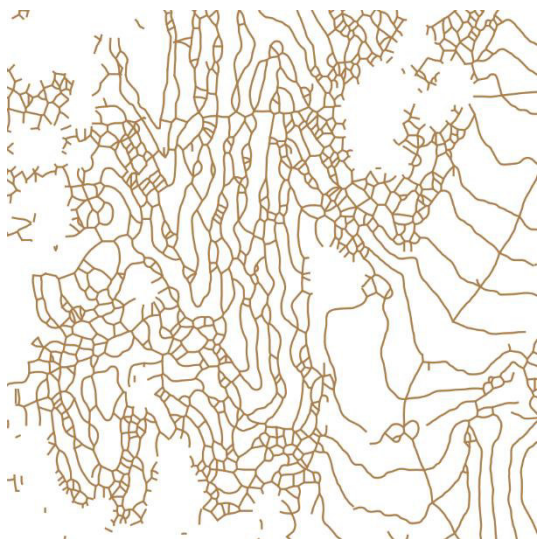
Figure 16: Vectorized contour lines produced by the ArcScan Toolset in ArcMap 10.6.
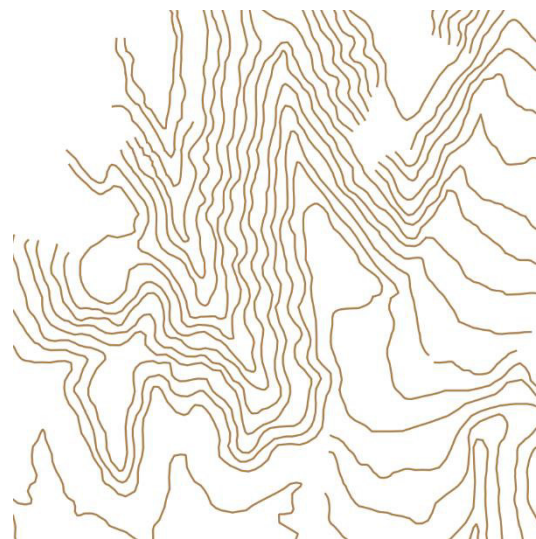
Figure 17: Manually corrected contour lines produced by deleting unwanted lines and redrawing coalescing parts.

Lastly, the contour lines need to be attributed manually with their respective elevation to be able to interpolate the elevation data. In areas consisting mostly of steeper slopes, no contours were digitized due to insufficient readability. There, the DEM values are derived entirely through the interpolation algorithm.

5.3 Deriving the Digital Elevation Model

Next, the contour lines are used to interpolate the DEM describing the historical maps. The derivation of a surface raster from line data can be achieved through various types of interpolation such as Inverse Distance Weighted (IDW), Kriging or following a trend line (Pellitero *et al.*, 2016). In this thesis, the ArcMap Tool "Topo to raster" is applied. The tool interpolates a surface by calculating grids at progressively finer scales. This creates a smooth, continuous surface by passing through all the input data. An additional benefit is that it works even for sparse and irregularly spread input data (Hutchinson, 1989). The main drawback of this approach is that it results in a hydrologically correct surface which is not an ideal match for a glacial surface (Pellitero *et al.*, 2016). But, although it may produce unrealistic concavities, the interpolation method is a good fit for this study as it preserves the input data accurately.

The setup for this thesis includes Contour Lines, distinct Elevation Points (such as mountain tops) and Lakes as input data. The standard of a maximum of 20 iterations is applied, as suggested by Hutchinson et al. (2011). The resulting spatial resolution is set to 4 m, which is at par with the TanDEM-X elevation data and allows a comparison to ArcticDEM (2 m resolution). As mentioned above, hydrological correctness does not describe glacial surfaces well, which is why drainage enforcement in the tool was turned off. This allows the preservation of terrain sinks, such as the smaller glacial lakes to the side of Thompson Glacier. The resulting DEM is referred to as the 'historical DEM' throughout this thesis.

5.4 Co-Registration

To be able to compare the historical DEM to the contemporary elevation models, it needs to be checked for shifts in x-, y- and z-direction. This process is crucial to assessing a potential systematic error in the comparison of elevation data, as even small horizontal shifts can cause a large bias in elevation change estimates (Paul *et al.*, 2015). For that purpose, the contemporary DEMs are used as the main reference (referred to as Master DEM) to which the historical DEM (termed Slave DEM) is fitted. As changes over time are to be expected within glaciated areas, only areas regarded as stable terrain are taken into consideration. This thesis relies on the universal Co-Registration correction approach by Nuth & Kääb (2011), which is a prevalent method regarding DEM differencing (e.g. Gardelle *et al.*, 2013; Zemp *et al.*, 2015).

The approach allows to check the changes over the assumed stable terrain for three potential biases:

1. The location of the data in x-, y- and z-direction
2. The elevation dependent bias
3. Biases related to the acquisition geometry of the data

Here, only the first bias is assessed and corrected, as the other would go beyond the scope of this thesis. The shift vectors in x and y direction can be calculated using the equations below.

Equation 1

$$\frac{dh}{\tan(\alpha)} = a * \cos(b - \Psi) + c$$

where

Equation 2

$$c = \frac{\overline{dh}}{\tan(\overline{\alpha})}$$

The formula is composed of the following parameters: dh, which is the difference in elevation between the master and the slave DEM. α, the slope angle of the master DEM. Ψ, the aspect of the master DEM. a and b are variables describing the magnitude and the direction of the horizontal shift vector. The variable c describes the vertical bias over stable terrain between both DEMs. The offset between two DEMs can be described as a relationship between the elevation differences and the aspect of the terrain ($dh/tan(\alpha)$). Thus, the parameters a, b and c can be calculated using a sinusoidal curve fit, as shown in Figure 18.
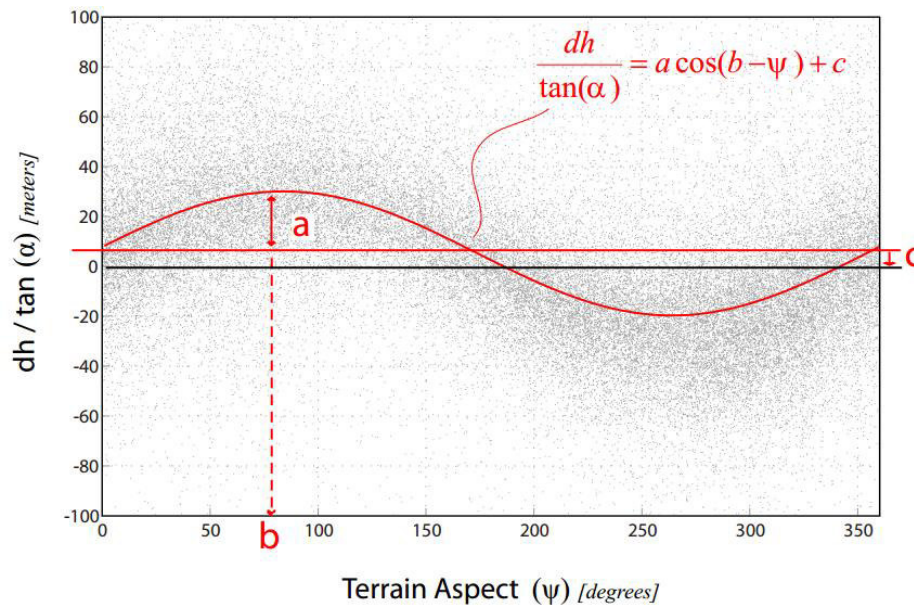
Figure 18: Sinusoidal curve fit achieved through Co-Registration. This results in the three parameters necessary to resolve the shift between two DEMs. The point cloud represents each pixel within the designated stable terrain. Figure by Nuth & Kääb (2011:275).

5. Methods

From the resulting curve, the shift vectors for *Δx*, *Δy* and *Δz* can be derived as follows:

Equation 3

$$\Delta x = a * \sin(b)$$

Equation 4

$$\Delta y = a * \cos(b)$$

Equation 5

$$\Delta z = \frac{c}{\tan(\bar{a})}$$

The resulting values are applied to the slave DEM to correct the misalignment. Ideally, this reduces the mean value and standard deviation of elevation differences over stable terrain. The Co-Registration process is applied iteratively until there is no significant improvement of the standard deviation or the magnitude of the shift vector. Nuth & Kääb (2011) suggest stopping the iteration if the change in standard deviation is less than 2%, or, if the resulting shift vector is less than 0.5 m.

5.4.1 Masking Stable Terrain

The mask of stable terrain used for the Co-Registration process is determined through the following steps: First, the historical maps offer a graphic distinction of glaciated and ice-free areas. On the TGR map, the colour-coding of contour lines helps to delimit glacierized areas from terrain with no ice cover. Similarly, nunataks are clearly distinguishable from glacier ice. On the EXA map, ice-covered and ice-free areas are classified by colour. Using this information, a polygon dataset containing all ice-free areas on the historical maps was created in ArcMap.

As the historical DEM is based on interpolated data, the ice-free terrain is further narrowed down to terrain with highly detailed elevation information. Only areas which are completely described with contour lines are included. That way, steep cliffs and ragged mountain tops are eliminated from the stable terrain mask, as they lack specific elevation information due to their graphical representation. These constraints result in a relatively small area with stable terrain (12.6 km²) compared to the total of masked ice-free terrain (135.2 km²) (Figure 19). The optimal stable terrain is chosen based on contour line accuracy and taking each major terrain aspect into consideration.
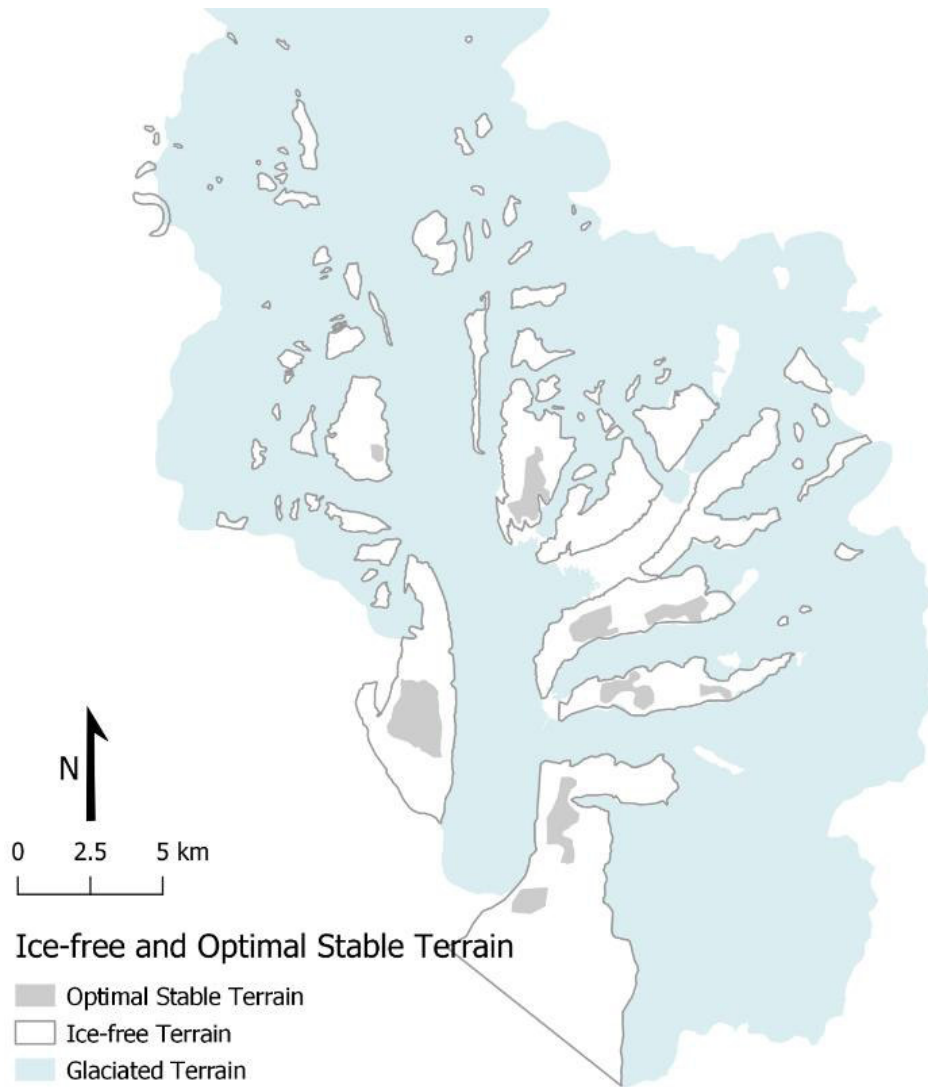
Figure 19: Overview on ice-free and glaciated terrain. Only the optimal stable terrain (in filled grey) measures up to the requirements of the Co-Registration process.

As the optimal stable terrain used for Co-Registration is rather small compared to the size of the glaciated terrain, the use of the entirety of the ice-free terrain as stable terrain input was tested additionally. Results were however unsatisfactory, as high standard deviation in the elevation difference of ice-free terrain caused inconsistent shift vectors with each iteration. Thus, this thesis relies on a qualitative approach to stable terrain rather than quantitative.

5.4.2 Co-Registration Workflow

The steps to extract the used information from the stable terrain were implemented in ArcMap following a tutorial compiled by Philip Rastner. The calculations of the shift vector are based on an Excel-Tool provided by Chris Nuth.

First, the elevation difference between the Master and Slave DEM is calculated. The resulting raster image is converted into a point dataset. Then, the slope (α) and aspect (Ψ) values from the Master DEM are assigned to each point. In case of the ArcticDEM dataset, the point cloud was resampled to a coarser resolution Here, the data within the stable terrain is further constrained by eliminating values from slopes which are outside of slope range from 5° to 30° (Thomson *et al.*, 2017). The values for *dh*, α and Ψ are then exported to the Excel-Tool. Using the Solver function, a sinusoidal curve is fitted to the scatter plot, which calculates the values for Δx, Δy and Δz. The latter are then applied to the Slave DEM.

Following Paul *et al.* (2017), the horizontal offset needs to be applied in any case, but the vertical offset needs to be checked carefully, to decide if it is to be applied to the difference DEM. This is particularly important for the comparison of DEMs from different sources or different spatial resolutions. It is likely that the elevation differences have a non-constant shift and thus cannot be corrected using the mean value resulting from the co-registration process (Racoviteanu *et al.*, 2007). As mentioned above, co-registration is implemented iteratively until the resulting shift is no longer improving. In this thesis, the iteration was run at least 3 times for each of the contemporary DEMs, as well as using both ice-free terrain and stable terrain masks as input. The resulting correction of the offset is presented in detail in Chapter 6.2.

5.5 Determination of Glacier Outlines

A new glacier outline dataset was created based on a Sentinel 2 satellite image and the contemporary DEMs. The image dates from late summer (3rd of August, 2018) and is therefore useful to trace glacier boundaries below the permanent snow line as glaciers are easily distinguishable from the rest of the terrain. In parts of the image where readability is low due to a lack of contrast, the hillshade derived from the contemporary DEMs was used additionally.

The drainage divides for each glacier were mapped using an approach based on the watershed divide method described in Bolch et al. (2010). Using this method, the aspect of the terrain withing the contemporary DEMs is used to calculate hydrological flow directions. This allows the creation of clear boundaries for each glacier in the area. Under the assumption that the flow divides do not migrate through time, these drainage divides were also used to delimit the historical glacier outlines in the accumulation area.

5.6 Assessing Data Voids

The indefinite contour lines of the EXA map impact the quality of the derived DEM greatly. In order to create a best guess scenario, the entirety of the EXA map is dismissed and treated as a data void. Then, two approaches are implemented to reconstruct the accumulation area in order to obtain a reliable geodetic mass balance.

5.6.1 Zero-Change Void Filling

The first approach to resolve the lacking data on the EXA map, is to reconstruct the data on the assumption that there have been no changes in elevation in the accumulation area. While glacierized regions in the Arctic are more likely to have experienced a loss in ice coverage over time (e.g. Gardner *et al.*, 2011), strong negative elevation changes within the accumulation area are highly unlikely (Paul *et al.*, 2017). On Axel Heiberg Island, larger glaciers with higher altitude accumulation areas, such as Thompson Glacier, were advancing over the majority of the observed period, which argues for at least stable values in the accumulation area (Thomson, Osinski and Ommanney, 2011).

The zero-change DEM is derived from the contour lines derived from TanDEM-X elevation data and the ArcticDEM dataset where necessary. For that purpose, the contour lines are clipped to the extent of the parts of the accumulation area, which are only depicted on the EXA map. As this creates a relatively abrupt break to the TGR map, contour lines near the break line are thinned out to allow for a smoother transition. Rather than reconstructing an accurate historical state of the accumulation area, the DEM generated by this approach indicates the range of more plausible rates of elevation change.

5.6.2 Hypsometric Void Filling

The second approach relies on a glacier's hypsometry to reconstruct the elevation data within the void. It is based on the assumption that elevation change is dependent on elevation itself. In McNabb *et al.* (2019), the hypsometric method is subdivided into either local or global approaches. Local, if the method is applied to fill data voids within an individual glacier. Global, if the calculations are used on an entire dataset or area of interest. Although the latter is usually applied to extrapolate from a few glaciers to a regional scale (e.g. Berthier *et al.*, 2010; Nilsson *et al.*, 2015), it is used here to extrapolate values from a single glacier to the entire study area.

Here, the mean elevation by elevation bin approach is implemented. This method relies on altitudinal belts (the so-called elevation bins) for which the mean elevation difference is derived and multiplied by their area. The results is a volume change which can then be used to calculate the volume change suitable for the voids on the glacier (McNabb *et al.*, 2019). In this study, the elevation bins are created within the perimeter of the Hidden Ice Field (HIF). The entirety of the ice field is mapped on the TGR map, presenting the best possible elevation data to reconstruct the 1960's accumulation area. As a smaller ice field, the HIF's topographic features resemble the conditions on Mueller Ice Cap best. Therefore, its values are more suitable to derive the mean elevation change bins than those of the more valley-like glaciers on the TGR map.

McNabb et al. (2019) suggest 50 m wide bins for glaciers with an elevation range of 500 m or more, or 10% of the elevation range if the range in altitude is smaller. The elevation data for Thompson Glacier is portrayed accurately on the TGR map up to an altitude of 850 m. Thus, only the upper range of HIF (850 m a.s.l. to 1500 m a.s.l.) is used to derive elevation bins. Due to the size of the range elevation bins of 50 m are implemented. The mean elevation changes are calculated after eliminating all values that differ ±3 standard deviations from the mean, which is a widely used way to ignore outliers (e.g. Berthier *et al.*, 2004; Gardelle *et al.*, 2013; Dussaillant *et al.*, 2018). The values for the elevation bins from 1550 m a.s.l. upwards are assumed to be 0 since they include less than 1% of the area of HIF. This has no larger impact on the extrapolated areas, as less than 4% of the study area are situated above that altitude.

Tributaries of Thompson Glacier, that are more similar to valley glaciers (e.g. Crook Glacier) are modified with elevation bin values from White Glacier presented in (Thomson *et al.*, 2017) to account for their different topography in the accumulation area. In doing so, the bias towards the changes found on HIF can be counteracted to some extent. All applied elevation bin values are presented in Appendix C.

5.6.3 Modifying the historical DEM

Since the topography created by the EXA map contour lines is considered wrong, contemporary contour lines are used to reconstruct the historical accumulation area. This is also based on the assumption that the glacier's bedrock topography should not change substantially over time (Zemp *et al.*, 2013). Using the contour tool in ArcMap, contour lines with a 25 m equidistance (on par with the TGR map) are derived from the TanDEM-X and ArcticDEM images. Their elevation data is adjusted using the mean elevation bin values from HIF for ice field-like topography and the mean elevation bin values from White Glacier for valley glacier-like topography. The subdivision into different contour types is presented in Figure 20.
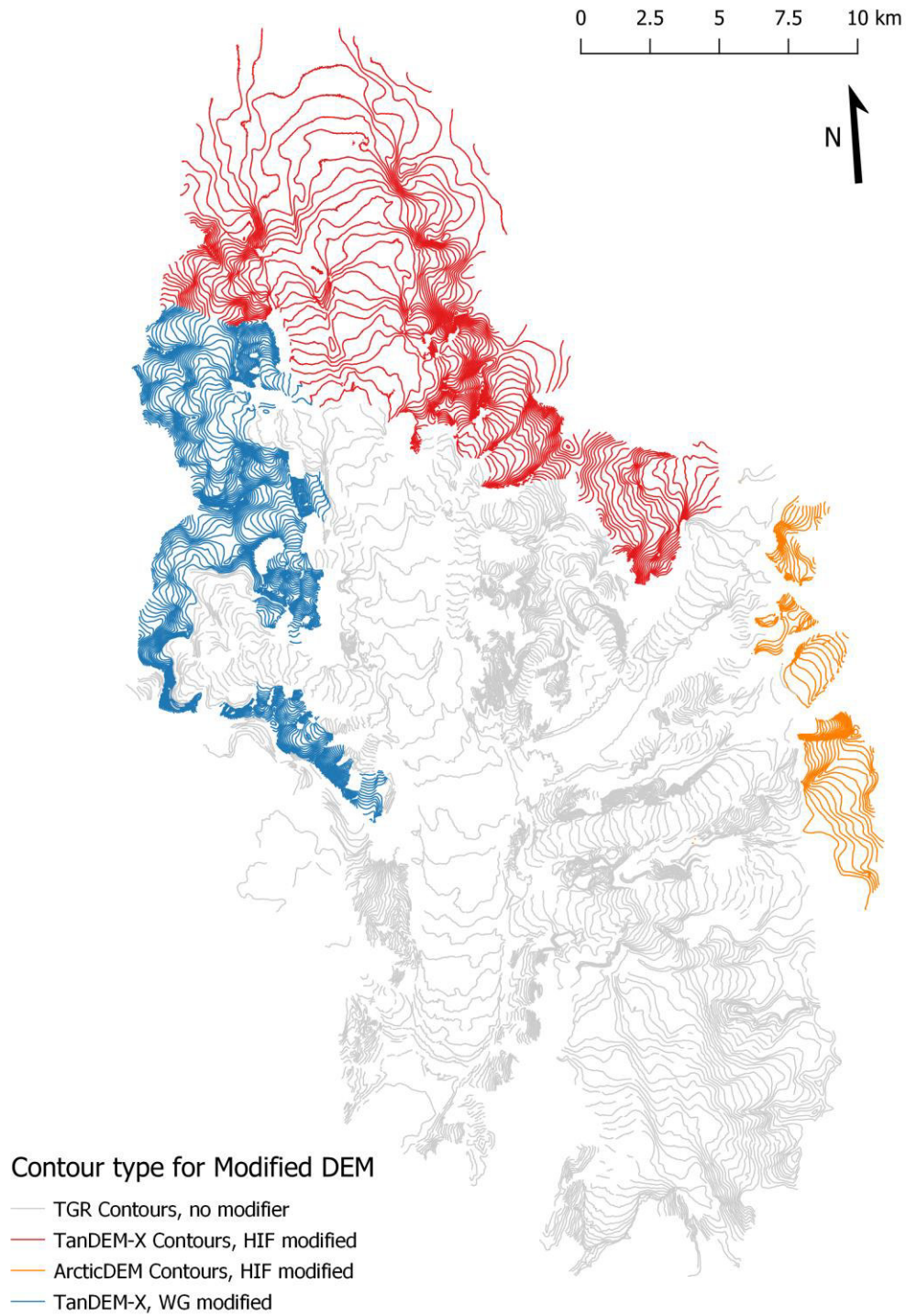
Figure 20: Contour line classification for the Modified DEM. Contour lines are modified in areas where only EXA map contours are available as input, respectively where preliminary results showed a change in elevation that was deemed too large.

5.7 Geodetic Mass Balance

The geodetic method is a widely used approach for the assessment of changes in the mass balance of a glacier (Huss, 2013). It relies on repeated surveying of a glacier's surface elevation which can be implemented at intervals of a few years to a few decades, depending on the rate of change found on a glacier (Fountain, Krimmel and Trabant, 1997). By differencing the monitored elevations and applying a density conversion, the glacier-wide cumulative mass balance can be derived for the time period between measurements (Cox and March, 2004). In this study, volume change and geodetic mass balance are calculated following the formulas presented in Zemp *et al.* (2013).

The glacier's volume change is derived from the sum of the difference in altitude of each measured pixel times the number of measured pixels:

Equation 6

$$\Delta V = r^2 \sum_{k=1}^{K} \Delta h_k$$

K equals the number of pixels covering the glacier at the maximum extent, Δh_k is the difference in elevation at a certain pixel k, while r represents the pixel size. To derive the geodetic mass balance B_{geod} for a specific period of record (PoR), the volume change is divided by the average glacier area times the conversion into glacier ice. The latter is described as the ratio of average ice density to water density. The result is in the unit metre water equivalent (m w.e.).

Equation 7

$$B_{geod.PoR} = \frac{\Delta V}{\bar{S}} * \frac{\overline{\rho_{ice}}}{\rho_{water}}$$

The required average glacier area $\bar{S}$ is calculated using the surface area of the glacier at time t_0 and t_1, assuming a linear change in time:

Equation 8

$$\bar{S} = \frac{S_{t0} + S_{t1}}{2}$$

To obtain the annual geodetic mass balance $B_{geod.a}$, the balance calculated in equation 7 is further divided by the PoR itself. This results in a value in the unit meter water equivalent per year (m w.e. a^{-1}):

Equation 9

$$B_{geod.a} = \frac{B_{geod.PoR}}{PoR}$$

5.8 Error Propagation

In the process of deriving a glacier-wide mass balance from DEMs a variety of uncertainties are introduced in each step of the workflow. Potential errors, such as plotting errors in the historical map, misrepresentation of elevation data due to co-registration or wrongly assumed glacier areas affect the resulting values greatly. However, direct information on these errors is not available for the most part. This is why a statistical approach is implemented to account for uncorrelated and random errors within the used data (Zemp *et al.*, 2013).

5.8.1 Uncertainty in glacier-wide elevation changes

For each glacier in this thesis, the uncertainties within glacier-wide elevation changes are calculated following the formula by Huber *et al.* (2020) below. The error in glacier-wide specific elevation change $\sigma_{\Delta h}$ consists of three individual components:

Equation 10

$$\sigma_{\Delta h} = \sqrt{\sigma_{DEM}{}^2 + \sigma_{void}{}^2 + \sigma_{date}{}^2}$$

σ_{DEM} describes the uncertainty that is entailed in the difference image of two DEMs. This is expressed in equation 11 by McNabb *et al.* (2019).

Equation 11

$$\sigma_{DEM} = \sqrt{\frac{\varepsilon_{random}^2}{\sqrt{n/(L/r)^2}} + \varepsilon_{bias}^2}$$

The random error ε_{random} is based on 1.96 times the standard deviation of the elevation difference over stable terrain which is derived from the co-registration process, corresponding to the 95% confidence interval of a normal distribution. In the study of McNabb *et al.* (2019), the comparison of multiple DEMs from the same timeframe entails a certain bias which they express in ε_{bias}. Since this does not appear in this thesis the bias is omitted. Next, *n* is the number of independent samples that are inside the observed glacier outline. According to Zemp *et al.* (2013), the number of independent items is not equal to the sample size, which in this case would be the number of on-glacier pixels. Thus, the term is divided by the term *(L/r)* where *L* is the spatial autocorrelation distance and *r* is the pixel size. The autocorrelation distance is often approximated to 500 m (e.g. Magnússon *et al.*, 2016; Brun *et al.*, 2017).

Alternatively, *n/(L/r)* can also be approximated as the half of the number of contour lines on the observed glacier (Thomson *et al.* 2017). The total of contours *c* is divided by two to conservatively consider the error in the contour lines themselves. This results in a more conservative estimate of the error, but accounts for the fact that the entire historical DEM is interpolated based on contour line information. In order include both approaches, the mean value of both estimates $\bar{n}$ is used to calculate σ_{DEM}:

Equation 12

$$\sigma_{DEM} = \left(\sqrt{\frac{(1.96 * StDev_{stable})^2}{\sqrt{\bar{n}^2}}} \right)$$

5. Methods

As each derived DEM is using the identical stable terrain for co-registration, the random error to calculate the DEM related uncertainty σ_{DEM} are the same. The different uncertainties of each DEM are included in the term σ_{void}, which entails the error introduced through the implemented void filling methods. Following Huber et al. (2020), this component is described as 1.96 times the standard deviation of the elevation changes within the filled voids, calculated for each void filling approach. As the void filling does not affect the entire glacier area, σ_{void} is described as a ratio. The size of the void fill is included by dividing through the root of $\bar{n}_{void}$, which is calculated in the same way as described above, using the number of pixels, or half the number of contours within the filled voids.

Equation 13

$$\sigma_{void} = \left(\sqrt{\frac{(1.96 * StDev_{void})^2}{\sqrt{\bar{n}_{void}^2}}} \right)$$

Next, the term σ_{date} contains the error stemming from the vague date of the contemporary DEM data. Both DEMs used in this thesis are based on a composite of images which were taken over a longer time period. Thus, they do not show an exact date but rather a time period which is compressed into one image. To account for that, the date related uncertainty is estimated as the mean deviation of years within a DEM, times the annual average elevation change rate (Huber, McNabb and Zemp, 2020). For example, the temporal coverage of the TanDEM-X dataset ranges from 2010 to 2014, thus introducing a temporal uncertainty of ± 2 years.

Equation 14

$$\sigma_{date} = MeanDev_{yr} * \frac{\Delta h}{PoR}$$

5.8.2 Uncertainty in glacier-wide mass changes

As soon as the change in elevation is converted into an assessment of volume change, more uncertainties are introduced. Namely, there is an uncertainty in the estimate of the glacier's area σ_S and an uncertainty in the density conversion σ_ρ. The latter is important for the conversion of elevation change into meter water equivalent.

The differencing of two DEMs results in a change in glacier volume instead of mass, which would be the desired quantity to assess impacts such as sea-level rise contribution. The conversion factor implemented by most glaciological studies equals to 850±60 kg m^{-3}, established in Huss (2013). The uncertainty of ±60 kg m^{-3} is expressed as σ_ρ. This is then combined with the error in elevation change $\sigma_{\Delta h}$ from above to describe the error in the glacier-wide geodetic mass balance σ_B.

Equation 15

$$\sigma_B = |B| * \sqrt{\left(\frac{\sigma_{\Delta h}}{\overline{\Delta h}} \right)^2 + \left(\frac{\sigma_{\bar{\rho}}}{\bar{\rho}} \right)^2}$$

In this thesis, the error in glacier area σ_S is approximated as 0.05. This accounts for the misjudgement of the glacier area, which according to Rastner *et al.* (2012) is usually around 5% of the measured area. This is then applied to the uncertainty related to glacier mass change, which is described as:

Equation 16

$$\sigma_{\Delta M} = |\Delta M| * \sqrt{\left(\frac{\sigma_B}{\bar{B}}\right)^2 + \left(\frac{\sigma_{\bar{S}}}{\bar{S}}\right)^2}$$

6. Results

6.1 The historical DEM

The historical DEM resulting from contour line interpretation represents the 1960 state of the Thompson Glacier Region with varying quality (Figure 21). The contour line equidistance changes from 25 m on the TGR map to 100 m on the EXA map. Therefore, areas that are only present on the EXA map consist of larger swaths of interpolated data with less detail in comparison to their TGR counterpart. The contour line input is presented in Figure 22 on the following page, showing the division in TGR derived elevation data (blue) and EXA derived elevation data (red). All contour lines derived from the EXA map are marked as indefinite, which increases the uncertainty in this part of the study area even further.

Furthermore, contour lines in steep ice-free areas were not digitized. These areas are therefore generated entirely through the interpolation algorithm with little to no input data. This leads to smooth surface artefacts which do not represent the actual terrain and are thus not suitable for further use. In areas where cliffs are situated directly by the side of a glacier, these artefacts impact the interpolated values within glaciated areas. But as the results presented in this thesis are glacier-wide values they are of little consequence.
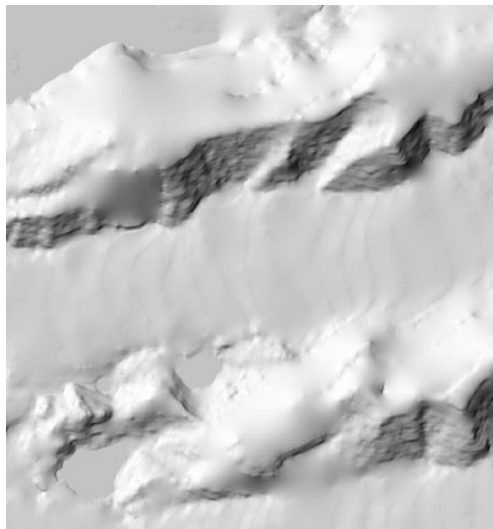
Figure 21: Hillshade of the historical DEM with visible differences in DEM quality. Where contour line information is dense, the DEM appears more rugged. Areas which are based on interpolated values appear as smooth surfaces. These appear most frequently in steep cliffs where contour information could not be interpreted (see the differences along the upper ridge). The flat areas in the upper left and lower left corners are glacier lakes and thus accurately represented.

6. Results
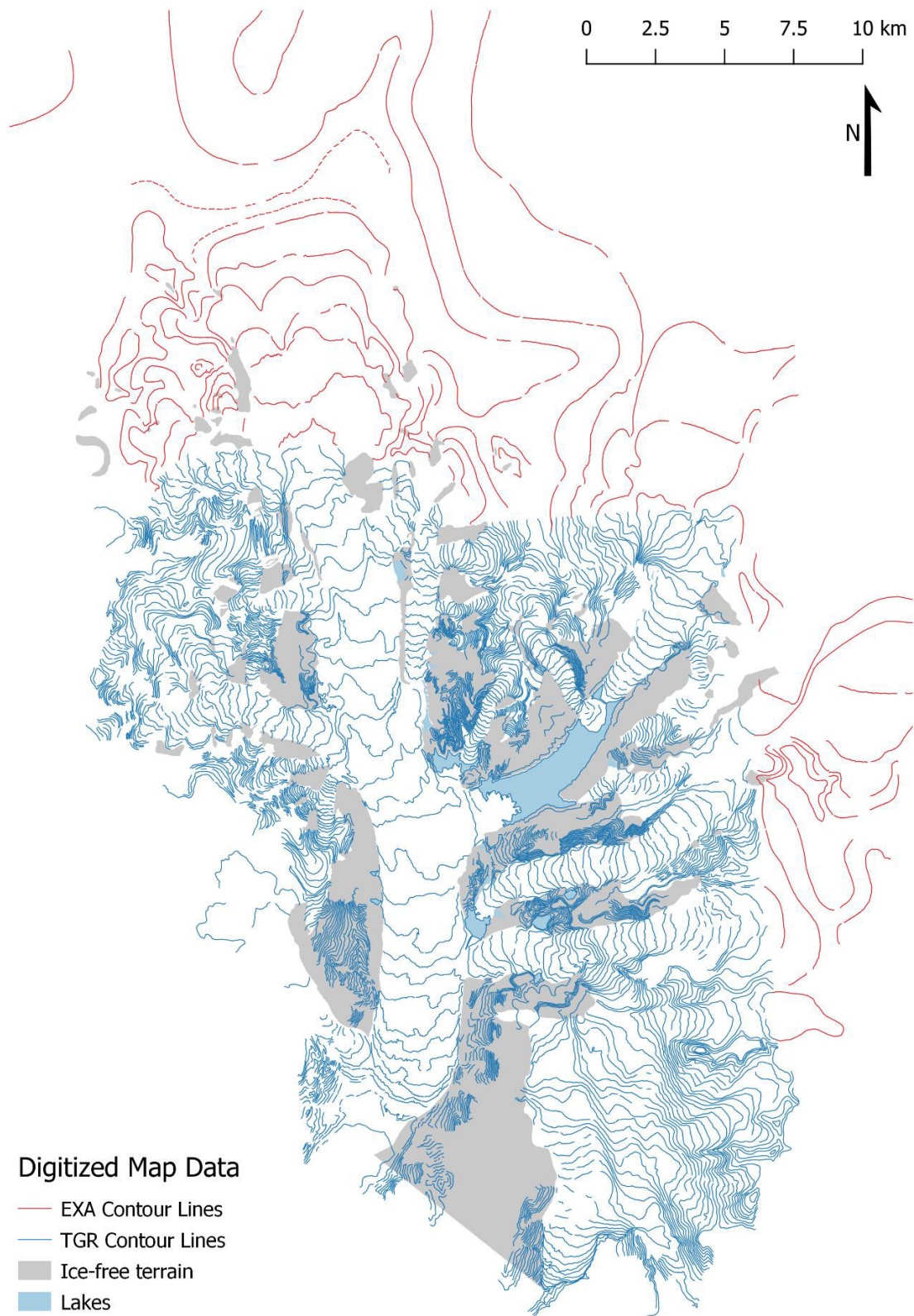
Figure 22: Digitized map data from the TGR and EXA map used to interpolate the historical DEM. Note that ice-free terrain without contour lines results in the smooth surfaces shown in Figure 19.

6.2 Co-Registration

The Co-Registration process improved the misalignment of the historical DEM to both TanDEM-X and ArcticDEM datasets. In the comparison to the ArcticDEM dataset five iterations were implemented. However, the mean and standard deviation values reached an optimum after three iterations, with the additional two iterations being used to check the reliability of the literature value. For the comparison between the historical DEM and the TanDEM-X data three iterations were implemented.

Using the stable terrain mask as input area, a small shift in x-direction (-0.7 m) and a more significant shift in y-direction (-34.3 m) are visible in the comparison to the TanDEM-X dataset. The same input area resulted in an equally small difference in x-direction (+5.7 m) and large difference in y-direction (-48.8 m) in the comparison to the ArcticDEM mosaic. In vertical direction, there is a similar shift of -6.3 m to the TanDEM-X raster, and -7.6 m to the ArcticDEM. More detailed values for each iteration are presented in Appendix B.

Table 2: Overview on Co-Registration Results

Master DEM		Dh of Stable Terrain		Iterations	Applied Shift [m]		
		Mean	Std. dev.		Δx	Δy	Δz
TanDEM-X	Before	-6.6	13.49	3	-0.7	-34.3	-6.3
	After	-5.88	10.04				
ArcticDEM	Before	-11.9	24.02	5	+5.7	-48.8	-7.6
	After	-5.53	21.55				

The co-registration process does not resolve the misalignment entirely (Figure 23). This is visible in the trend of west-facing slopes tending to be more negative than east-facing slopes. Similarly, north-facing slopes are more negative than south-facing slopes. However, the latter case is less pronounced as north-south ridges are almost undetectable over stable terrain. Still, it implies that the historical maps suffer from tilted and distorted features which are not resolved by correcting the horizontal shift. This needs to be taken into account, especially when assessing the elevation changes of glaciers that flow primarily on steep west-, or east-facing slopes, such as Finger Glacier and Phantom Glacier.
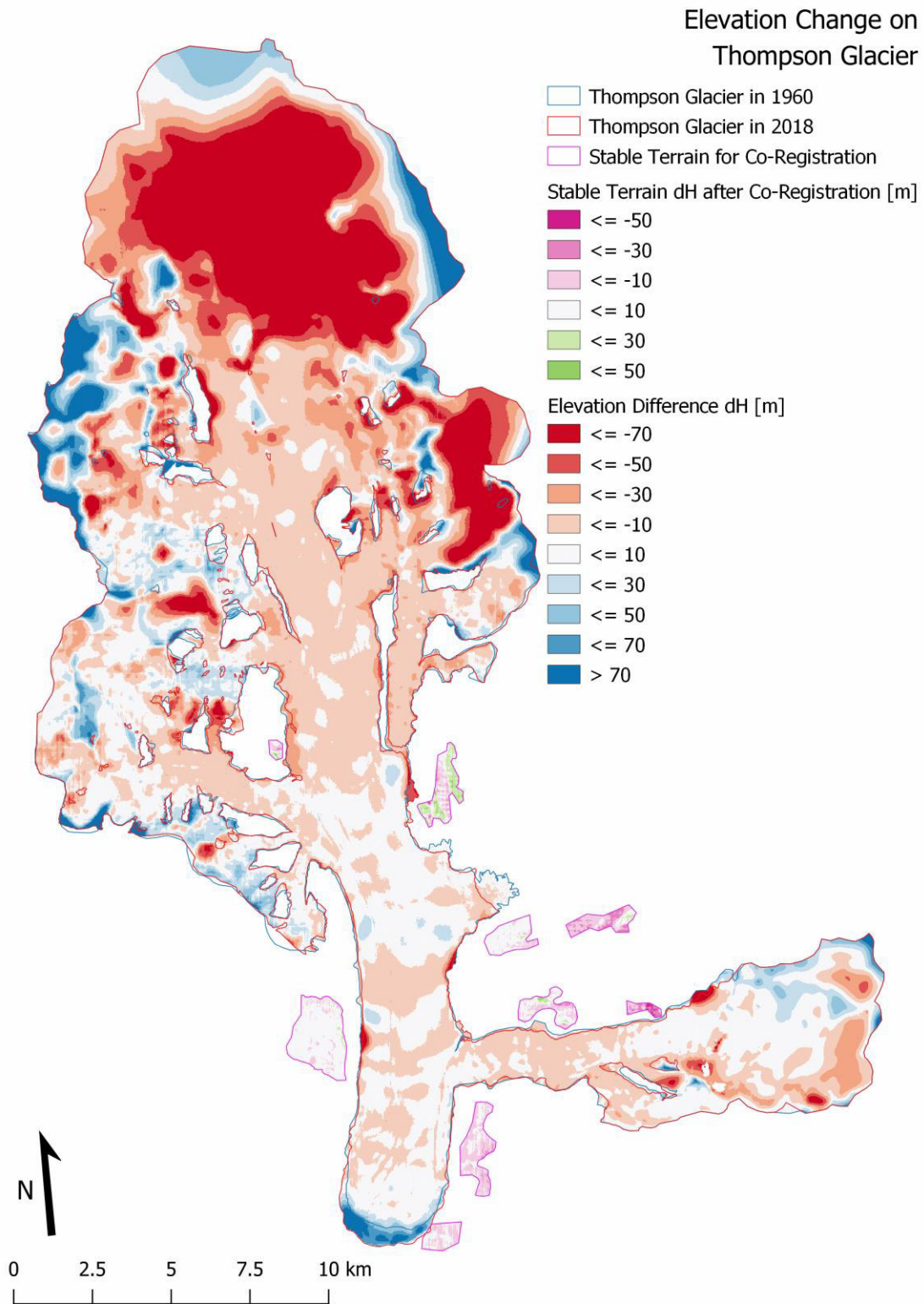
Figure 23: Historical dDEM showing the elevation changes on Thompson Glacier. Note how elevation differences on stable terrain are still present. The steeper the underlying terrain, the larger is the error in elevation.

6.3 Elevation Differences

6.3.1 Historical Difference DEM

The difference image (dDEM) resulting from the subtraction of the historical DEM from the contemporary DEMs presents a first overview on the changes in elevation. The several trends visible on the glacier's tongue are presented in Figure 24 on the following page. The elevation changes below are broad and without error estimates as they are only intended to give an impression on the trends in the study area.

The glacier front (a) shows highly positive values which are expected since the glacier was advancing over the observed time period. Here, values range mostly in between +60 and +90 m with a few points reaching more than 100 m in elevation gain. The lower third of the tongue, between 200 and 400 m altitude, shows slightly negative values. Here, the eastern half of the glacier shows values close to 0 m, while the western half is slightly more negative with values down to -20 m. To the west near Basalt Ridge (b), there are strongly negative artefacts (-150 m) due to the interpolation of elevation data within a steep cliff. The same effect is visible next to Astro Ridge (c, -120 m) on the eastern side of the glacier.

The middle third of the tongue, between 400 and 600 m altitude, shows similar values but there are spots of elevation gain across the glacier. In those, the increase ranges mostly between +10 and +20 m. A notable difference is visible near Phantom Lake and Five Finger Lake (d), where there is a thinning of -10 to -20 m, accompanied by an increasing size of the glacier lakes. The upper third of the tongue, between 600 and 900 m altitude, shows a decrease in elevation in between -15 and -20 m across the entire width of the glacier. Negative values to the side of the glacier are again attributed to artefacts generated by the interpolation in steep cliffsides.

The most striking feature of the difference image are the extremely negative values in the accumulation area of Thompson Glacier (e). Here, both TanDEM-X and ArcticDEM elevation values are over 200 m lower than the values derived from the EXA map. The most extremes being lower than the presumed historical value by over 230 m. Such a strong negative elevation change is highly unlikely within the accumulation area of a glacier and is therefore regarded as a fault in the input data (e.g. Paul *et al.*, 2017; Pieczonka and Bolch, 2015). Nonetheless, geodetic mass balance values are calculated with the historical DEM to obtain comparative values.

While the historical dDEM is unsuitable to assess the geodetic mass balance of Thompson Glacier, some of the smaller surrounding glaciers (Finger Glacier, Parallel Glacier and Phantom Glacier) are portrayed entirely on the TGR map. Thus, their historical information is represented accurately enough on the historical dDEM. All three of the smaller glaciers exhibit negative changes in elevation. Finger Glacier (f) shows the most negative trend with overall values in between -30 and -50 m. However, Finger Glacier is situated almost entirely on a steep western-facing slope, which tend to have more negative values on the historical dDEM – even after co-registration. Thus, its values have to be taken with a pinch of salt. The same issue, in reverse, explains the less negative values (between -5 and -20 m) of the neighbouring, east-facing Phantom Glacier. Parallel Glacier shows negative values with a loss of at least 20 m in height across its tongue. Consequently, the glacier is now distinctly disconnected from Thompson Glacier's tongue (g).
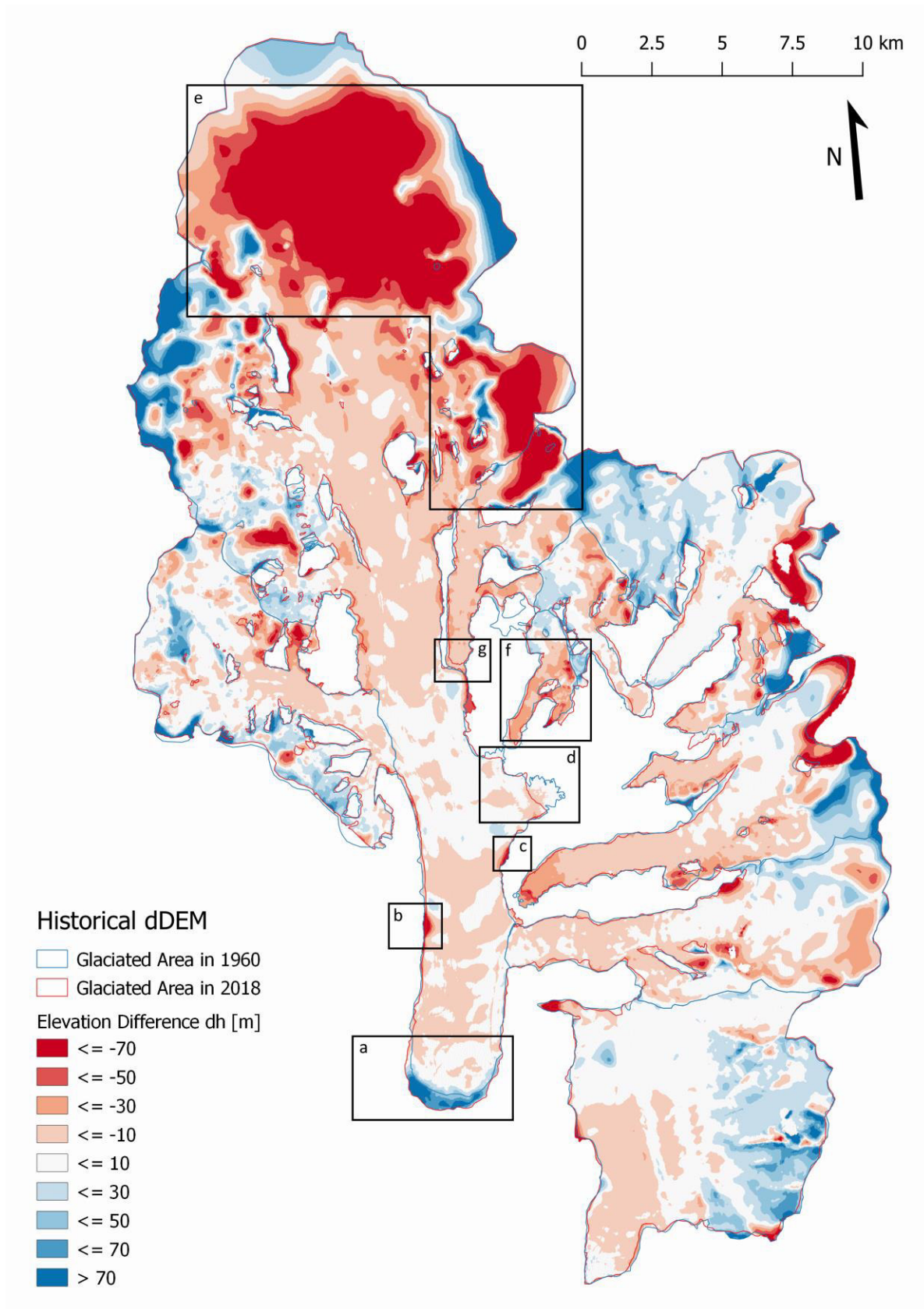
Figure 24: Difference DEM derived by subtracting the historical DEM from the ArcticDEM dataset.
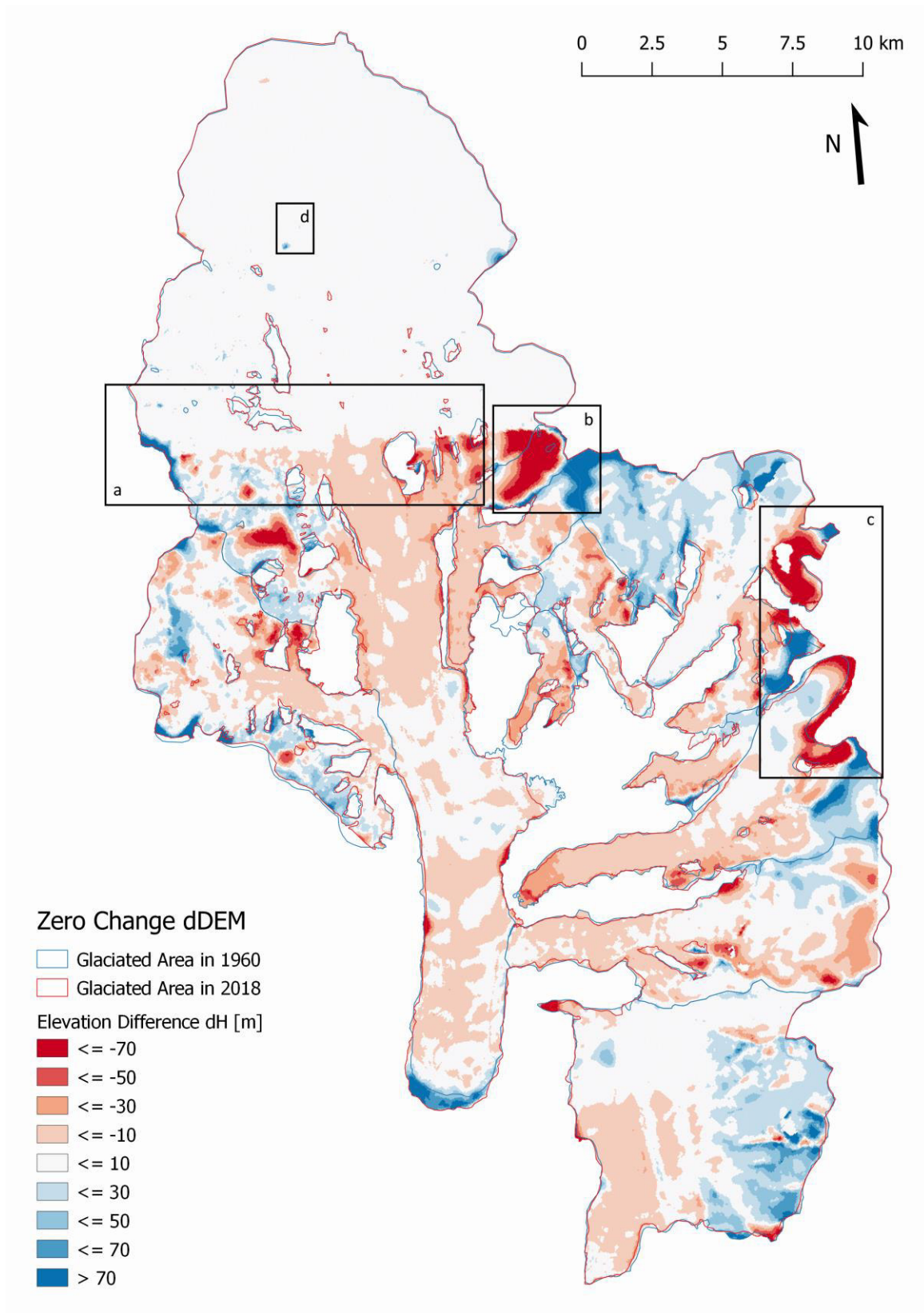
Figure 25: Zero Change difference DEM derived by exchanging EXA map data with contemporary elevation values, followed by subtracting the historical DEM from the ArcticDEM dataset.

6.3.2 Zero Change Difference DEM

The zero change dDEM nullifies the impact of the large error within the accumulation area on Thompson Glacier (Figure 25, previous page). By omitting any elevation change in the area only present on the EXA map, the impact of the formerly present negative extremes can be quantified. However, the resulting difference image does not represent a realistic scenario since it produces a sharp border along the perimeter of the EXA map (a). The remaining areas with extremely negative values (b & c) have no further impact on the purpose of the zero change dDEM. They are all located outside of Thompson Glacier's perimeter and do not affect the derivation of its 'zero-change' mass balance. The sparse points within the accumulation area showing elevation change (d) are the results of artefacts within the ArcticDEM dataset. Since they are rather small, they do not impact the derived glacier-wide values.

The entirety of the TGR map is left untouched; any values derived from the zero change dDEM therefore still entail potential errors found on the TGR map. Corrections to TGR map are introduced to the modified historical DEM. Thus, mass balances for surrounding glaciers which extend on the EXA map are directly derived from the modified dDEM.

6.3.3 Modified Difference DEM

The modified dDEM also cancels out the negative impact of the error in the accumulation area, but unlike the zero-change approach, it uses the regional trends of mean elevation change by elevation. In doing so, parts of the accumulation area turn slightly negative (in between -30 and -10 m elevation difference). As the modified DEM tries to include characteristic topographies into its values, there are different trends visible within the observed area (see Figure 26 on the following page). To the west of the area (a), both positive and negative extreme values from the historical dDEM are smoothed out by using the elevation change trend found on White Glacier according to Thomson *et al.* (2017). This results in an overall stable accumulation area. Slightly negative elevation change can be found in its lower parts, yet the mountain ranges to the west include positive changes in between +10 and +30 m.

The ice fields to the east (b) follow the trend of the Hidden Ice Field. Here, values tend to be slightly negative, predominantly in the range of -30 to -10 m. The same approach was also used to correct the accumulation area of Astro Glacier (c). A peculiarity is the positive outlier in the accumulation area of Transit Glacier (d). This is the result of a relatively large artefact in the ArcticDEM dataset which is visible in the sharp border between values larger than +70 m and values in between +10 and +30 m. The artefact is set to a zero-change area in the calculations for Transit Glacier.
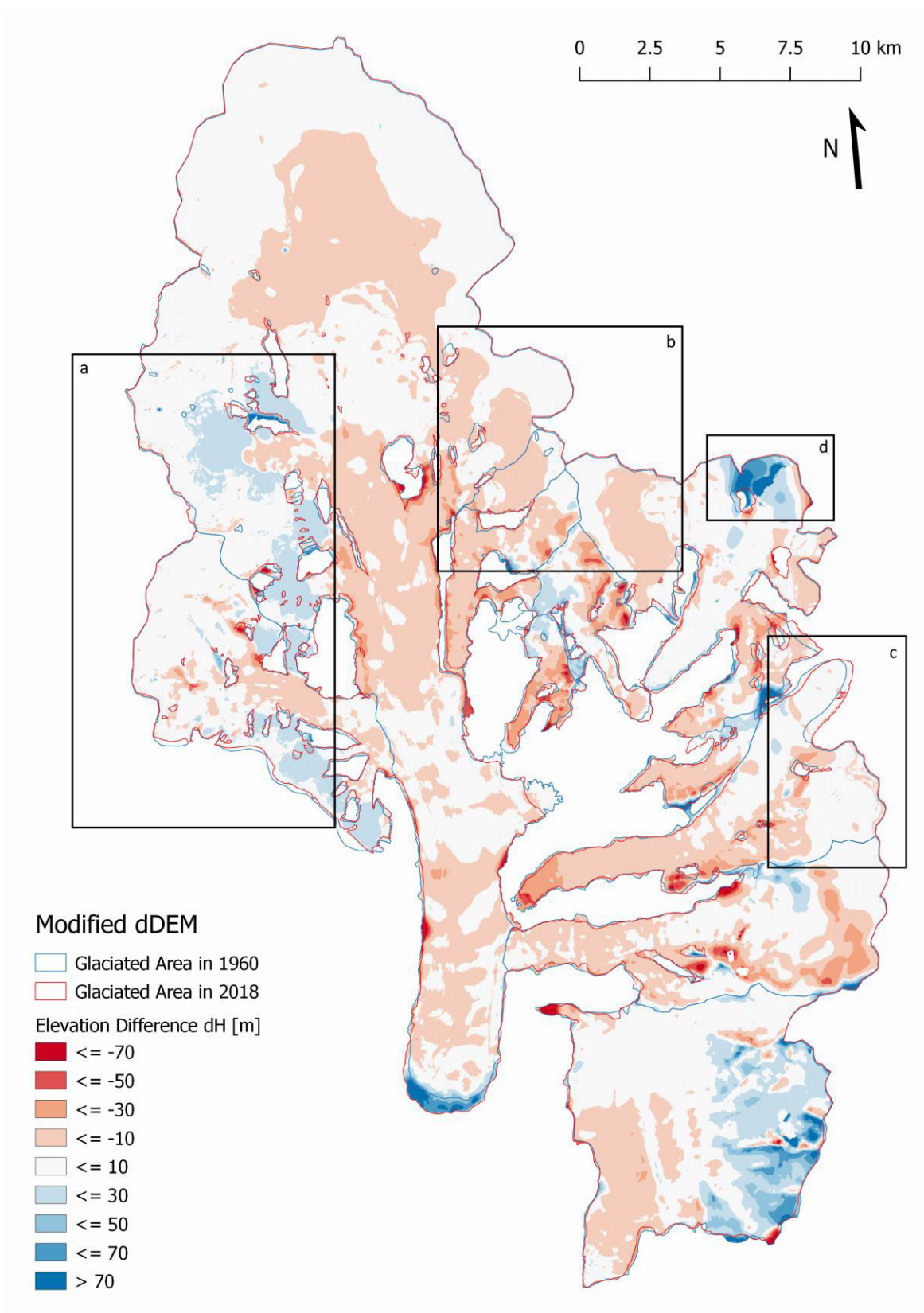
Figure 26: Modified difference DEM, derived by subtracting the modified historical DEM from the ArcticDEM dataset. Note that changes appear on the perimeter of the observed area, where input data from the EXA map was replaced with modified contour lines.

6.4 Geodetic Mass Balance

Geodetic mass balances (B_{geod}) were calculated for each dDEM. Presented below are the values of the geodetic mass balance over the entire period of record $B_{geod.PoR}$ and the annual geodetic mass balance $B_{geod.a}$.

6.4.1 Thompson Glacier

Thompson Glacier suffers greatly from the impact of the large error in the accumulation area on the historical dDEM. This area alone forces the glacier-wide elevation change down below –20 m. By declaring the area to be a data void and using the void filling approaches presented above, the values derived for Thompson Glacier are quartered (Table 3).

Table 3: Derived values for elevation change (Δh), geodetic mass balance over period of record ($B_{geod.PoR}$) and annual geodetic mass balance ($B_{geod.a}$) for each difference DEM.

dDEM	Δh [m]	$B_{geod.PoR}$ [m w.e.]	$B_{geod.a}$ [m w.e. a^{-1}]
Historical dDEM	-24.41	-20.81	-0.38
Zero-Change dDEM	-4.48	-3.82	-0.07
Modified dDEM	-6.44	-5.49	-0.1

The zero-change approach uses no knowledge of regional changes, which ultimately results in a relatively small elevation change. In comparison, the results derived from the modified dDEM are more realistic, as they include the trend in elevation change by elevation extracted from the TGR map. It is notable that while the modified dDEM drastically reduces the elevation change of the entire Thompson Glacier, the rates for the two distinct tributaries turn out more negative (Table 4).

Table 4: Comparison of values from tributary glaciers derived from the historical dDEM and modified dDEM. Note the increase in elevation difference (Δh) and geodetic mass balance ($B_{geod.PoR}$) for both glaciers.

	Δh [m]		$B_{geod.PoR}$ [m w.e.]	
	Hist.dDEM	Mod.dDEM	Hist.dDEM	Mod.dDEM
Crook Glacier	-0.62	-1.07	-0.53	-0.91
Wreck Glacier	-8.46	-9.53	-0.13	-0.15

Regardless of the implemented void filling, the negative mass balance values for Thompson Glacier are most likely the result of glacier thinning predominantly present on the glacier's tongue. The glacier's advance until the early 2000s is still visible as a gain of around 650 m in length. Given that the PoR spans over the point in time when the glacier started retreating, the impact of the recent retreat cannot be assessed.

6.4.2 Surrounding Glaciers

Regarding the surrounding glaciers, the results are divided into different blocks, as not all glaciers are present on all dDEMs due to their location. Firstly, Finger Glacier, Phantom Glacier and Parallel Glacier are all included entirely on the TGR map. Thus, they are not affected by any changes introduced in the zero-change or modified DEM. They are therefore analysed directly on the historical DEM. Their location allows for an analysis of their mass balance using both TanDEM-X and ArcticDEM data for comparison. Table 5 below summarizes the resulting values for the difference image to both contemporary datasets.

Table 5: Calculation of glacier-wide Elevation Change Δh, Geodetic Mass Balance over the Period of Record $B_{geod.PoR}$ and annual geodetic mass balance $B_{geod.a}$. The results are based on the subtraction of the historical DEM from the TanDEM-X and ArcticDEM dataset respectively.

	Δh [m]		$B_{geod.PoR}$ [m w.e.]		$B_{geod.a}$ [m w.e. a^{-1}]	
	TanDEM-X	ArcticDEM	TanDEM-X	ArcticDEM	TanDEM-X	ArcticDEM
Finger Glacier	-15.97	-18.03	-13.63	-15.37	-0.26	-0.28
Phantom Glacier	-7.99	-7.23	-6.82	-6.16	-0.13	-0.11
Parallel Glacier	-7.91	-9.59	-6.74	-8.17	-0.13	-0.15

Secondly, the accumulation areas of Astro and Transit Glacier are situated on the EXA map. Thus, both glaciers are impacted by the changes in the modified DEM. As they are located outside of the perimeter of the TanDEM-X elevation model, the values presented in Table 6 result from the comparison to the ArcticDEM image.

Table 6: Calculation of glacier-wide Elevation Change Δh, Geodetic Mass Balance over the Period of Record $B_{geod.PoR}$, and Annual Geodetic Mass Balance $B_{geod.a}$. The results are based on the subtraction of the historical and modified DEM from the ArcticDEM elevation model.

	Δh [m]		$B_{geod.PoR}$ [m w.e.]		$B_{geod.a}$ [m w.e. a^{-1}]	
	Hist.dDEM	Mod.dDEM	Hist.dDEM	Mod.dDEM	Hist.dDEM	Mod.dDEM
Astro Glacier	-8.44	-10.15	-7.2	-8.65	-0.13	-0.16
Transit Glacier	+6.29	-4.03	+5.36	-3.43	+0.1	-0.06

Lastly, Hidden Ice Field and Bellevue glacier are both depicted on the TGR map. Only the ArcticDEM image portrays them entirely as they are located on the edge of the TanDEM-X dataset. However, as only parts of the accumulation area are missing in the TanDEM-X elevation model, it can be used to derive "zero-change" comparison values. The same approach is also tested for Astro Glacier, although almost two thirds of the glacier are missing in the TanDEM-X dataset. The results are compiled in Table 7 below.

Table 7: Calculation of glacier-wide Elevation Change Δh, Geodetic Mass Balance over the Period of Record $B_{geod.PoR}$, and Annual Geodetic Mass Balance $B_{geod.a}$. The results are based on the subtraction of the historical DEM from both ArcticDEM and TanDEM-X. Note that all glaciers are not entirely positioned on the TanDEM-X dataset. The missing area is stated as percentage of the glacier's total area.

	Δh [m]		$B_{geod.PoR}$ [m w.e.]		$B_{geod.a}$ [m w.e. a^{-1}]		Area missing on TDX [%]
	ArcticDEM	ZeroChange TDX	ArcticDEM	ZeroChange TDX	ArcticDEM	ZeroChange TDX	
Bellevue Glacier	-9.18	-8.61	-7.83	-7.34	-0.14	-0.14	12
Hidden Ice Field	+2.36	+0.84	+2.01	+0.72	+0.04	+0.01	17
Astro Glacier	-8.44	-5.96	-7.2	-5.08	-0.13	-0.1	61

The full overview on the calculations used to derive all geodetic mass balances, as well as elevation change maps for all glaciers surrounding Thompson Glacier are presented in Appendix D.

6.5 Error propagation

The uncertainties within the elevation changes are mostly dependent on values related to the input dataset. For the most part, the difference images are based on the same input data – the only difference being the different void filling approaches. Uncertainties within the used DEM are assessed using the standard deviation over stable terrain, which is the same in all datasets. Thus, σ_{DEM} remains the same. In the case of Thompson Glacier, all three dDEMs are based on a comparison of the Historical DEM to the ArcticDEM dataset. Visible differences appear in the void filling uncertainty σ_{void}, which is larger for the Modified dDEM as the affected area is bigger. The date related uncertainty σ_{date} is largest for the historical dDEM. This is related to the calculation of σ_{date}, as it uses the derived annual average elevation change. The error in the accumulation area results in a more negative elevation change which causes a larger σ_{date}.

Table 8: Error estimates for the glacier-wide elevation change Δh derived for each dDEM. σ_{void} is omitted in historical dDEM as no void filling was implemented.

	Historical dDEM	Zero-Change dDEM	Modified dDEM
Δh [m]	-24.41	-4.48	-6.44
σ_{DEM} [m]	*0.14*	*0.14*	*0.14*
σ_{void} [m]	*–*	*0.003*	*0.1*
σ_{date} [m]	*-1.11*	*-0.2*	*-0.29*
$\sigma_{\Delta h}$ [m]	**1.12**	**0.24**	**0.34**

These differences also appear between each dDEM when assessing the uncertainties in the geodetic mass balance and mass change. As the uncertainty in the conversion is related to a ratio between the uncertainty in elevation change and the specific elevation change itself, the differences between the three dDEMs propagate into the error in the geodetic mass balance σ_B. Thus, the largest error is again found in the historical dDEM. The errors in density conversion σ_ρ and area σ_{area} remain the same for all three dDEMs.

Table 9: Error estimates for geodetic mass balance and mass change derived for each dDEM.

	Historical dDEM	Zero-Change dDEM	Modified dDEM
B_{geod} [m w.e.]	**-20.81**	**-3.82**	**-5.49**
ΔM [Gt]	-7.81	-1.43	-2.06
σ_ρ [kg m^{-3}]	*60*	*60*	*60*
σ_{area} [m^2]	*18.76*10^6*	*18.76*10^6*	*18.76*10^6*
σ_B [m w.e.]	**1.75**	**0.34**	**0.48**
$\sigma_{\Delta M}$ [Gt]	0.76	0.15	0.21

6. Results

The full overview of the most plausible results with error estimates for all observed glaciers is presented in Table 10 below. The detailed calculation including all derived values can be found in Appendix D.

Table 10: Overview of the most plausible results for glacier-wide mass balances of all observed glaciers.

Glacier	$B_{geod.PoR}$ [m w.e.]
Thompson Glacier	**-5.49**±0.48
Astro Glacier	**-8.65**±0.81
Bellevue Glacier	**-7.83**±0.76
Finger Glacier	**-15.37**±1.59
Hidden Ice Field	**+2.01**±0.32
Parallel Glacier	**-8.17**±0.92
Phantom Glacier	**-6.26**±0.83
Transit Glacier[2]	**-3.43**±0.53

---

[2] Due to a large artefact on Transit Glacier in the ArcticDEM dataset, some elevation change values within its accumulation area were set to zero. Consequently, the resulting mass balance is likely mitigated.

7. Discussion

7.1 Interpretation of Thompson Glacier's Mass Balance

Thompson Glacier shows negative mass balance values in all three difference images (Figure 27). As presented above, the direct comparison of the historical maps to contemporary DEMs results in glacier-wide values which are too negative due to the extreme values in the accumulation area. The zero-change approach offers the easiest solution to the lack of accurate data in the accumulation area. However, the derived mass balance of –3.82±0.87 m w.e. describes a scenario where any elevation changes in the accumulation area over the last decades are dismissed. Comparative values from the neighbouring White Glacier offer some support for small elevation changes above an altitude of 1400 m a.s.l. (Thomson *et al.*, 2017), but the topography of the valley glacier's accumulation area differs greatly from Thompson Glacier's ice cap origin.
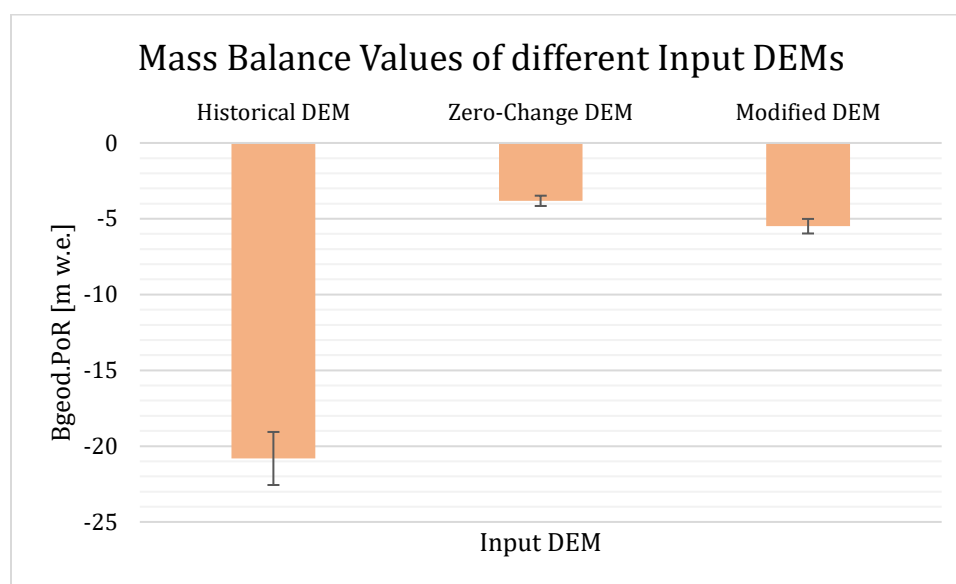
Figure 27: Geodetic Mass Balance values $B_{geod.PoR}$ derived from each of the three Input DEMs. The strongly negative values resulting from the historical DEM are interpreted as an error in the input data and thus not regarded as a realistic scenario.

More probable values are represented in the modified dDEM, which includes the influence of local topographic features on elevation change. While the Hidden Ice Field is an order of magnitude smaller than Mueller Ice Cap, its elevation changes are assumingly more appropriate to reconstruct Thompson Glacier's accumulation area. The resulting mass balance turns more negative (–5.49±0.48 m w.e.), including both negative and positive elevation changes within the accumulation area. The downside of this approach is that a relatively small area is used for extrapolation, which limits the representativeness of the data (Pieczonka *et al.*, 2013). This is counteracted by including values of White Glacier to reconstruct the parts of the accumulation area which can be described as more "valley-glacier-like". The modified dDEM therefore includes as much knowledge of the local characteristics as possible, rendering its values the best guess for Thompson Glacier's changes.

7.2 Interpretation of Mass Balances in the Study Area

According to the best guess scenario, the observed glaciers within the study area exhibit negative mass balances in the range of –5 to –8 m w.e., which translates into a yearly rate in between –0.10 and –0.15 m w.e. (Figure 28). The entire region of the northern Canadian Arctic (ACN) lost less than -0.25 m w.e. per year in the same timeframe according to Zemp *et al.* (2019). It is noteworthy that the estimates for ACN are based on a very limited data sample including only few long-term series from dozen glaciers only. Nonetheless, the derived results fit within the bounds of expectations.
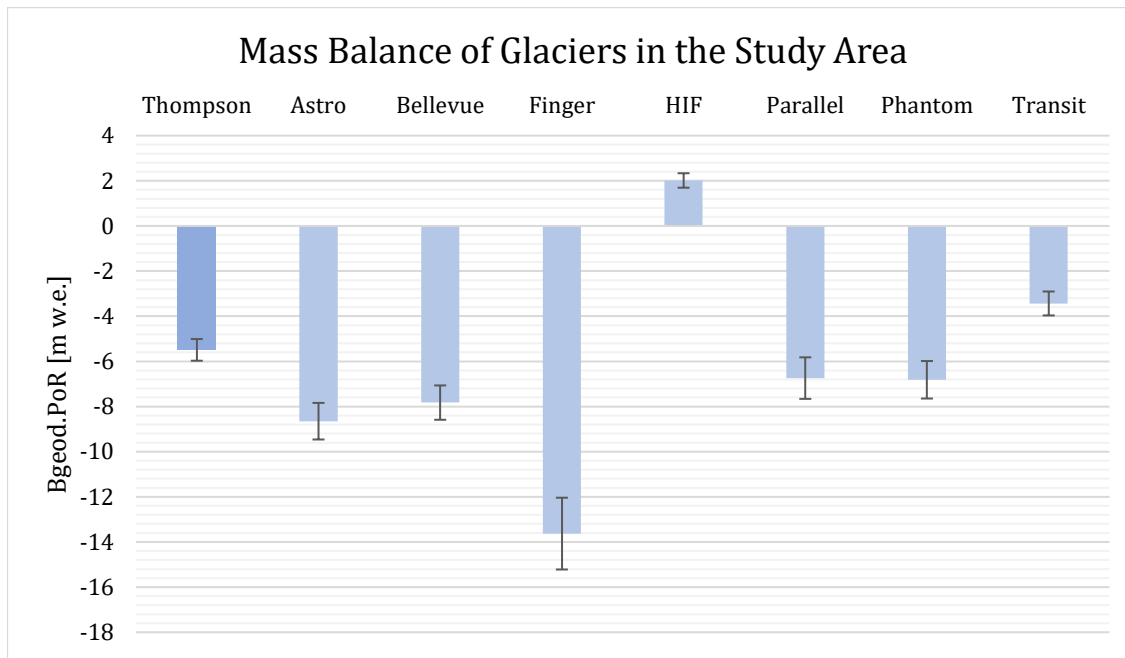
Figure 28: Comparison of mass balance values for all observed glaciers within the study area. Error estimates are based on the error propagation assessment presented in Chapter 5.7.

The outliers are the Hidden Ice Field, Finger Glacier, and to some extent Transit Glacier. Especially peculiar are the positive mass balance values for Hidden Ice Field (+2.01±0.32 m w.e). A possible explanation for this is its relatively high average altitude, with less than 20% of the ice field being situated below 750 m a.s.l.. Thus, slightly positive values are acceptable, as regional mass balance models show values above zero for higher altitude areas even in periods of increased mass loss (Gardner *et al.*, 2011). Nonetheless, the derived mass balance values seem rather high, which could also be linked to a collection of positive outliers in the historical DEM. However, the mass balance values for HIF stay positive even if the most positive areas are disregarded.

The more negative values of Finger Glacier can be related to the smaller size of the glacier and its location on a relatively steep slope. However, a potential bias remaining from co-registration is not excludable, as steep west-facing slopes tend to be more negative – which affects the entirety of Finger Glacier (see Chapter 6.2). Mass balance values for Transit Glacier are potentially mitigated, as parts of the accumulation area were set to zero due to an artefact in the ArcticDEM dataset. Furthermore, the area contributing to Transit Glacier is highly subjected to misinterpretation as the actual drainage divide in its flat accumulation area is difficult to define. The misjudgement of the glacier area propagates directly to the derived values (Zemp *et al.*, 2013).

7.3 Comparison of changes on Thompson Glacier

The WGMS lists four glaciers as reference glaciers in the northern Canadian Arctic (ACN) with ongoing glaciological mass balance records for at least 30 years. All observations on the four glaciers were started in the early 1960s which amounts to the same period of record studied in this thesis. This allows a solid comparison to the values derived for Thompson Glacier (Figure 28). Here, the contrast in mass balance between Thompson Glacier and its immediate neighbour White Glacier is noticeable. Over 54 years, the former exhibits a mass balance of –5.41±0.48 m w.e., while the latter lost an equal of –9.61±0.87 m w.e. of ice (Thomson *et al.*, 2017). The difference is according to the expectations, as it falls in line with the behaviour of both glaciers. As mentioned previously, White Glacier retreated persistently while Thompson Glacier advanced until the early 2000s. Furthermore, the size of Thompson Glacier conditions a longer response time to climatic impacts (Cogley, Adams and Ecclestone, 2011). Overall, the similar behaviour of all glaciers visible in Figure 29 can be expected due to the long period of record. At the same time, absolute mass changes are expected to vary greatly (Figure 30), as differences in a glacier's hypsometry influences both the short time reaction, as well as the long-term trend (Kuhn *et al.*, 1985).
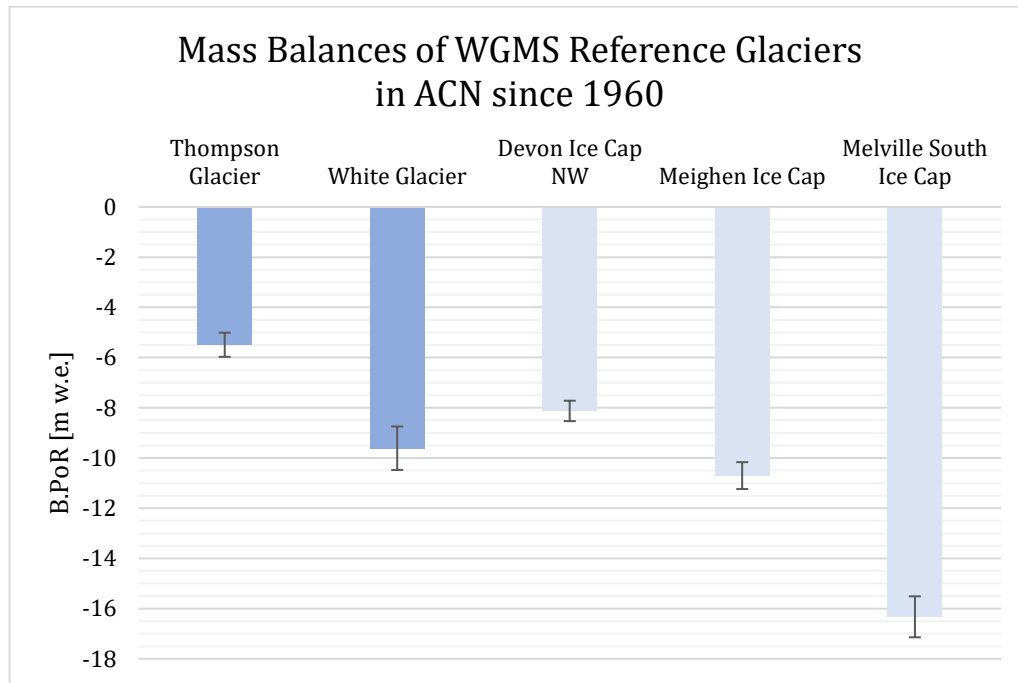
Figure 29: The geodetic mass balance of Thompson Glacier compared to the mass balances of WGMS reference glaciers in the subregion Arctic Canada North. Data for White Glacier from Thomson et al. (2017), ice cap data from the Fluctuations of Glaciers database (WGMS, 2019). Records for Thompson Glacier, White Glacier and Meighen Ice Cap start in 1960, Devon Ice Cap in 1961 and Melville South Ice Cap in 1963. Geodetic mass balances in dark blue, cumulative glaciological mass balances in light blue. Cumulative glaciological mass balances are given with a 95% confidence interval.

7. Discussion

Due to its larger size, values for mass change are more insightful to assess the impact of Thompson Glacier's changes. The conversion shows that the glacier has lost –2.06±0.21 Gt of ice, which is about a hundredfold of the mass change of White Glacier. This shows that the contribution to global sea level rise from the CAA is greatly dependent on the mass changes of larger glaciers. Even relatively low mass balance rates result in larger losses of ice mass. Keeping the dependence on glacier hypsometry in mind, the scale of mass loss on Thompson Glacier is still less extreme than those of the reference ice caps in the region. The outlet basin of Devon Ice Cap, which is more than four times larger, experienced a mass change almost seven times more negative. Similarly, the significantly smaller Meighen and Melville ice caps still show nearly half the amount of Thompson Glacier's ice loss (WGMS, 2019).
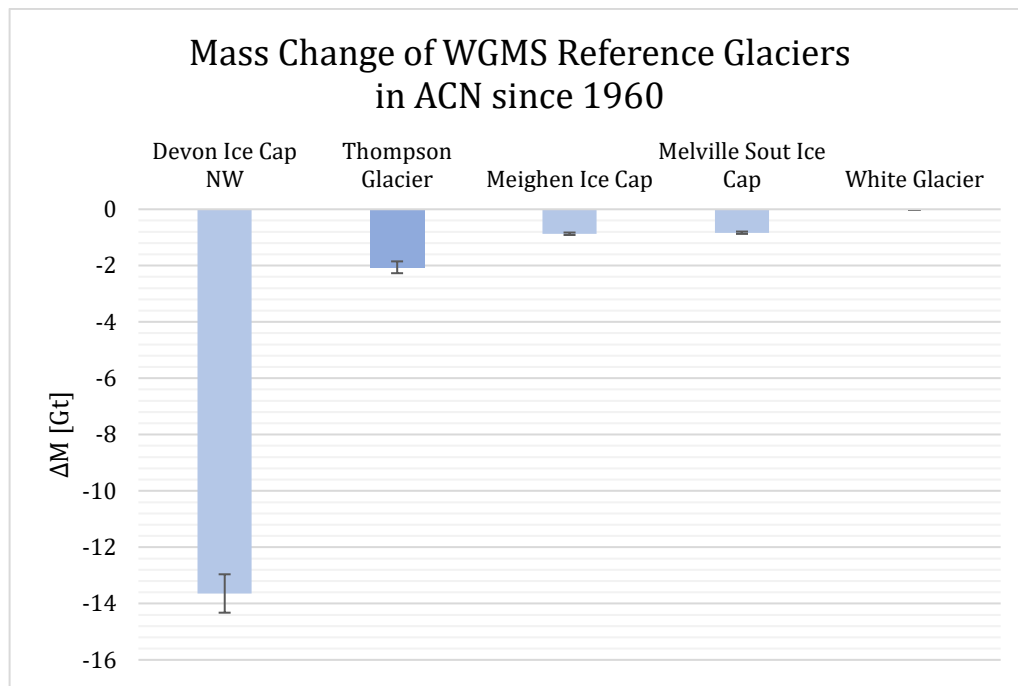
Figure 30: Mass change in Gt of Thompson Glacier compared to the WGMS reference glaciers in ACN. Ice cap data is derived from the cumulative glaciological mass balance and average area from the Fluctuations of Glaciers database (WGMS, 2019). White glacier data from Thompson et al. (2017). Ice cap mass changes are given with a 95% confidence interval.

On a global scale, the Thompson Glacier exhibits one of the least negative mass balances when compared to reference glacier from different regions (Figure 31). In the same timeframe, valley glaciers in Alaska (e.g. Gulkana Glacier) show mass balances more than six-times more negative. In the Alps in Central Europe values are even more extreme (e.g. Gries Glacier) (WGMS, 2019). This is to be expected, since glaciers in the High Arctic regime have a relatively low mass turnover and are less sensitive to changes in temperature and precipitation compared to more maritime glacier regimes with high mass turnover (e.g. in Alaska) (Zemp *et al.*, 2015). However, regarding the contribution to global sea level rise, glaciers in the size of Thompson Glacier have a large impact. The comparison to North American valley glaciers (Figure 32) shows the differences in specific mass change highlighting the strong effects of climatic changes on Thompson Glacier.
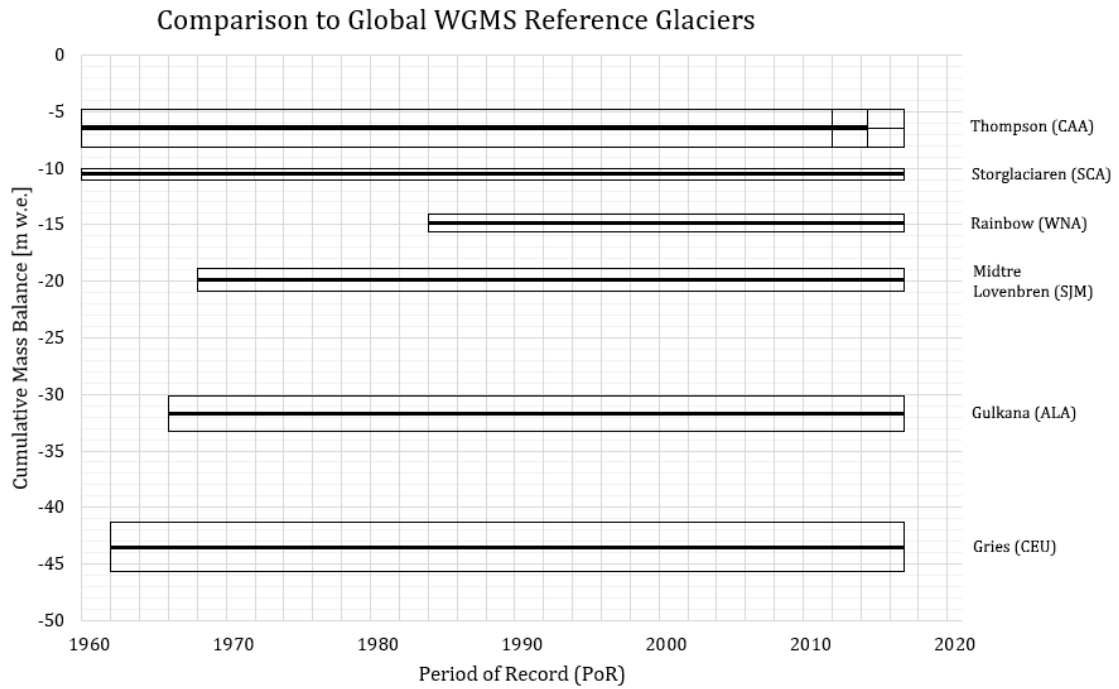
Figure 31: Thompson Glacier in comparison to cumulative glaciological mass balance of reference glaciers from different GTN-G regions. SCA: Scandinavia, WNA: Western North America, SJM: Svalbard & Jan Mayen, ALA: Alaska, CEU: Central Europe. Except for Thompson Glacier, all errors are given in a 95% confidence interval. Data from the Fluctuations of Glaciers database (WGMS, 2019).
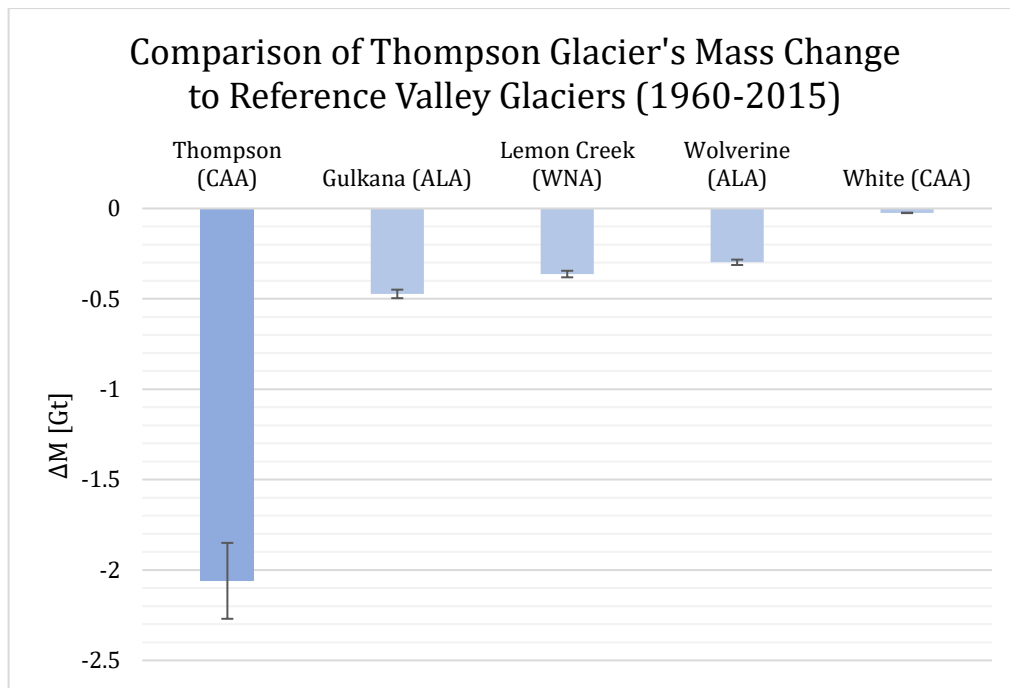
Figure 32: Comparison of Thompson Glacier's mass change since 1960 to WGMS reference valley glaciers in North America (ALA: Alaska, WNA: Western North America). Data derived from cumulative glaciological mass balances from the Fluctuations of Glaciers database (WGMS, 2019).

49

7.4 Reliability of Historical Maps

While the TGR map can seemingly be implemented into a scientific study with reliable results, the EXA map shows that historical maps cannot be readily trusted as a valid data source. The contour lines pictured on it are far from being accurate, which is already hinted at on the map where they are classified as indefinite. Why there is such a large error in the EXA map cannot be answered conclusively. Various measurement points, including sites with direct altitude measurements on the glacier are present on the map, yet contour lines in between them are off by a couple hundred meters. As the map is based on photogrammetry, the large error on Mueller Ice Cap is most likely the result of a misinterpretation of aerial images. Since the accumulation area is largely feature less, optical reading errors are facilitated (Paul *et al.*, 2017). The poor illumination documented in the reports of the flights, as well as the low number of flights over the accumulation area (Haumann, 1963) point to this explanation.

The data error on the EXA map roughly corresponds to one seventh of Thompson Glacier's total area with a substantial impact on values derived for a glacier-wide scale. The benefit of such a large error is its easy discoverability. However, the appearance of optical reading errors on the EXA map implicates that the same kind of error may be present on the TGR map, as optical photogrammetry was used supplementary to ground survey (Cogley and Jung-Rothenhäusler, 2002). In general, this thesis shows that historical map material needs to be questioned if used for geodetic mass balance calculations. The error on the EXA map translate into a strongly negative mass balance for Thompson Glacier while at the same time resulting in a highly positive glacier wide elevation gain for Transit Glacier. This demonstrates the importance of considering uncertainties in historical elevation data, especially in cases where map metadata is limited.

7.5 Influence of Void Filling

The different methods to fill the data void in the accumulation area have a great impact on the derived results. Each approach directly influences the estimates of geodetic mass balance values (McNabb *et al.*, 2019). Thus, assessing the strengths and weaknesses of both methods is necessary.

Using a zero-change approach is the easiest method to quickly draw up a comparison scenario to the values derived from the historical maps. As strong negative changes are unlikely in the accumulation area (Paul *et al.*, 2017), the zero-change approach demonstrates which order of magnitude for glacier-wide changes is more plausible. The method thus helps to assess the impact of extreme values within the accumulation area. In the case of Thompson Glacier, switching from the historical map input to a zero-change accumulation area reduces the glacier-wide elevation change by a factor of six, showing how far off the values from the EXA map are. However, the values derived from the zero-change approach should not be interpreted as reliable results either, as the method includes little knowledge of the local setting, and produces sharp borders within the generated DEM.

The issue of lacking detail in the zero-change approach is resolved by implementing the hypsometric method. Structuring the void filling based on the assumption that elevation change rates are dependent on elevation itself allows for a more nuanced reconstruction of altitude bands. Nonetheless, using elevation bins to fill the void is impaired by the uncertainty within the values used to define the bins. Undetected errors in the area where elevation bins are defined greatly impact the reconstructed area. In this thesis, the accuracy of the elevation data used to derive elevation bins is

uncertain. The resulting void fill is based on the assumption that the TGR map input is reliable. Furthermore, it assumes that elevation change values found on HIF represent the conditions on MIC, which introduces a bias towards the setting on HIF. Therefore, values presented for the modified DEM are estimates of the most plausible scenario using as many of the available information as possible.

7.6 Importance of Assessing Error Propagation

The mass balance estimates derived in this thesis aim to incorporate all quantifiable errors which helps to quantify the results. However, a variety of uncertainties appearing throughout the workflow cannot be measured directly. For example: The uncertainty regarding the accuracy of contour lines is integrated into the number of independent samples by declaring only half of them as valid. In doing so, the uncertainty within the resulting DEM can be statistically represented, but it does not describe the error in detail. Sources of errors within contour lines are manifold: First, there is no indication for the accuracy of contour lines on the historical map. Second, the ArcScan algorithm generates contour lines by following a centre line fitted to certain pixel values. This entails uncertainties in both the derived centre line and the pixels which are classified as a contour. Next, faultily generated contour lines were corrected manually using the historical map for comparison. This introduces the potential of reading errors.

The number of potential uncertainties is unlimited. Yet, the modelling of error propagation is only possible if full information of each step is available (Paul *et al.*, 2017). Since this is unlikely the case, the application of the statistical approach to error propagation offers a more practical toolset to assess uncertainties (Zemp *et al.*, 2013). This is a necessary step in quantifying any obtained results, as it indicates if the implemented methods fit the objective of the study. In this thesis, the statistical error bars turn out relatively small. This can be explained by the error assessment's reliance on assumptions for uncertainty and certain statistical considerations (Zemp *et al.*, 2015). Nonetheless, the calculated uncertainties demonstrate where values are least reliable. In the case of the outliers within the observed glaciers, the detected error for the HIF is smaller, rendering its positive mass balance more plausible. The strongly negative mass balance of Finger Glacier shows a larger error, which indicating that its values might be too low.

Equally important is the assessment of uncertainties that are not included in the statistical approach to error propagation. The large uncertainty in the accumulation area on the EXA map, while visually detected, is not represented within the resulting error bars. Thus, if only uncorrelated and random errors are considered, the historical dDEM of Thompson Glacier shows a strongly negative glacier-wide elevation change with an acceptable range of error (-24.41 ± 1.12 m). Given that the assessment of error propagation accounts for many uncertainties, the result is seemingly plausible. But, as shown above, ridding the accumulation area of implausible values leads to a much smaller change in glacier-wide elevation. In sum, the assessment of both random and correlated errors is crucial. The statistical approach to error propagation delivers the means to quantify results and offers support for their discussion. Yet, clear faults in the input data need to be detected and omitted to clear the way for statistical testing.

8. Conclusion & Outlook

8.1 Conclusion

The main goal of this thesis was to derive the geodetic mass balance of Thompson Glacier, to gain more insight into the changes in the glacierized regions of the Canadian Arctic Archipelago. As most of the glacier's historical accumulation area is only available on unreliable maps, the thesis further tackled the issue of handling large data voids in order to reconstruct a plausible historical glacier state. The process of deriving the glacier's mass balance is thus accompanied by many uncertainties, which are assessed by a statistical approach. The outcome is concluded below, along with the research questions posed at the beginning of this thesis.

a.) How did Thompson Glacier's ice mass change during the period of 1960 to 2014±4?

This thesis shows that Thompson Glacier, despite advancing for most of the past decades, exhibits a negative mass balance which translates into a relatively large loss of ice mass. Using a reconstructed historical accumulation area to omit overly negative elevation change, the geodetic mass balance amounts to –5.49±0.91 m w.e. over the period of record. This falls in line with mass balances of other glaciers in the Canadian Arctic, albeit being slightly less negative in comparison. Nonetheless, the geodetic mass balance corresponds to a loss of –2.06±0.42 Gt of ice, showing the large impact of a changing climate on Thompson Glacier.

b.) How reliable is the use of historical maps in deriving geodetic mass balances for glaciers?

The detailed historical maps are useful to derive a DEM of past glacier states with good spatial resolution. However, the historical input data undergoes a variety of processes until it can be compared to its contemporary counterpart. Digitization, interpolation, co-registration, and void-filling each introduce errors to the elevation data, increasing the total uncertainty within the obtained results. Here, the quality of the historical map directly translates to applicability of its derived DEM. Furthermore, the inaccuracies in the accumulation area encountered in this thesis demonstrate that errors on historical maps impact resulting mass balances to a high degree. Such errors might not be easily detectable in other cases, especially where little information on the map's production is documented. The reliability of historical maps is thus dependent on both the detail on the map, as well as the detail in the map's metadata.

c.) How do different approaches to reconstruct large data voids affect the obtained results?

Regardless of the implemented void-filling method, Thompson Glacier's mass balance results negative. But, the obtained values from both approaches diverge significantly. Assuming a zero-change scenario in the accumulation area yields the least negative mass balance values. However, this approach includes little of the knowledge on local changes resulting in a probable underestimation of the glacier's mass change. On the other hand, using a hypsometric void-filling method results in values which are strongly influenced by the elevation change derived from the area where elevation bins were defined. While this leads to more nuanced results, uncertainties within the elevation bins directly propagate to the filled data void. In sum, the method chosen to fill a large data void controls the consequent results. This needs to be reflected in the presentation of obtained data. The better explicable an assumption for a void fill is, the more supportable are the resulting values.

d.) How relevant is the assessment of error propagation regarding the quantification of obtained results?

This thesis shows that the assessment of error propagation is a necessary step to quantify the results of geodetic mass balance calculations. Uncertainties within the used input data may cause strongly distorted results which highlights the importance of checking the used data for its reliability. However, not all errors are evident. The implementation of the statistical approach to test error propagation allows for an assessment of these uncertainties. This process helps to support or reject obtained results, offering the means to judge whether the derived values are reliable.

8.2 Outlook

The findings of this thesis demonstrate that Thompson Glacier exhibits a considerable loss in ice-mass, despite advancing over most of the period of record. Since the glacier started its retreat only recently, it can be assumed that most of the negative changes happened over a relatively short time span. Assessing the current behaviour of Thompson Glacier, including short-term trends, in more detail would help to identify the speed of the glacier's retreat. Due to its large size, negative changes on Thompson Glacier significantly contribute to the Canadian Arctic's contribution to global sea level rise. Thus, future monitoring of the glacier is vital.

As for the methods implemented to fill data voids, a more comprehensive assessment of the accuracy of a reconstructed accumulation is desirable. Testing if known glacier areas can be reconstructed accurately with the applied approaches would contribute to further support the findings of this thesis. Further assessing the reliability of large, reconstructed glacier areas allows the implementation of the methods in other areas where large parts of glaciers are missing.

9. Literature

Berthier, E. *et al.* (2004) 'Recent rapid thinning of the '"Mer de Glace'" glacier derived from satellite optical images', *Geophysical Research Letters*, 31, pp. 2–5.

Berthier, E. *et al.* (2010) 'Contribution of Alaskan glaciers to sea-level rise derived from satellite imagery', *Nature Geoscience*. Nature Publishing Group, 3(2), pp. 92–95. doi: 10.1038/ngeo737.

Blachut, T. J. and Müller, F. (1966) 'Some fundemental Considerations on Glacier Mapping', *Canadian Journal of Earth Sciences*, 3(6), pp. 747–759.

Bolch, T., Menounos, B. and Wheate, R. (2010) 'Remote Sensing of Environment Landsat-based inventory of glaciers in western Canada , 1985 – 2005', *Remote Sensing of Environment*, 114(1), pp. 127–137. doi: 10.1016/j.rse.2009.08.015.

Brun, F. *et al.* (2017) 'A spatially resolved estimate of High Mountain Asia glacier mass balances from 2000 to 2016', *Nature Geoscience*, 10(9), pp. 668–673. doi: 10.1038/ngeo2999.

Cogley, J. G. and Adams, W. P. (2000) 'Remote-Sensing Resources for Monitoring Glacier Fluctuations on Axel Heiberg Island', *Arctic*, 53(3), pp. 248–259.

Cogley, J. G., Adams, W. P. and Ecclestone, M. A. (2011) 'Half a Century of Measurements of Glaciers on Axel Heiberg Island, Nunavut, Canada', *Arctic*, 64(3), pp. 371–375.

Cogley, J. G. and Jung-Rothenhäusler, F. (2002) 'Digital Elevation Models of Axel Heiberg Island Glaciers', *Trent Technical Note*, 1(May).

Copland, L., Sharp, M. J. and Dowdeswell, J. A. (2003) 'The distribution and flow characteristics of surge-type glaciers in the Canadian High Arctic', *Annals of Glaciology*, 36, pp. 73–81. doi: 10.3189/172756403781816301.

Cox, L. H. and March, R. S. (2004) 'Comparison of geodetic and glaciological mass-balance techniques, Gulkana Glacier, Alaska, U.S.A', *Journal of Glaciology*, 50(170), pp. 363–370. doi: 10.3189/172756504781829855.

Dussaillant, I., Berthier, E. and Brun, F. (2018) 'Geodetic Mass Balance of the Northern Patagonian Icefield from 2000 to 2012 Using Two Independent Methods', *Frontiers in Earth Science*, 6(8), pp. 1–13. doi: 10.3389/feart.2018.00008.

Fountain, A. G., Krimmel, R. M. and Trabant, D. C. (1997) 'A Strategy for Monitoring Glaciers', *U.S. Geological Survey circular*, 1132, pp. 1–19.

Gardelle, J. *et al.* (2013) 'Region-wide glacier mass balances over the Pamir-Karakoram-Himalaya during 1999-2011 (vol 7, pg 1263, 2013)', *The Cryosphere*, 7, pp. 1885–1886. doi: 10.5194/tc-7-1263-2013.

Gardner, A. S. *et al.* (2011) 'Sharply increased mass loss from glaciers and ice caps in the Canadian Arctic Archipelago', *Nature*, 473(7347), pp. 357–360. doi: 10.1038/nature10089.

Haumann, D. (1963) 'Surveying glaciers in Axel Heiberg Island', *The Canadian Surveyor*, 17(12), pp. 81–93.

Haumann, D. and Honegger, D. (1962) 'Thompson Glacier - Axel Heiberg Island, Northwest Territories, Canada, 1:50'000', in *WGMS (2018): Glacier Map Collection (GMC)*. Zurich, Switzerland: World Glacier Monitoring Service (WGMS).

Huber, J., McNabb, R. and Zemp, M. (2020) 'Elevation Changes of West-Central Greenland Glaciers From 1985 to 2012 From Remote Sensing', *Frontiers in Earth Science*, 8(35), pp. 1–16. doi: 10.3389/feart.2020.00035.

Huss, M. (2013) 'Density assumptions for converting geodetic glacier volume change to mass change', *The Cryosphere*, (4), pp. 877–887. doi: 10.5194/tc-7-877-2013.

Hutchinson, M. F. (1989) 'A new procedure for gridding elevation and stream line data with automatic removal of spurious pits', *Journal of Hydrology*, 106, pp. 211–232.

Hutchinson, M. F., Xu, T. and Stein, J. A. (2011) 'Recent Progress in the ANUDEM Elevation Gridding Procedure Recent Progress in the ANUDEM Elevation Gridding Procedure', in *Geomorphometry*, pp. 19–22.

Kälin, M. (1971) *The active push moraine of the Thompson Glacier, Axel Heiberg Island, Canadian Arctic Archipelago, Canada*. McGill University. doi: 10.3929/ethz-a-010782581.

Kuhn, M. *et al.* (1985) 'Fluctuations of climate and mass balance: different responses of two adjacent glaciers.', *Zeitschrift fur Gletscherkunde und Glazialgeologie*, 21, pp. 409–416.

Magnússon, E. *et al.* (2016) 'Geodetic mass balance record with rigorous uncertainty estimates deduced from aerial photographs and lidar data – Case study from Drangajökull ice cap, NW Iceland', *The Cryosphere*, 10(1), pp. 159–177. doi: 10.5194/tc-10-159-2016.

McNabb, R. *et al.* (2019) 'Sensitivity of glacier volume change estimation to DEM void interpolation', *The Cryosphere*, 13(3), pp. 895–910. doi: 10.5194/tc-13-895-2019.

Meredith, M. *et al.* (2019) 'Polar regions', in *IPCC Special Report on the Ocean and Cryosphere in a Changing Climate*, pp. 203–320. doi: 10.1016/S1366-7017(01)00066-6.

Moisan, Y. and Pollard, W. H. (1995) 'Processus d'edification de la structure de poussée du glacier thompson, Île Axel Heiberg, Territoires du Nord-Ouest', *Canadian Geographer*, 39(1), pp. 58–67.

Müller, F. (1962) *Glacier Mass-Budget Studies on Axel Heiberg Island, Canadian Arctic Archipelago*. Montreal, Canada: McGill University.

Müller, F. and Harrison, J. (1965) 'Expedition Area – Axel Heiberg Island Canadian Arctic Archipelago 1 : 100000', in *WGMS (2018): Glacier Map Collection (GMC)*. Zurich, Switzerland: World Glacier Monitoring Service (WGMS). doi: 10.5904/wgms-maps-2018-02.

Nilsson, J. *et al.* (2015) 'Mass changes in Arctic ice caps and glaciers : implications of regionalizing elevation changes', *The Cryosphere*, 9, pp. 139–150. doi: 10.5194/tc-9-139-2015.

Nuth, C. and Kääb, A. (2011) 'Co-registration and bias corrections of satellite elevation data sets for quantifying glacier thickness change', *The Cryosphere*, 5(1), pp. 271–290. doi: 10.5194/tc-5-271-2011.

Ommanney, C. S. L. (1969) *A study in glacier inventory; the ice masses of Axel Heiberg Island, Canadian Arctic archipelago*. Montreal, Canada: McGill University.

Paul, F. *et al.* (2015) 'The glaciers climate change initiative: Methods for creating glacier area, elevation change and velocity products', *Remote Sensing of Environment*. Elsevier Inc., 162, pp. 408–426. doi: 10.1016/j.rse.2013.07.043.

Paul, F. *et al.* (2017) 'Error sources and guidelines for quality assessment of glacier area, elevation change, and velocity products derived from satellite data in the Glaciers_cci project', *Remote*

Sensing of Environment. Elsevier, 203(November 2016), pp. 256–275. doi: 10.1016/j.rse.2017.08.038.

Pellitero, R. *et al.* (2016) 'GlaRe, a GIS tool to reconstruct the 3D surface of palaeoglaciers', *Computers and Geosciences*. Elsevier, 94, pp. 77–85. doi: 10.1016/j.cageo.2016.06.008.

Pieczonka, T. *et al.* (2013) 'Heterogeneous mass loss of glaciers in the Aksu-Tarim Catchment (Central Tien Shan) revealed by 1976 KH-9 Hexagon and 2009 SPOT-5 stereo imagery', *Remote Sensing of Environment*. Elsevier Inc., 130, pp. 233–244. doi: 10.1016/j.rse.2012.11.020.

Pieczonka, T. and Bolch, T. (2015) 'Region-wide glacier mass budgets and area changes for the Central Tien Shan between ~1975 and 1999 using Hexagon KH-9 imagery', *Global and Planetary Change*. Elsevier B.V., 128, pp. 1–13. doi: 10.1016/j.gloplacha.2014.11.014.

Rastner, P. *et al.* (2012) 'The first complete inventory of the local glaciers and ice caps on Greenland', *The Cryosphere*, 6(6), pp. 1483–1495. doi: 10.5194/tc-6-1483-2012.

Sharp, M. *et al.* (2011) 'Extreme melt on Canada's Arctic ice caps in the 21st century', *Geophysical Research Letters*, 38(11), pp. 3–7. doi: 10.1029/2011GL047381.

Thomson, L. I. *et al.* (2017) 'Comparison of geodetic and glaciological mass budgets for White Glacier, Axel Heiberg Island, Canada', *Journal of Glaciology*, 63(237), pp. 55–66. doi: 10.1017/jog.2016.112.

Thomson, L. I. and Copland, L. (2017) 'Multi-decadal reduction in glacier velocities and mechanisms driving deceleration at polythermal White Glacier , Arctic Canada', *Journal of Glaciology*, 63(239), pp. 450–463. doi: 10.1017/jog.2017.3.

Thomson, L. I., Osinski, G. R. and Ommanney, C. S. L. (2011) 'Glacier change on Axel Heiberg Island, Nunavut, Canada', *Journal of Glaciology*, 57(206), pp. 1079–1086. doi: 10.3189/002214311798843287.

WGMS (2019) 'Fluctuations of Glacier Database'. Zurich, Switzerland: World Glacier Monitoring Service. doi: 10.5904/wgms-fog-2019-12.

Zemp, M. *et al.* (2013) 'Reanalysing glacier mass balance measurement series', *The Cr*. doi: 10.5194/tc-7-1227-2013.

Zemp, M. *et al.* (2015) 'Historically unprecedented global glacier decline in the early 21st century', *Journal of Glaciology*, 61(228), pp. 745–762. doi: 10.3189/2015JoG15J017.

Zemp, M. *et al.* (2019) 'Global glacier mass changes and their contributions to sea-level rise from 1961 to 2016', *Nature*, 568(7752), pp. 382–386. doi: 10.1038/s41586-019-1071-0.

Appendix

A. Historical Maps
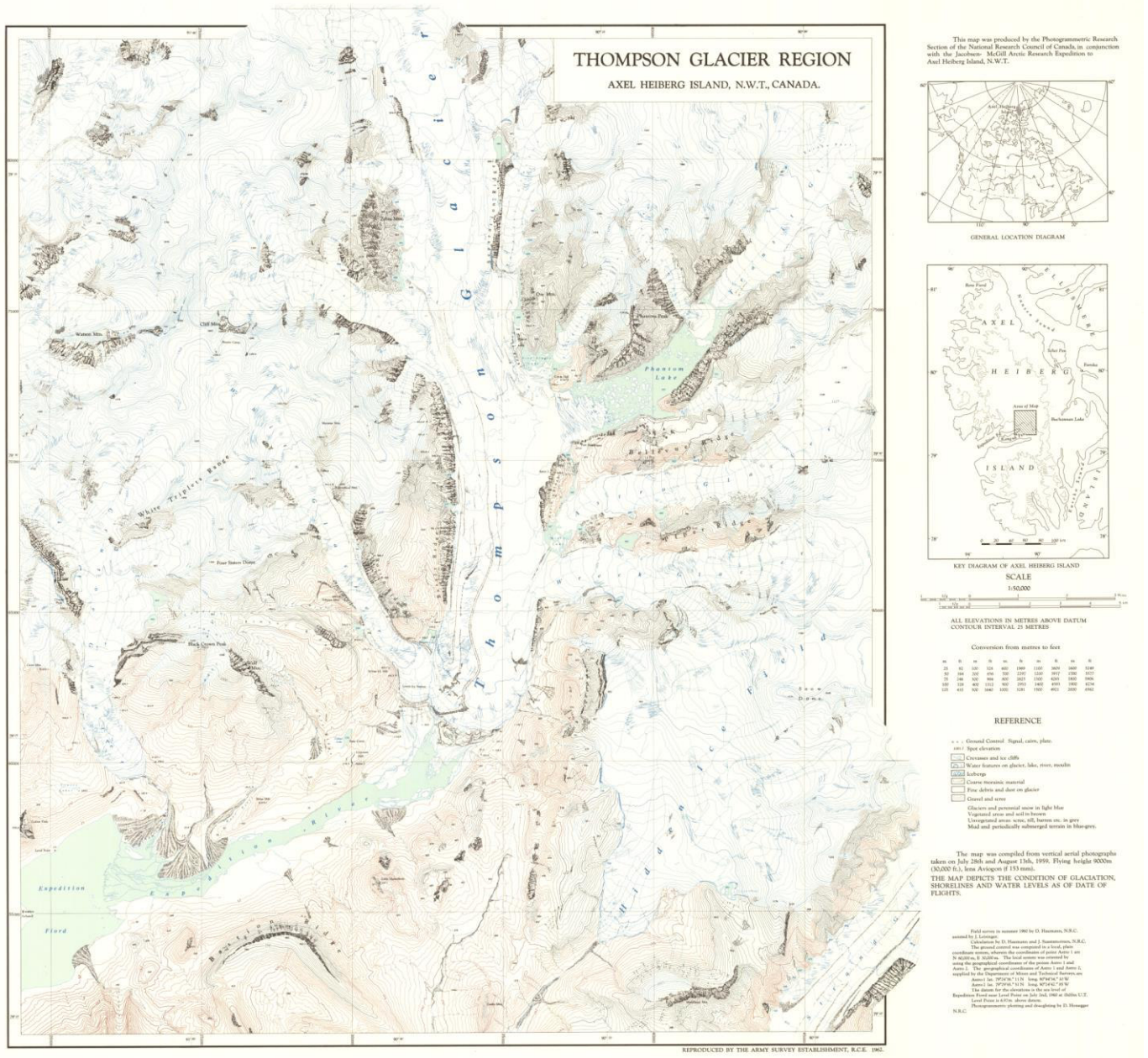
Appendix 1: National Research Council, 1962, Thompson Glacier Region, Axel Heiberg Island, N.W.T., Canada at 1:50'000 scale. Photogrammetric Research Section, National Research Council of Canada, Ottawa, in conjunction with Axel Heiberg Island Expedition, McGill University, Montreal.

ALL ELEVATIONS IN METRES ABOVE DATUM
CONTOUR INTERVAL 25 METRES

Conversion from metres to feet

m	ft	m	ft	m	ft	m	ft	m	ft
25	82	100	328	600	1969	1100	3609	1600	5249
50	164	200	656	700	2297	1200	3937	1700	5577
75	246	300	984	800	2625	1300	4265	1800	5906
100	328	400	1312	900	2953	1400	4593	1900	6234
125	410	500	1640	1000	3281	1500	4921	2000	6562

REFERENCE

▲ ■ . Ground Control Signal, cairn, plate.

1081.7 Spot elevation

Crevasses and ice cliffs

Water features on glacier, lake, river, moulin

Icebergs

Coarse morainic material

Fine debris and dust on glacier

Gravel and scree

Glaciers and perennial snow in light blue
Vegetated areas and soil in brown
Unvegetated areas: scree, till, barren etc. in grey
Mud and periodically submerged terrain in blue-grey.

The map was compiled from vertical aerial photographs taken on July 28th and August 13th, 1959. Flying height 9000m (30,000 ft.), lens Aviogon (f 153 mm).

THE MAP DEPICTS THE CONDITION OF GLACIATION, SHORELINES AND WATER LEVELS AS OF DATE OF FLIGHTS.

Field survey in summer 1960 by D. Haumann, N.R.C. assisted by J. Leisinger.
Calculation by D. Haumann and J. Saastamoinen, N.R.C.
The ground control was computed in a local, plain coordinate system, wherein the coordinates of point Astro 1 are N 60,000 m, E 30,000 m.   The local system was oriented by using the geographical coordinates of the points Astro 1 and Astro 2.   The geographical coordinates of Astro 1 and Astro 2, supplied by the Department of Mines and Technical Surveys, are
Astro 1 lat. 79°24'36." 11 N   long. 90°44'34." 10 W
Astro 2 lat. 79°29'45." 51 N   long. 90°24'42." 85 W
The datum for the elevations is the sea level of Expedition Fiord near Level Point on July 2nd, 1960 at 1h00m U.T.
Level Point is 6.97m above datum.
Photogrammetric plotting and draughting by D. Honegger N.R.C.

Appendix 2: Thompson Glacier Region Map metadata, presented on the map itself.
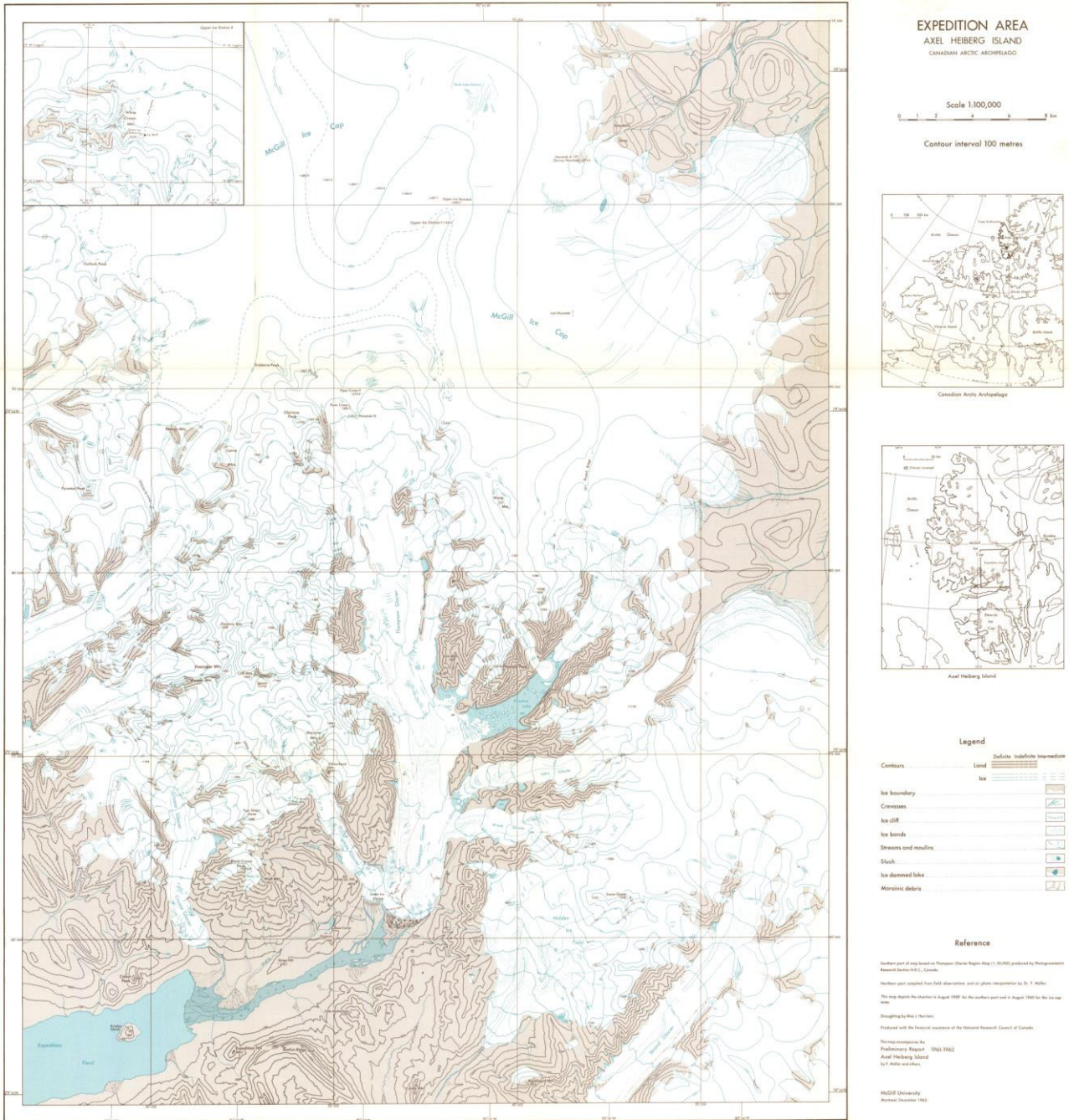
Appendix 3: McGill University, 1963, Expedition Area, Axel Heiberg Island, Canadian Arctic Archipelago. Map at 1:100'000 scale. Accompanies Müller, F., et al., 1963, Preliminary Report, 1961-1962, Axel Heiberg Island Research Reports, McGill University, Montreal.

Appendix

Legend

	Definite	Indefinite	Intermediate
Contours............ Land			
Ice			

Ice boundary...

Crevasses ....

Ice cliff...

Ice bands ....

Streams and moulins...

Slush...

Ice dammed lake ....

Morainic debris...

Reference

Southern part of map based on Thompson Glacier Region Map (1: 50,000) produced by Photogrammetric Research Section N.R.C., Canada.

Northern part compiled from field observations and air photo interpretation by Dr. F. Müller.

This map depicts the situation in August 1959 for the southern part and in August 1960 for the ice cap area.

Draughting by Miss J. Harrison.

Produced with the financial assistance of the National Research Council of Canada.

This map accompanies the
Preliminary Report   1961-1962
Axel Heiberg Island
by F. Müller and others.

McGill University
Montreal, December 1963.

Appendix 4: Expedition Area Map metadata, presented on the map itself.

B. Co-Registration

Appendix Table 1: First iteration results for Co-Registration parameters and shift vectors using the TanDEM-X digital elevation model as master DEM and the historical DEM as slave DEM.

TanDEM-X Iteration 1

Co-Registration Parameters		Output	
a	28.45	**ΔX**	-11.4
b	-23.59	**ΔY**	26.1
c	-19.86	**ΔZ**	-6.5
RMSE	35.95		
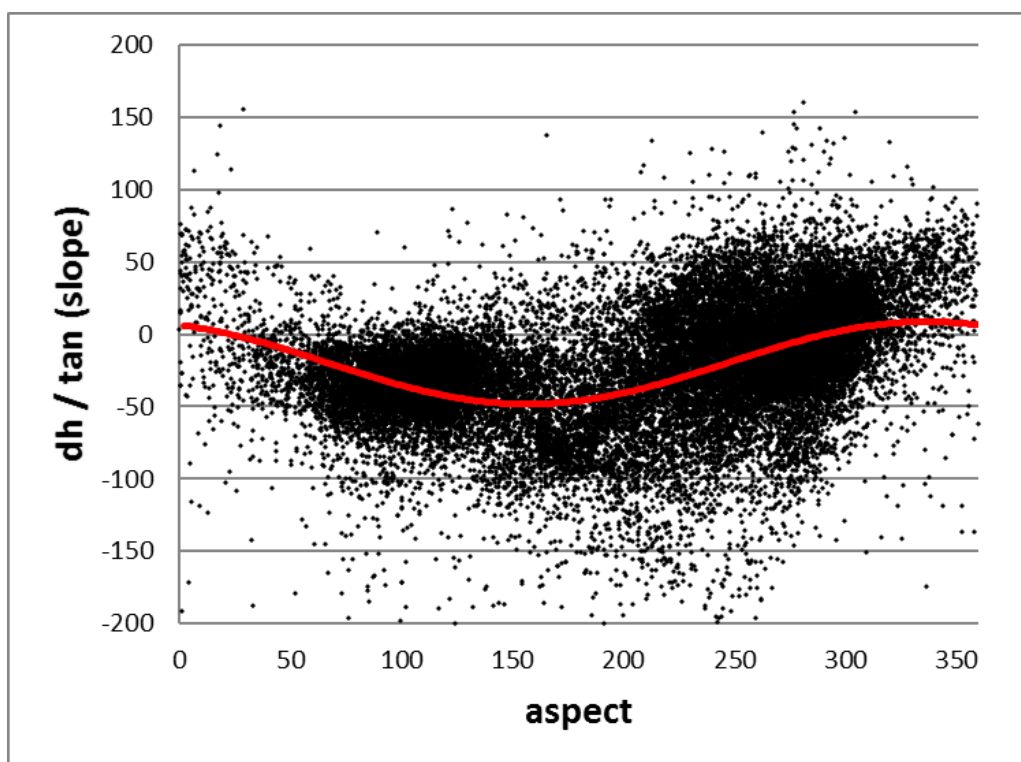
Appendix 5: Curve-fit for the first iteration of Co-Registration. Historical DEM against TanDEM-X.
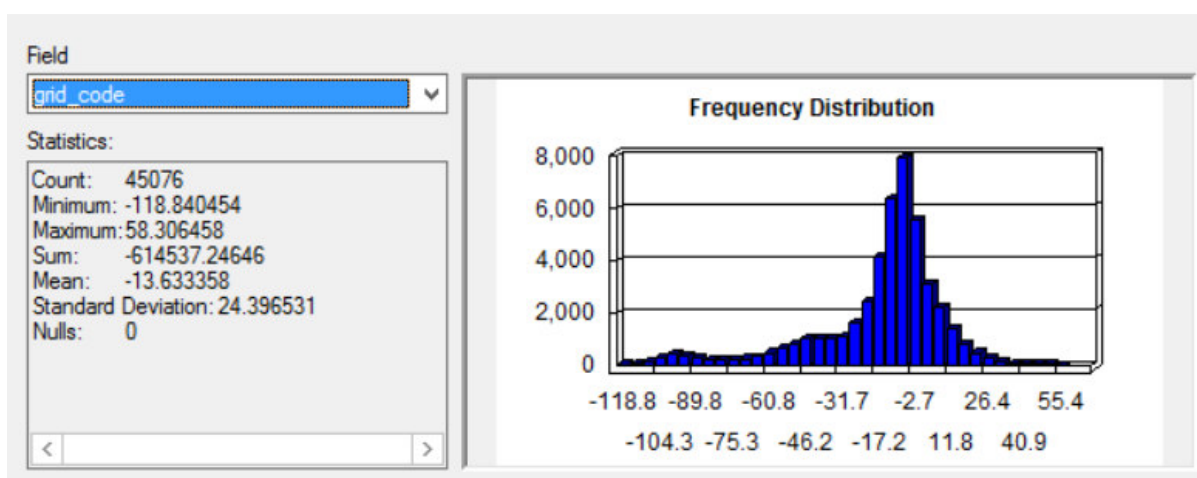
Appendix 6: ArcMap statistics and histogram of elevation difference over stable terrain before Co-Registration. Historical DEM against TanDEM-X

Appendix

Appendix Table 2: Resulting Co-Registration after the third and last iteration for the difference image of TanDEM-X and the historical DEM.

TanDEM-X Iteration 3

Co-Registration Parameters		Output	
a	6.55	ΔX	6.0
b	66.62	ΔY	2.6
c	-18.67	ΔZ	-6.1
RMSE	32.91		
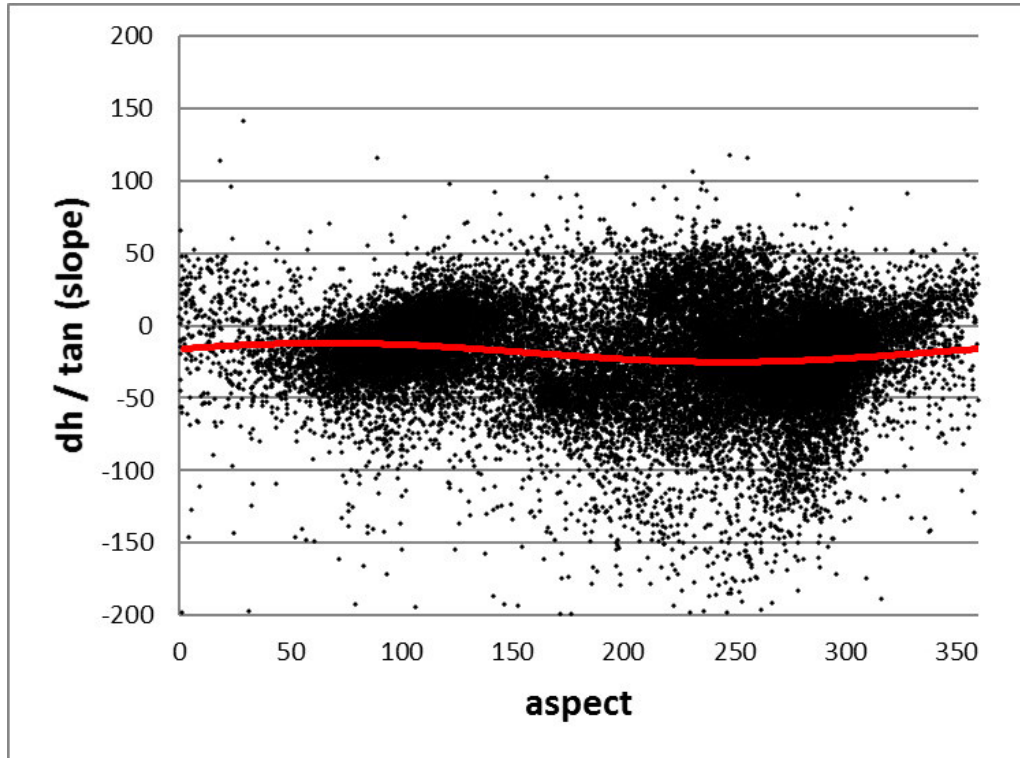
Appendix 7: Curve-fit for the third iteration of Co-Registration. Historical DEM against TanDEM-X.

Field

grid_code

Statistics:

Count: 45385
Minimum: -99.169617
Maximum: 69.164917
Sum: -343271.925552
Mean: -7.563555
Standard Deviation: 21.401558
Nulls: 0

Frequency Distribution
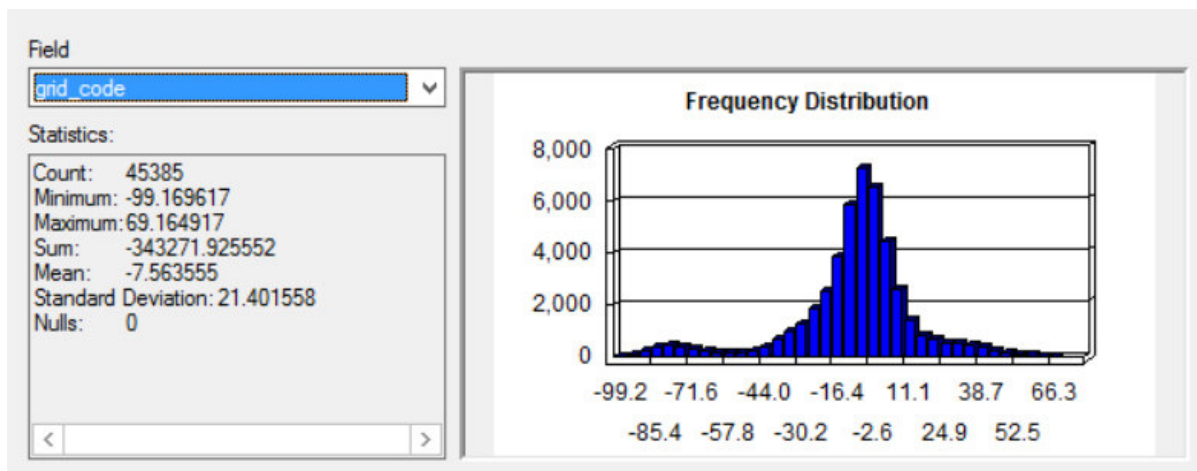
Appendix 8: ArcMap statistics and histogram of elevation differences over stable terrain after Co-Registration. Historical DEM against TanDEM-X.

Appendix Table 3: First iteration results for Co-Registration parameters and shift vectors using the ArcticDEM digital elevation model as master DEM and the historical DEM as slave DEM.

ArcticDEM Iteration 1

Co-Registration Parameters		Output	
a	33.44229	ΔX	27.16255
b	54.31356	ΔY	19.50853
c	-20.5391	ΔZ	-8.82007
RMSE	52.88376		
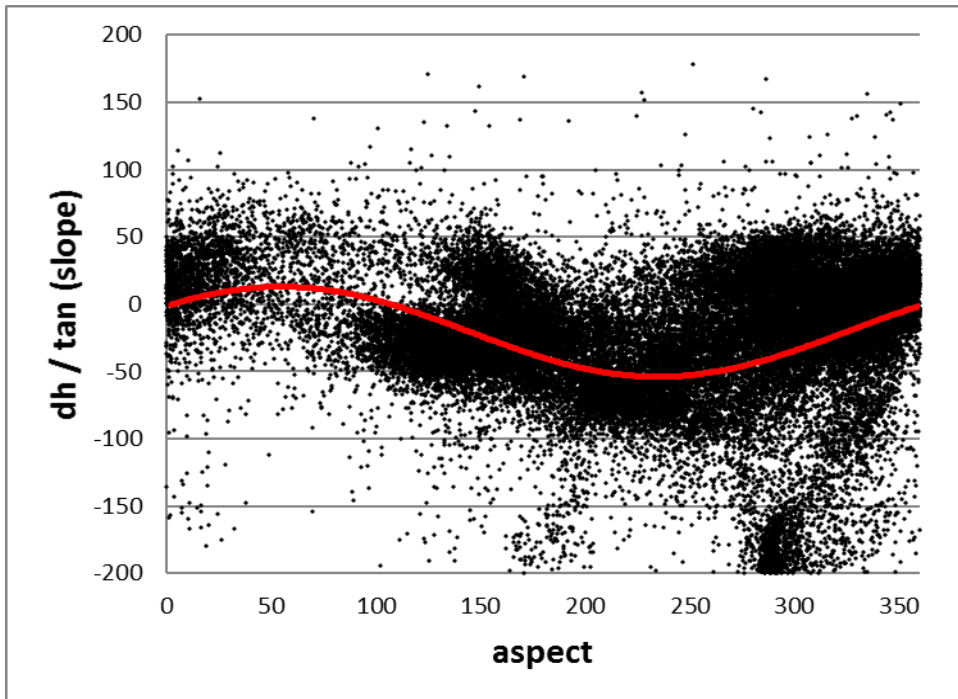
Appendix 9: Curve-fit for the first iteration of Co-Registration. Historical DEM against ArcticDEM.
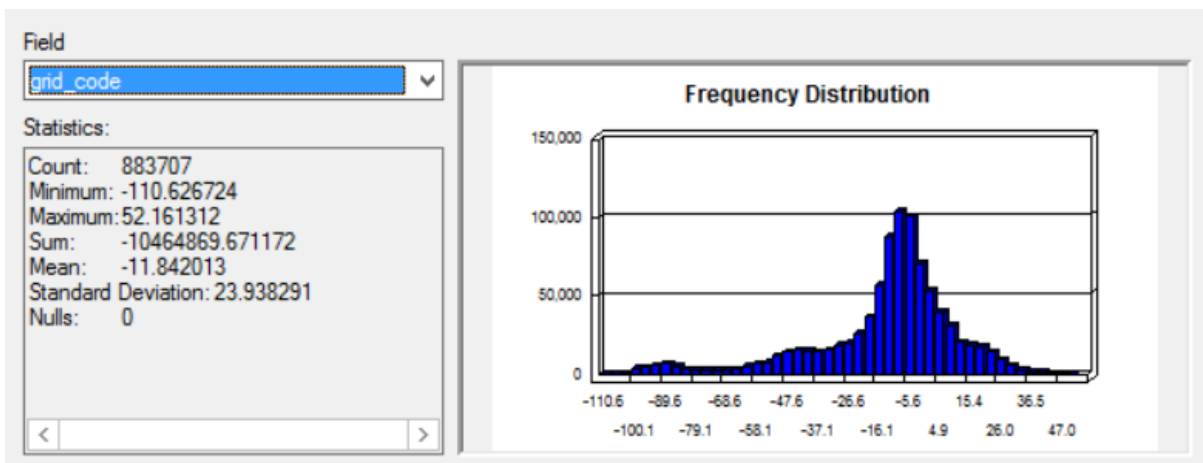
Appendix 10: ArcMap statistics and histogram of elevation change over stable terrain before Co-Registration. Historical DEM against ArcticDEM.

Appendix

Appendix Table 4: Resulting Co-Registration parameters and shift vectors after the fifth and final iteration for the difference image between the historical DEM and ArcticDEM digital elevation models.

ArcticDEM Iteration 5

Co-Registration Parameters		Output	
a	-12.794	ΔX	-4.88429
b	22.44303	ΔY	-11.825
c	-16.9712	ΔZ	-7.28791
RMSE	51.01621		
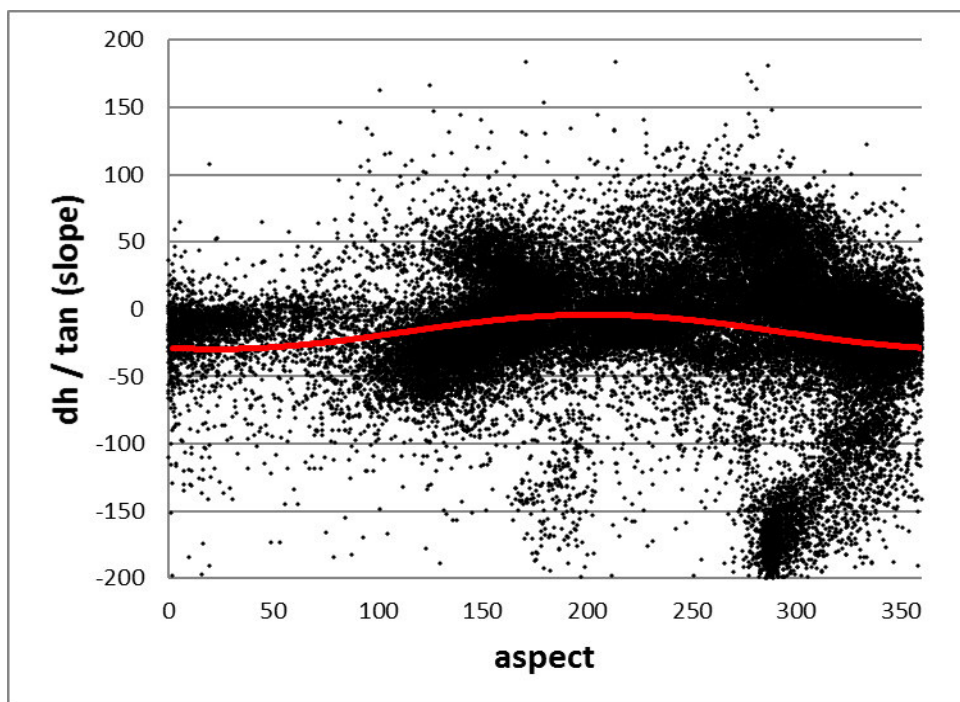
Appendix 11: Curve-fit for the fifth Co-Registration iteration. Historical DEM against ArcticDEM.
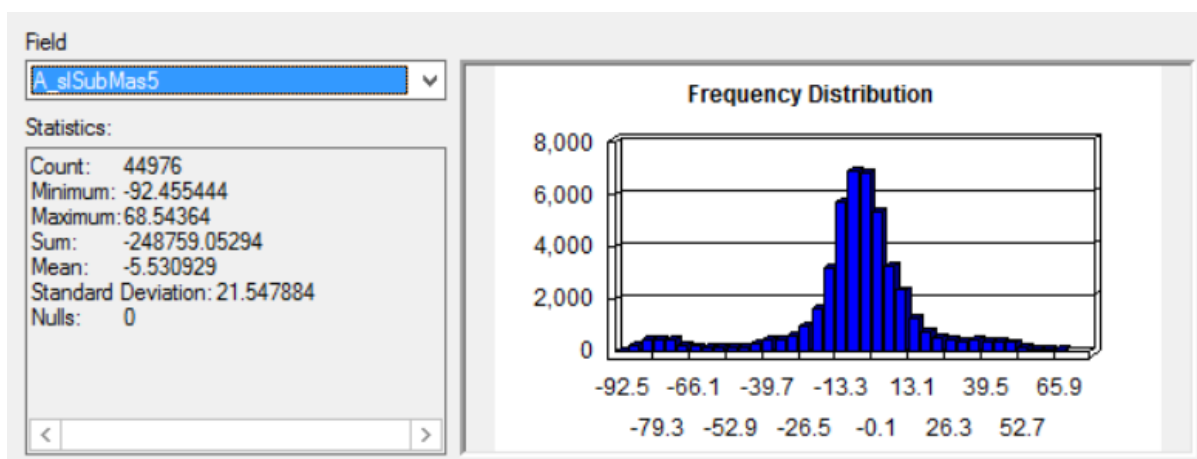
Appendix 12: ArcMap statistics and histogram of elevation change over stable terrain after Co-Registration. Historical DEM against ArcticDEM. The smaller sample size (Count) in comparison to the initial state is the result of resampling the stable terrain point cloud. This is due to the total number of points in the Co-Registration tool being limited.

C. Elevation Bin Modifiers

Appendix Table 5: HIF Mean elevation per elevation bin values and White Glacier mean elevation per elevation bin trend values from Thomson et al. (2017: 60). The mean values were used to modify contours in order to derive the Modified Historical DEM.

	HIF Value Modifier	WG Trend Modifier
Elevation Bin [m a.s.l.]	**Mean [m]**	**Mean [m]**
850	-4.571767	-22.5
900	0.412164	-25
950	7.738266	-22.5
1000	8.680869	-20
1050	7.858017	-20
1100	12.746616	-17.5
1150	19.548944	-15
1200	19.75275	-15
1250	19.487301	-10
1300	25.729283	-10
1350	14.139814	-5
1400	3.15009	-5
1450	3.770004	0
1500	-2.685283	2.5
1550	0	7.5
1600	0	7.5
1650	0	10
1700	0	10
1750	0	7.5
1800	0	5
1850	0	2.5

Appendix

D. Geodetic Mass Balances

Presented below are the calculations of geodetic mass balances for all observed glaciers. All derived values are highlighted in grey, blue font indicates an important intermediate result. Results presented as most probable value are highlighted in yellow.

Appendix Table 6: Calculation of geodetic mass balances with error assessment for Thompson Glacier. All results use ArcticDEM elevation data as contemporary input data.

Thompson Glacier		dDEM		
		Historical dDEM	Modified dDEM	ZeroChange dDEM
Area [m²]	S_1960		378324467.83	
	S_2014		372106808.27	
	S_avg		375215638.05	
Volume Change	r² [m²]		16	
	K		23951947	
	Σ_Δh_k [m]	-572518593	-151034379	-105011932
	ΔV [m³]	-9160297488	-2416550064	-1680190912
Conversion Factor	ρ_glac [kg m⁻³]		850	
	ρ_water [kg m⁻³]		997	
	ρ_ratio		0.852557673	
B_geod	Δh_avg	-24.41	-6.44	-4.48
	B_geod.PoR (m w.e.)	-20.81	-5.49	-3.82
	B_geod.a (m w.e. yr⁻¹)	-0.38	-0.10	-0.07
Error Assessment				
Calc. σ_DEM	CoReg_StDev		21.55	
	L		500	
	(n/(L/r))		191615.576	
	(c/2)		2250	
	n_mean		96932.788	
	σ_DEM		0.14	
Calc. σ_void	n_void		9399706	8825352
	(c/2)_void		603	120
	(n_void/(L/r))		75197.648	70602.816
	n_void_mean		37900.324	4412736
	Void_stdDev		19.894	6.86
	σ_void		0.10	0.003
Calc. σ_B	σ_date	-1.11	-0.29	-0.20
	σ_Δh	1.12	0.34	0.24
	σ_ρ		60	
	σ_B	1.75	0.48	0.34
Calc. σ_ΔM	ΔM [Gt]	-7.81	-2.06	-1.43
	σ_S		18760781.9	
	σ_ΔM	0.76	0.21	0.15
Results	B_geod.PoR [m w.e.]	-20.81±1.75	-5.49±0.48	-3.82±0.34
	ΔM [Gt]	-7.81±0.76	-2.06±0.21	-1.43±0.15

X

Appendix Table 7: Calculation of geodetic mass balances with error assessment for Astro Glacier. All results use ArcticDEM elevation data as contemporary input.

Astro Glacier

		dDEM	
		Historical dDEM	Modified dDEM
Area [m²]	S_1960	38446321.00	
	S_2014	38354485.19	
	S_avg	38400403.10	
Volume Change	r² [m²]	16	
	K	2343229	
	Σ_Δh_k [m]	-572518593	-151034379
	ΔV [m³]	-324112272	-389615040
Conversion Factor	ρ_glac [kg m⁻³]	850	
	ρ_water [kg m⁻³]	997	
	ρ_ratio	0.852557673	
B_geod	Δh_avg	-8.44	-10.15
	B_geod.PoR (m w.e.)	**-7.20**	**-8.65**
	B_geod.a (m w.e. yr⁻¹)	-0.13	-0.16
Error Assessment			
Calc. σ_DEM	CoReg_StDev	21.55	
	L	500	
	(n/(L/r))	18745.832	
	(c/2)	220	
	n_mean	9482.916	
	σ_DEM	0.43	
Calc. σ_void	n_void		756630
	(c/2)		44
	(n_void/(L/r))		6053.04
	n_void_mean		3048.52
	Void_stdDev		13.1516
	σ_void		0.24
Calc. σ_B	σ_date	-0.38	-0.46
	σ_Δh	0.58	0.63
	σ_ρ	60	
	σ_B	0.71	0.81
Calc. σ_ΔM	ΔM [Gt]	-0.28	-0.33
	σ_S	1920020.155	
	σ_ΔM	0.03	0.04
Results	B_geod.PoR [m w.e.]	**-7.2±0.71**	**-8.65±0.81**
	ΔM [Gt]	-0.28±0.03	-0.33±0.04

Appendix

Finger Glacier		dDEM	
		Hist. dDEM TDX	Hist. dDEM ARC
Area [m²]	S_1960	5536611.354	5536611.354
	S_2014	5689303.057	5689303.057
	S_avg	5612957.206	5612957.206
Volume Change	r² [m²]	289	16
	K	20273	367175
	Σ_Δh_k [m]	-310482	-6325734
	ΔV [m³]	-89729298	-101211744
Conversion Factor	ρ_glac [kg m⁻³]	850	
	ρ_water [kg m⁻³]	997	
	ρ_ratio	0.852557673	
B_geod	Δh_avg	-15.99	-18.03
	B_geod.PoR (m w.e.)	**-13.63**	**-15.37**
	B_geod.a (m w.e. yr⁻¹)	-0.25	-0.28
Error Assessment			
Calc. σ_DEM	CoReg_StDev	10.04	21.55
	L	500	
	(n/(L/r))	689.282	2937.4
	(c/2)	110	
	n_mean	399.641	1523.7
	σ_DEM	0.98	1.08
Calc. σ_B	σ_date	-0.61	-0.82
	σ_Δh	1.16	1.36
	σ_ρ	60	
	σ_B	1.38	1.59
Calc. σ_ΔM	ΔM [Gt]	**-0.08**	**-0.09**
	σ_S	280647.8603	
	σ_ΔM	0.01	0.01
Results	B_geod.PoR [m w.e.]	**-13.63±1.38**	**-15.37±1.59**
	ΔM [Gt]	-0.08±0.01	-0.09±0.01

Appendix Table 9: Calculations of geodetic mass balances with error assessment for Phantom Glacier. The values presented below compare TanDEM-X against ArcticDEM as contemporary data input.

Phantom Glacier			
		dDEM	
		Hist. dDEM TDX	Hist. dDEM ARC
Area [m²]	**S_1960**	11774484.96	11774484.96
	S_2014	12060742.52	12060742.52
	S_avg	11917613.74	11917613.74
Volume Change	**r² [m²]**	289	16
	K	42292	752694
	Σ_Δh_k [m]	-329653	-5382847
	ΔV [m³]	-95269717	-86125552
Conversion Factor	**ρ_glac [kg m⁻³]**	850	
	ρ_water [kg m⁻³]	997	
	ρ_ratio	0.852557673	
B_geod	**Δh_avg**	-7.99	-7.23
	B_geod.PoR (m w.e.)	**-6.82**	**-6.16**
	B_geod.a (m w.e. yr⁻¹)	-0.13	-0.11
Error Assessment			
Calc. σ_DEM	**CoReg_StDev**	10.04	21.55
	L	500	
	(n/(L/r))	1437.928	6021.552
	(c/2)	110	
	n_mean	773.964	3065.776
	σ_DEM	0.71	0.76
Calc. σ_B	**σ_date**	-0.31	-0.33
	σ_Δh	0.77	0.83
	σ_ρ	60	
	σ_B	0.81	0.83
Calc. σ_ΔM	**ΔM [Gt]**	**-0.081**	**-0.073**
	σ_S	595880.6871	
	σ_ΔM	0.01	0.01
Results	**B_geod.PoR [m w.e.]**	**-6.82±0.81**	**-6.16±0.83**
	ΔM [Gt]	-0.081±0.01	-0.073±0.01

Appendix Table 10: Calculations of geodetic mass balances with error assessment for Parallel Glacier. The values below compare TanDEM-X against ArcticDEM as contemporary input data.

Parallel Glacier			
		dDEM	
		Hist. dDEM TDX	Hist. dDEM ARC
Area [m²]	**S_1960**	14594480.56	14594481.56
	S_2014	13493277.89	13493277.89
	S_avg	14043879.22	14043879.72
Volume Change	**r² [m²]**	289	16
	K	46767	841318
	Σ_Δh_k [m]	-384246	-8414260
	ΔV [m³]	-111047094	-134628160
Conversion Factor	**ρ_glac [kg m⁻³]**	850	
	ρ_water [kg m⁻³]	997	
	ρ_ratio	0.852557673	
B_geod	**Δh_avg**	-7.91	-9.59
	B_geod.PoR (m w.e.)	**-6.74**	**-8.17**
	B_geod.a (m w.e. yr⁻¹)	-0.13	-0.15
Error Assessment			
Calc. σ_DEM	**CoReg_StDev**	10.04	21.55
	L	500	
	(n/(L/r))	1590.078	6730.544
	(c/2)	110	
	n_mean	850.039	3420.272
	σ_DEM	0.67	0.72
Calc. σ_B	**σ_date**	-0.30	-0.44
	σ_Δh	0.74	0.84
	σ_ρ	60	
	σ_B	0.79	0.92
Calc. σ_ΔM	**ΔM [Gt]**	**-0.095**	**-0.115**
	σ_S	702193.9612	
	σ_ΔM	0.01	0.01
Results	**B_geod.PoR [m w.e.]**	**-6.74±0.79**	**-8.17±0.92**
	ΔM [Gt]	-0.095±0.01	-0.115±0.01

Appendix Table 11: Calculations for geodetic mass balances with error assessment for Transit Glacier. Note how the introduction of modified input data changes the mass balance from positive to negative. All results use ArcticDEM elevation data as contemporary input.

Transit Glacier			
		dDEM	
		Historical dDEM	Modified dDEM
Area [m²]	**S_1960**	52232268.87	52232268.87
	S_2014	49811445.4	49811445.4
	S_avg	51021857.14	
Volume Change	**r² [m²]**	16	
	K	3093057	
	Σ_Δh_k [m]	20063692	-12843260
	ΔV [m³]	321019072	-205492160
Conversion Factor	**ρ_glac [kg m⁻³]**	850	
	ρ_water [kg m⁻³]	997	
	ρ_ratio	0.852557673	
B_geod	**Δh_avg**	6.29	-4.03
	B_geod.PoR (m w.e.)	**5.36**	**-3.43**
	B_geod.a (m w.e. yr⁻¹)	0.10	-0.06
Error Assessment			
Calc. σ_DEM	**CoReg_StDev**	21.55	
	L	500	
	(n/(L/r))	24744.456	
	(c/2)	50	
	n_mean	12397.228	
	σ_DEM	0.38	
Calc. σ_void	**n_void**		12372.228
	(c/2)		50
	(n_void/(L/r))		12372.228
	n_void_mean		6211.114
	Void_stdDev		22.344
	σ_void		0.28
Calc. σ_B	**σ_date**	0.29	-0.18
	σ_Δh	0.48	0.55
	σ_ρ	60	
	σ_B	0.55	0.53
Calc. σ_ΔM	**ΔM [Gt]**	0.27	-0.18
	σ_S	2551092.857	
	σ_ΔM	0.03	0.03
Results	**B_geod.PoR [m w.e.]**	**+5.36±0.55**	**-3.43±0.53**
	ΔM [Gt]	+0.27±0.03	-0.18±0.03

Appendix Table 12: Calculations of geodetic mass balances with error assessment for Bellevue Glacier. Values presented for ZeroChange TDX are based on the assumption that the missing area in the TanDEM-X dataset did not change over time.

Bellevue Glacier			
		dDEM	
		Hist. dDEM ARC	ZeroChange TDX
Area [m²]	**S_1960**	5854580.761	5854580.761
	S_2014	5991680.661	5991680.661
	S_avg	5923130.711	5923130.711
Volume Change	**r² [m²]**	16	289
	K	387467	22792
	Σ_Δh_k [m]	-3398252	-176542
	ΔV [m³]	-54372032	-51020638
Conversion Factor	**ρ_glac [kg m⁻³]**	850	
	ρ_water [kg m⁻³]	997	
	ρ_ratio	0.852557673	
B_geod	**Δh_avg**	-9.18	-8.61
	B_geod.PoR (m w.e.)	**-7.83**	**-7.34**
	B_geod.a (m w.e. yr⁻¹)	-0.15	-0.13
Error Assessment			
Calc. σ_DEM	**CoReg_StDev**	10.04	21.55
	L	500	
	(n/(L/r))	3099.736	774.934
	(c/2)	20	
	n_mean	1559.868	397.467
	σ_DEM	0.50	2.12
Calc. σ_B	**σ_date**	-0.35	-0.39
	σ_Δh	0.61	2.15
	σ_ρ	60	
	σ_B	0.76	1.91
Calc. σ_ΔM	**ΔM [Gt]**	**-0.046**	**-0.043**
	σ_S	296156.5356	
	σ_ΔM	0.01	0.01
Results	**B_geod.PoR [m w.e.]**	**-7.83±0.76**	**-7.34±1.91**
	ΔM [Gt]	-0.046±0.01	-0.043±0.01

Appendix Table 13: Calculations of geodetic mass balances with error assessment for the Hidden Ice Field. Values for ZeroChange TDX are based on the assumption that the missing area in the TanDEM-X dataset did not change over time.

Hidden Ice Field			
		dDEM	
		Hist. dDEM ARC	ZeroChange TDX
Area [m²]	**S_1960**	73397555.51	73397555.51
	S_2014	72879257.66	72879257.66
	S_avg	73138406.58	73138406.58
Volume Change	**r² [m²]**	16	289
	K	4308285	197447
	Σ_Δh_k [m]	10796388	212518
	ΔV [m³]	172742208	61417702
Conversion Factor	**ρ_glac [kg m⁻³]**	850	
	ρ_water [kg m⁻³]	997	
	ρ_ratio	0.852557673	
B_geod	**Δh_avg**	2.36	0.84
	B_geod.PoR (m w.e.)	**2.01**	**0.72**
	B_geod.a (m w.e. yr⁻¹)	0.04	0.01
Error Assessment			
Calc. σ_DEM	**CoReg_StDev**	21.55	10.04
	L	500	
	(n/(L/r))	34466.28	6713.198
	(c/2)	20	
	n_mean	17243.14	3366.599
	σ_DEM	0.32	0.34
Calc. σ_B	**σ_date**	0.09	0.04
	σ_Δh	0.33	0.34
	σ_ρ	60	
	σ_B	0.32	0.30
Calc. σ_ΔM	**ΔM [Gt]**	**0.147**	**0.052**
	σ_S	3656920.329	
	σ_ΔM	0.024	0.022
Results	**B_geod.PoR [m w.e.]**	**+2.01±0.32**	**+0.72±0.3**
	ΔM [Gt]	+0.147±0.02	+0.052±0.02
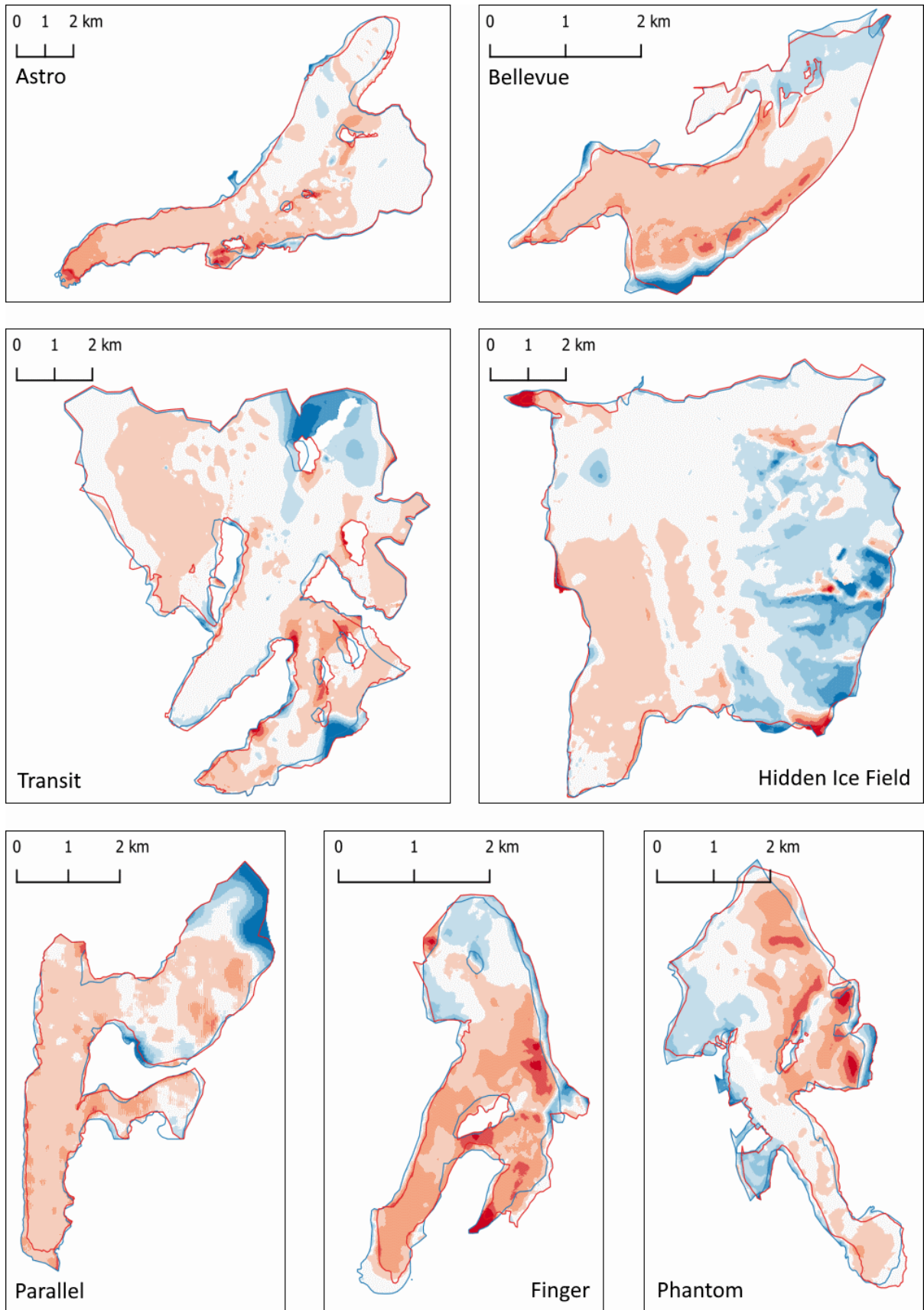
Appendix 13: Elevation change dH [m] on all observed glaciers as seen on the modified dDEM.

Difference Images of Surrounding Glaciers

☐ Glacier Outline in 1960
☐ Glacier Outline in 2018

Elevation Change dH [m]
■ <= -70
■ <= -50
■ <= -30
■ <= -10
☐ <= 10
☐ <= 30
■ <= 50
■ <= 70
■ > 70

Appendix 14: Legend for Appendix 13. All elevation change maps are orientated to the north.

Appendix

Personal Declaration

Personal declaration: I hereby declare that the submitted thesis is the result of my own, independent work. All external sources are explicitly acknowledged in the thesis.

Andreas Gantner

Zurich, 14.04.2020